



**UNIVERSITY of the
WESTERN CAPE**

Polypyrrole supports for direct alcohol fuel cells.

By

Zicabangele Mseleku

Dissertation in fulfilment of the requirement for the degree

MASTERS in Chemical Science

Faculty of Natural Science

of the

University of the Western Cape

Supervisor: Prof Lindiwe Khotseng

Co-supervisor: Dr Sivakumar Pasupathi

Keywords

Electro-catalyst, catalysts' support material, Polypyrrole, reduced graphene oxide, direct alcohol fuel cell, Multi-walled carbon nanotubes, alcohol oxidation reaction.

Abstract

Anode catalysts are one of the key components of direct alcohol fuel cells (DAFCs). They play a huge role in the alcohol oxidation reaction (AOR) that occurs on the anode side. Palladium (Pd) supported on carbon material has been reported to have good catalytic activity towards alcohol oxidation reactions. Better stability and activity has been reported for catalysts supported on conductive polymers like polypyrrole (PPy) when compared to traditional carbon support material. This study investigated the effect of support materials on Pd and PdCo electro-catalysts while concurrently determining the support material that can improve the activity and stability of Pd and PdCo electro-catalysts used as direct alcohol fuel cells catalysts. All Pd and PdCo catalysts supported on PPy (prepared using oxidative polymerization method), reduced graphene oxide (rGO) and prepared using modified Hammers method and multi-walled carbon nanotubes and pre-treated by acid. All the catalysts were synthesized using the modified polyol method. The synthesized catalysts were: palladium on reduced graphene oxide (Pd/rGO), palladium on multi-walled carbon nanotubes (Pd/MWCNT), (Pd/PPy), palladium on polypyrrole-reduced graphene oxide (Pd/PPy-rGO), palladium on polypyrrole-multi-walled carbon nanotubes (Pd/PPy-MWCNT), palladium-Cobalt on reduced graphene oxide (PdCo/rGO), PdCo/MWCNT, PdCo/PPy, PdCo/PPy-rGO and PdCo/PPy-MWCNT.

Electrochemical, chemical and physical properties were investigated by cyclic voltammetry (CV), linear sweep voltammetry (LSV), electrochemical impedance spectroscopy (EIS), chronoamperometry, Fourier transform Infrared spectroscopy, high-resolution transmission electron microscopy (HRTEM), energy dispersive spectroscopy (EDS) and X-ray diffraction (XRD).


Firstly, all of the support materials were prepared before use by various methods. Reduced graphene oxide (rGO) was prepared and functional groups were confirmed through FTIR. MWCNTs were functionalized in a ratio of (3:1) HNO₃/H₂SO₄ mixture, and the functionalized MWCNTs were investigated through FTIR and the spectrum obtained revealed the presence of significant functional groups. Lastly, Polypyrrole (PPy) was investigated through FTIR and the spectrum obtained revealed the presence of all significant functional groups. The electrochemical active surface area (ECSA) of the synthesized catalysts was calculated from cyclic voltammograms. Pd/PPy showed the highest ECSA of 68.01 m².g⁻¹ followed by Pd/rGO with ECSA of 50.72 m².g⁻¹, because the metal particles were well dispersed on the surface of the support material. Among the binary catalysts PdCo/rGO showed the highest ECSA of 33.9 m².g⁻¹ followed by PdCo/PPy-MWCNT. The LSV results showed that Pd/rGO was the most active catalyst followed by Pd/PPy with the current density of 0.64 mAcm⁻² and 0.32 mAcm⁻² in methanol oxidation. Pd/rGO was found to be the most stable among mono catalysts followed by Pd/PPy, Pd/PPy-rGO, Pd/PPy-MWCNT and Pd/MWCNT respectively. PdCo/MWCNT showed to be the most stable among binary catalysts followed by PdCo/PPy, PdCo/PPy-rGO, PdCo/rGO and PdCo/PPy-MWCNT in methanol observed using chronoamperometry. The highest current density from the mono catalysts was 0.64 mAcm⁻² of Pd/rGO whereas binary catalysts showed the maximum current density of 0.37 mAcm⁻² from PdCo/MWCNT. Pd/PPy also showed a higher current density of 0.32 mAcm⁻² compared to

PdCo/PPy with the lowest current density of 0.014 mAcm^{-2} in methanol. Among hybrid supported mono catalysts Pd/PPy-rGO showed a better catalytic activity and stability compared to Pd/PPy-MWCNT, also the hybrid supported mono catalysts displayed a better catalytic activity on methanol oxidation compared to the hybrid supported binary catalysts namely PdCo/PPy-rGO and PdCo/PPy-MWCNT. However binary catalysts collectively showed a better stability compare to mono catalysts. The HR-TEM and XRD studies, showed that particle sizes were in the range of 7.7-13.5 nm for HRTEM and 6.0-8.32 nm for XRD with some agglomeration observed from HRTEM images for most of the catalysts.



Declaration

I Zicabangele Mseleku hereby declare that “Polypyrrole supports for Direct Alcohol Fuel Cells” is the result of my own work that was done by me under the supervision of Prof. Lindiwe Khotseng and co-supervision of Prof. Sivakumar Pasupathi, and that it has not been previously submitted for any degree or examination in any other university or higher education; and that all the sources and quotations have been indicated and acknowledged by complete references.

_____  _____ on this 20 day of December _____

(Candidate)

_____ on this _____ day of _____

(Supervisor)

_____ on this _____ day of _____

(Co-supervisor)



Dedication

This work is dedicated to my loving family, friends and my church. The support they have shown me throughout my studies, not only for this degree but throughout my schooling career is highly appreciated. A special dedication goes to my late grandmother Yintombi Mseleku losing her made me realize how unpredictable life is, and to always appreciate those around you in every chance you get. It is also dedicated to every kid from my home town “Nquthu” with a dream hoping to achieve.

Acknowledgements

Above everything my gratitude goes to the Lord God Almighty for the strength and wisdom to carry me this far, I could not have made it on my own.

My outmost thank you to my supervisor Prof. Lindiwe Khotseng for giving me this opportunity to further my studies and career and for her guidance and patience during the course of the research work.

The University of the Western Cape, Chemistry Department for giving the opportunity to further my studies.

HySA systems and NRF for the financial support.

Fellow postgraduate students within the department especially Akindeji Jerome Sabejeje for helping me with the lab work guidance.

I would like to thank my friends especially Lungelo Sithole and S’fundo Nene for their constant checking up on me. Thank you for being reliable and kind friends and for being my brothers.

To my family, my cousins I truly thank you for support and pushing me to achieve my goals in life.

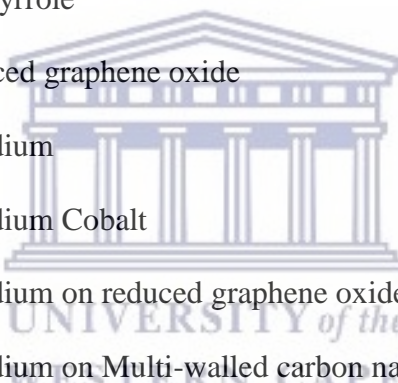
To my church and everyone who covered me in prayer during challenging times I thank you.



List of Abbreviations

DAFCs	: Direct Alcohol Fuel Cells
DMFC	: Direct Methanol Fuel Cells
AORs	: Alcohol Oxidation Reactions
CV	: Cyclic Voltammetry

MOR	: Methanol Oxidation Reaction
EG	: Ethylene glycol
EIS	: Electrochemical Impedance Spectroscopy
EDS	: Energy Dispersive Spectroscopy
FTIR	: Fourier Transform Infra-Red Spectroscopy
HRTEM	: High Resolution Transmission Electron Microscopy
XRD	: X-ray Diffraction Spectroscopy
LSV	: Linear Sweep Voltammetry
MWCNTs	: Multi Walled Carbon nanotubes
PPy	: Polypyrrole
rGO	: Reduced graphene oxide
Pd	: Palladium
PdCo	: Palladium Cobalt
Pd/rGO	: Palladium on reduced graphene oxide
Pd/MWCNT	: Palladium on Multi-walled carbon nanotubes
Pd/PPy	: Palladium on Polypyrrole
Pd/PPy-rGO	: Palladium on Polypyrrole-reduced graphene oxide
Pd/PPy-MWCNT	: Palladium on Polypyrrole-multi-walled nanotubes
PdCo/rGO	: Palladium-cobalt on reduced graphene oxide
PdCo/MWCNT	: Palladium-cobalt on multi-walled carbon nanotubes
PdCo/PPy	: Palladium-cobalt on Polypyrrole
PdCo/PPy-rGO	: Polypyrrole-reduced graphene oxide
PdCo/PPy-MWCNT	: Palladium-cobalt on Polypyrrole-multi-walled nanotubes
Ag/AgCl	: Silver-silver chloride
ECSA	: Electrochemical Surface Area



GCRDE : Glassy Carbon Rotating Disk Electrode

L_{Pd} [mg.cm⁻²] : Palladium loading per unit geometric electrode area

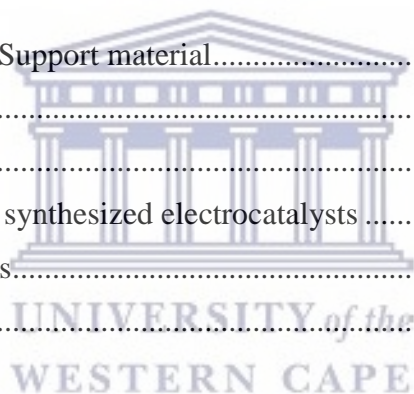


Table of Contents

Keywords	2
Abstract	2
Declaration	4
Dedication	5
List of Abbreviations	7
Table of Contents	10
List of Figures	12
List of Tables	13
Chapter 1	14
Introduction	14
1.1 Background	14
1.2 Overview of fuel cells	16
Rationale of the project	18
Aim and objectives	19
Research questions	20
References	21
Chapter 2	24
Literature review	24
Chapter overview	24
2.1. Types of fuel cells	24
2.2 Catalyst	31
2.3 Support material for catalysts	34



2.4 Fuel cells catalyst preparation methods	39
References	42
Chapter 3	51
Experimental	51
3. Introduction	51
3.1 Chemicals	51
3.2 Methodology	52
3.3 CHARACTERIZATION TECHNIQUES	57
References	70
Chapter 4	73
Results and Discussion	73
4.1 Functionalization of The Support material	73
4.2 XRD Analysis	78
4.3. Internal structure	82
4.4 Elemental analysis of the synthesized electrocatalysts	91
4.5 Electrochemistry Analysis	94
Chapter 5	115
Conclusion and recommendation	115
5.1. Conclusion	115
5.2 Recommendations	117
References	111



List of Figures

Figure 1.1 schematic diagram of a fuel cell. [14]	17
Figure 2.1 schematic diagram of a direct methanol fuel cell [53].	30
Figure 2.2 schematic diagram of pyrrole polymerization to form polypyrrole [52].....	39
Figure 3.1 working station of FTIR [12]	63
Figure 3.2 cyclic voltammogram of Pd/MWCNT (at the fifth cycle) in 2M KOH solution. Pd loading $17 \mu\text{g cm}^{-2}$. scan rate: 50 mV s^{-1} [18]......	65
Figure 4.1.1 FTIR spectra of functionalized MWCNTs with COOH.....	74
Figure 4.1.2 FTIR spectra of go and rGO	75
Figure 4.1.4 FTIR spectra of PPy	77
Figure 4.2.1 XRD patterns of the in house supports material (ppy, MWCNT and rGO).....	78
Figure 4.2.2 the XRD patterns of the in house catalysts namely Pd/rGO, Pd/MWCNT, Pd/PPy, Pd/PPy-rGO, Pd/PPy-MWCNT.....	79
Figure 4.2.3a the XRD patterns of the palladium cobalt catalysts namely PdCo/rGO, PdCo/MWCNT, PdCo/PPy, PdCo/PPy-rGO, PdCo/PPy-MWCNT with a zoomed patterns in the diagram labelled b.....	80
Figure 4.3.1 HRTEM images of the prepared supports material of (a) MWCNT, (b)rGO and (c)PPy at low and high magnification.	84
Figure 4.4 EDS plots of the synthesized catalysts of (a) Pd/rGO, (b) Pd/MWCNT, (c) Pd/PPy, (d)Pd/PPy-rGO, (e) Pd/PPy-MWCNT, (f) PdCo/rGO, (g) PdCo/MWCNT, (h) PdCo/PPy, (i) PdCo/PPy-rGO and (j) PdCo/PPy-MWCNT.....	94
Figure 4.5.1 cyclic voltammetry of Pd in house electro-catalyst supported on rGO, MWCNT, PPy and on a hybrid support of PPy-rGO and PPy-MWCNT in N_2 saturated 1.0 M of KOH at a scan rate of 20 mV.s^{-1}	96
Figure 4.5.2 cyclic voltammetry of Pd in house electro-catalyst supported on rGO, MWCNT, PPy and on a hybrid support of PPy-rGO and PPy-MWCNT in N_2 saturated 1.0 M of KOH and 1.0 M of methanol at a scan rate of 20 mV.s^{-1}	99
Figure 4.5.3 EIS of the synthesized electrocatalysts of Pd/rGO, Pd/MWCNT, Pd/PPy, Pd/PPy-rGO and Pd/PPy-MWCNT in 1.0 M KOH with 1.0 M methanol.....	101
Figure 4.5.4 chronoamperometry of Pd in-house electro-catalysts on rGO, MWCNT, PPy, PPy-rGO and PPy-MWCNT support in N_2 saturated 1.0 M KOH and 1.0 M methanol comparing their stability at a -0.3V.	103

Figure 4.5.5 cyclic voltammetry of PdCo in house electro-catalyst supported on rGO, MWCNT, PPy and on a hybrid support of PPy-rGO and PPy-MWCNT in N ₂ saturated 1.0 m of KOH at a scan rate of 20 mv.s ⁻¹	104
Figure 4.5.6 cyclic voltammetry of PdCo in house electro-catalyst supported on rGO, MWCNT, PPy and on a hybrid support of PPy-rGO and PPy-MWCNT in N ₂ saturated 1.0 m of KOH and 1.0 m of methanol at a scan rate of 20 mv.s ⁻¹	105
Figure 4.5.7 EIS of PdCo synthesized electro-catalyst supported on rGO, MWCNT, PPy and on a hybrid support of PPy-rGO and PPy-MWCNT in N ₂ saturated 1.0 M of KOH and 1.0 M of methanol.	107
Figure 4.5.8 chronoamperometry of PdCo in-house electro-catalysts on rGO, MWCNT, PPy, PPy-rGO and PPy-MWCNT support in N ₂ saturated 1.0M KOH and 1.0 M methanol comparing their stability at -0.3v.....	109



List of Tables

Table 2.1: The table below shows different types of fuel cells [3-5]	25
Table 2.2: The application of different catalyst in direct alcohol fuel cells and their performance	32
Table 3.1: The list of chemicals used for the study, and their suppliers.....	51
Table 3.1 XRD sample preparation	61
Table 3.3: Sample preparation and operating parameters for LSV	66
Table 4. 1: XRD data of Gaussian Fit for (111) plane and HRTEM for crystal size calculation	81
Table 4.5.1: Summary data of ECSA.....	97
Table 4.5.2: All the data collected from figure 4.5.2 of methanol oxidation.....	100
Table 4.5.3 the table below shows charge transfer resistance (R _{ct}) of the synthesized mono-catalysts	102
Table 4.5.4: Current density values and onset potentials of PdCo/rGO, PdCo/MWCNT, PdCo/PPy, PdCo/PPy-rGO and PdCo/PPy-MWCNT in 1.0MKOH with 1.0M methanol at a scan rate of 20mV.s ⁻¹	106
Table 4.5.5 the table below shows charge transfer resistance (R _{ct}) of the synthesized binary catalysts	107

Chapter 1

Introduction

1.1 Background

The world is facing a serious problem of energy demand caused by the population increase and fossil fuels depletion as well as the issue of climate change caused by the high CO₂ emission from the fossil fuels that are currently used as the main source of energy. Due to these problems scientists are compelled to find a better renewable source of energy. Among the discovered sources of renewable energy, fuel cells have been found to be the promising alternative mainly for future use. Fuel cells has attracted a broad attention from the researchers because of their intriguing ability to produce energy with high efficiency and high density [1]. Fuel cell is an electrochemical device that converts chemical energy of a fuel (e.g. hydrogen, alcohol, etc.) to produce electricity through electro-catalytic reaction. Currently fuel cells are the most promising source for renewable energy production because they produce less to none pollution. At present, human population globally depends on fossil fuels as the major source of energy and in the meantime the use of rapidly depleting fossil fuels to meet the increasing global demand for energy is economically and environmentally unsustainable. Concurrently, the reserves of easily-accessible fossil fuels are declining as they are not produced from renewable sources, resulting in continually escalating financial and environmental costs in utilization, extraction and processing activities, especially as the use of non-ideal deposits in complex areas becomes necessary to meet global demand. Greenhouse gas emissions (e.g. CO₂, CH₄ and N₂O) that are linked to the extraction, processing and use of fossil fuels have raised atmospheric

concentrations of CO₂ significantly beyond the natural historical maximum of around 300 ppm. The concentration now of approximately 390 ppm is considered to be a substantial global risk of irreversible climatic changes and it still continues to increase [2-4]. According to the World Energy Outlook, the world's energy demands are expected to exceed 50% by 2030 than today [3-5].

In order to reduce the risk of global warming, emission of greenhouse gases needs to be reduced. To attain such dramatic emission reductions, whilst concurrently addressing the issue of increasing energy demand and improving energy security requires a change-over to renewable primary energy sources. The adoption of clean and efficient energy distribution and conversion technologies to replace hydrocarbon fuels and thermo-mechanical engines [3-4]. Renewable energy sources have a lower efficiency compared to fossil fuels, making it difficult to have renewable energy sources as fossil fuel replacements. However fuel cells have a high efficiency compared to photovoltaic cells and wind turbines. Emit no greenhouse gases this makes fuel cells a good candidate to replace or work with fossil fuels to decrease greenhouse gases [6]. Their reliability is still evolving; and there are safety concerns with hydrogen fuel cells and also with hydrogen not being readily available. The fuel used for fuel cells also has a low density compared to gasoline. Although fuel cells have their fair share of drawbacks they hold promise for our energy crisis in the future. Fuel cells have a high efficiency, and they use renewable fuels. Fuel cells can run continuously as long as fuel is available, they do not require recharging. Another advantage of fuel cells is that they can run in reverse process known as electrolysis for energy storage, producing hydrogen from electricity and water [7].

Fuel cells are advantageous in many ways. One of the key advantages is their ability to operate at low temperature which makes them suitable for use in motorized applications. Quiet

operation, their nature of operation is amazingly quiet which allows them to be used in the places where noise is not required like residential areas. They are also environmentally friendly meaning they do not emit harmful greenhouse gases. Higher efficiency, fuel cells can produce more energy with less fuel as compared to the combustion engines. In a fuel cell stack there are no moving parts hence the absence of mechanical inefficiencies [8-10].

1.2 Overview of fuel cells

A fuel cell can be defined as a device that converts the energy of a fuel (e.g. hydrogen, alcohol, and etc.) and oxidant in the presence of a catalyst into electricity, heat and water. Fuel cells could result in innovative improvement in energy production and shortly they might become a future world economy. Fuel cells are economically achievable for business energy production and also the developed fuel cells are becoming more competent for energy production [11-13]. These days the types of fuel cells are differentiated by their electrolytes; proton exchange membrane fuel cell (PEMFCs), solid oxide fuel cell (SOFCs), phosphoric acid fuel cell (PAFCs), molten carbonate fuel cell (MCFCs), alkaline fuel cell (AFCs) and direct alcohol fuel cell (DMFCs). Fuel cells can differ from tiny devices that produce a few watts of electricity to large power plants producing megawatts of electricity. A fuel cell is composed of an anode, cathode, and an electrolyte membrane. A typical fuel cell works by passing hydrogen through the anode of a fuel cell and oxygen through the cathode. At the anode site, a catalyst splits the hydrogen molecules into electrons and protons. The protons pass through the porous electrolyte membrane, while the electrons are forced through a circuit, generating an electric current and excess heat. At the cathode, the protons, electrons, and oxygen combine to produce water molecules. The figure below shows a schematic diagram of a fuel cell as described above.

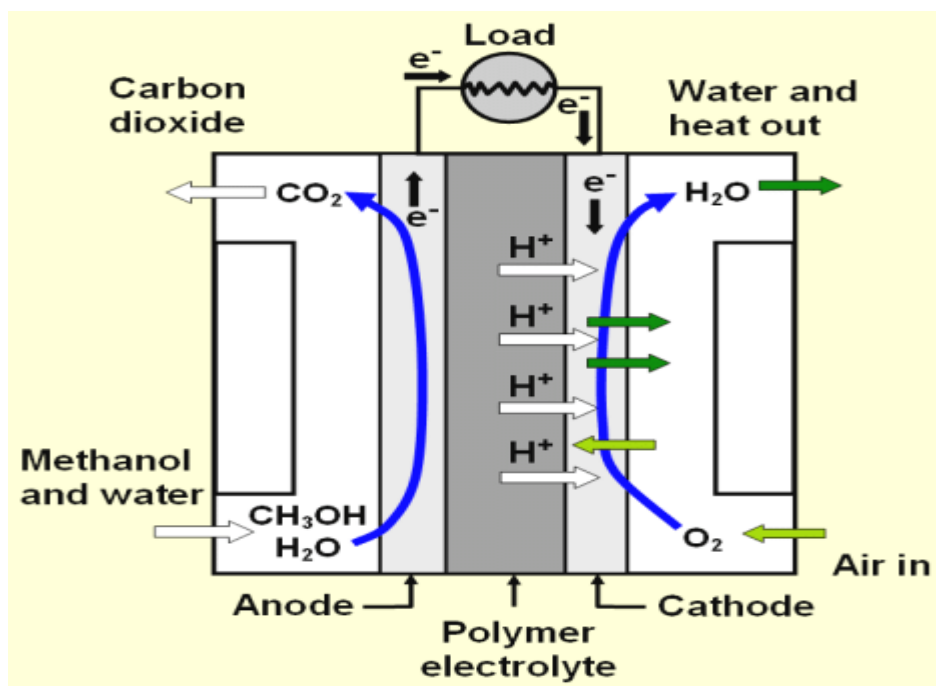


Figure 1.1 Schematic diagram of a direct methanol fuel cell. [14]

Among the different types of fuel cells, direct alcohol fuel cells (DMFCs) has attracted more attention for their use in portable application which makes it to be more advantageous as compared to other fuel cells. This is based on the fact that the liquid low-molecular-weight alcohols can easily be transported as compared to other conventional internal combustion engines. However, there problems related to the use of alcohol as fuel in fuel cells is the rapid poisoning of the anode during alcohol oxidation reaction (AOR) by adsorbed intermediate such as carbon monoxide making it impossible for the fuel cells to compete in the commercial market [15]. To address these problems a different metal palladium (Pd) has been used as the catalyst, showing resistance against poisoning by intermediate products [16]. The issue of low surface area and stability leading to a poor fuel cell performance has been solved by introducing carbon catalyst support material which provides a better and improved fuel cell performance through an increased surface area. But carbon supports material can be easily degraded in

alcohol fuel cells, to mitigate such challenges the ionomer was introduced. The ionomer is usually used as the electrolyte for proton production and to maintain the catalyst layer as a binder [17]. Anode catalysts are one of the key components which directly determine the performance output of DMFCs. This study investigated the effect of support (such as PPy, rGO, MWCNTs) of Pd and PdCo anode catalysts on the performance of DMFCs.

Rationale of the project

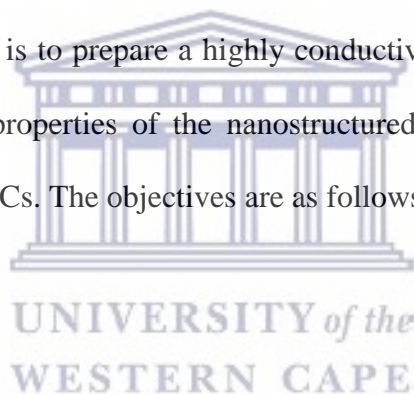
The focus of this investigation is on direct methanol fuel cell that is a low-temperature fuel cell. It has received more attention over the years as a promising technological development that may replace typical batteries as power sources for portable devices. This can be because of their distinctive features of utilizing liquid alcohol as fuel that offers, high specific energy density, the high energy conversion potency of 40-50%, low in operation temperatures (0 -100 °C), and also the use of alcohol as fuel permits for simple storage and transportation [15, 18-19], one thing that simplifies the fuel cell system.

One of the major problems associated with the DMFCs deals with the anode side of the fuel cell where oxidation of the fuel produces CO. The corrosion of the anode catalyst when carbon black is used as a support material results in a considerable loss in the overall efficiency of the DMFCs. Some great Measures have been made to solve such problem, carbon nanostructured materials like carbon nanotubes, graphene and etc. have been largely employed as the catalyst support material for low temperature fuel cells like DMFCs's. However still there are several drawbacks of these support materials, limiting the catalyst performance, which leads to a total fuel cell performance and stability being lowered. These drawbacks include their micro-pores which limits the surface accessibility lowering the surface area, easy corrosion. Therefore an advanced or modified carbon material is required to further enhance the fuel cell performance.

Due to the distinctive characteristics of Polypyrrole (PPy) like its high conductivity, it has been suggested as the promising alternative to carbon support material [20-21]. Studies have proven that fuel cell performance can be improved by means of ionomer as stated by Eguchi. M, et al, (2012) [17], hence in this study Polypyrrole is used as the ionomer. In light of these facts the development of research goals with regards to the project were developed.

Aim and objectives

The main purpose of the study is to prepare a highly conductive Polypyrrole material which will be used to enhance the properties of the nanostructured carbon support material for Palladium (Pd) catalyst in DAFCs. The objectives are as follows:



Objectives

- Preparation of a highly electron conductive Polypyrrole material
- The catalytic properties will be evaluated using analytical techniques such as cyclic voltammetry, Linear Sweep Voltammetry, Chronoamperometry and Electrochemical Impedance spectroscopy.
- The physical characterization will be done by employing X-ray diffraction (XRD) spectroscopy. Scanning electron microscope will be used for elemental composition and high resolution transmission electron microscope (HRTEM) for morphology and particle size. The FTIR and BET will also be used to study the functionality and surface area of the catalysts, respectively.

Research questions

What impact does a highly conductive Polypyrrole have on the electro-activity of the Pd catalyst and to the fuel cell efficiency and stability?



References

1. Carrette, L., Friedrich, K.A. and Stimming, U., 2000. Fuel cells: principles, types, fuels, and applications. *ChemPhysChem*, 1(4), pp.162-193.
2. Midilli, A., Dincer, I. and Ay, M., 2006. Green energy strategies for sustainable development. *Energy policy*, 34(18), pp.3623-3633.
3. Davis, S.J., Caldeira, K. and Matthews, H.D., 2010. Future CO₂ emissions and climate change from existing energy infrastructure. *Science*, 329(5997), pp.1330-1333.
4. Turner, J.A., 1999. A realizable renewable energy future. *Science*, 285(5428), pp.687-689.
5. Zerta, M., Schmidt, P.R., Stiller, C. and Landinger, H., 2008. Alternative World Energy Outlook (AWE0) and the role of hydrogen in a changing energy landscape. *International journal of hydrogen energy*, 33(12), pp.3021-3025.
6. Hoffert, M.I., Caldeira, K., Benford, G., Criswell, D.R., Green, C., Herzog, H., Jain, A.K., Kheshgi, H.S., Lackner, K.S., Lewis, J.S. and Lightfoot, H.D., 2002. Advanced technology paths to global climate stability: energy for a greenhouse planet. *science*, 298(5595), pp.981-987.
7. Cook, B., 2002. Introduction to fuel cells and hydrogen technology. *Engineering Science & Education Journal*, 11(6), pp.205-216.
8. Advantages and benefits of hydrogen and fuel cell technologies, Fuel cell Markets. (2002-2012). [www.fuelcellmarkets.com/fuel_cell_markets/5, 1, 1,663.html](http://www.fuelcellmarkets.com/fuel_cell_markets/5,1,1,663.html).
9. Costamagna, P. and Srinivasan, S., 2001. Quantum jumps in the PEMFC science and technology from the 1960s to the year 2000: Part II. Engineering, technology development and application aspects. *Journal of power sources*, 102(1-2), pp.253-269.
10. Rayment and S. Sherwin, 2003 Introduction to fuel cell University of Norte Dame, Notre Dame, IN 46556, USA. 14, p. 12-13.

11. Carrette, L., Friedrich, K.A. and Stimming, U., 2001. Fuel cells–fundamentals and applications. *Fuel cells*, 1(1), pp.5-39.
12. Dutta, S., 2014. A review on production, storage of hydrogen and its utilization as an energy resource. *Journal of Industrial and Engineering Chemistry*, 20(4), pp.1148-1156.
13. Badwal, S.P.S., Giddey, S., Kulkarni, A., Goel, J. and Basu, S., 2015. Direct ethanol fuel cells for transport and stationary applications–A comprehensive review. *Applied Energy*, 145, pp.80-103.
14. Long, N.V., Thi, C.M., Nogami, M. and Ohtaki, M., 2012. Novel Pt and Pd based core-shell catalysts with critical new issues of heat treatment, stability and stability for proton exchange membrane fuel cells and direct methanol fuel cells. *Heat Treatment- Conventional and Novel Applications, 1st ed.; Czwerwinski, F., Ed*, pp.235-268.
15. Zhao, T.S., Yang, W.W., Chen, R. and Wu, Q.X., 2010. Towards operating direct methanol fuel cells with highly concentrated fuel. *Journal of Power Sources*, 195(11), pp.3451-3462.
16. Cheng, X., Shi, Z., Glass, N., Zhang, L., Zhang, J., Song, D., Liu, Z.S., Wang, H. and Shen, J., 2007. A review of PEM hydrogen fuel cell contamination: Impacts, mechanisms, and mitigation. *Journal of Power Sources*, 165(2), pp.739-756.
17. Eguchi, M., Baba, K., Onuma, T., Yoshida, K., Iwasawa, K., Kobayashi, Y., Uno, K., Komatsu, K., Kobori, M., Nishitani-Gamo, M. and Ando, T., 2012. Influence of ionomer/carbon ratio on the performance of a polymer electrolyte fuel cell. *polymers*, 4(4), pp.1645-1656.
18. Liu, H., Song, C., Zhang, L., Zhang, J., Wang, H. and Wilkinson, D.P., 2006. A review of anode catalysis in the direct methanol fuel cell. *Journal of Power Sources*, 155(2), pp.95-110.

19. Zhao, T. and Xu, C., 2009. Fuel cells: direct alcohol fuel cells: direct methanol fuel cell: overview performance and operational conditions. *Encyclopedia of electrochemical power sources*.
20. Yuan, X., Ding, X.L., Wang, C.Y. and Ma, Z.F., 2013. Use of polypyrrole in catalysts for low temperature fuel cells. *Energy & Environmental Science*, 6(4), pp.1105-1124.
21. Huang, S.Y., Ganesan, P. and Popov, B.N., 2009. Development of conducting polypyrrole as corrosion-resistant catalyst support for polymer electrolyte membrane fuel cell (PEMFC) application. *Applied Catalysis B: Environmental*, 93(1-2), pp.75-81.

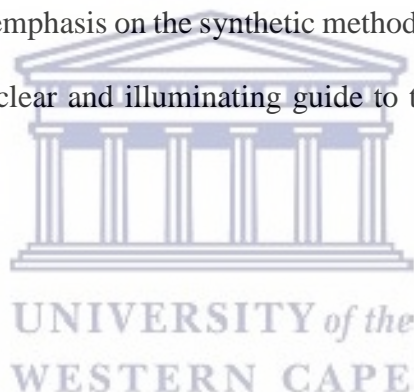


Chapter 2

Literature review

Chapter overview

This chapter focuses on the important concepts related to electro-catalysts of fuel cells. A brief look into the different types of materials used to modify support materials and catalysts for fuel cells and different types of fuel cells, with knowledgeable choice into the preference of catalyst and support material for this project. This chapter also introduces various synthetic routes for synthesizing catalysts, with an emphasis on the synthetic method used in this task. The purpose of this chapter is to provide a clear and illuminating guide to the literature reviewed for the proposed work.



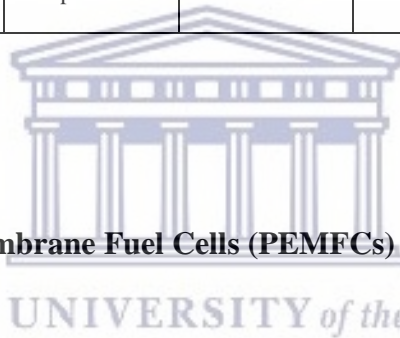
2.1. Types of fuel cells

Fuel cells are classified and differentiated by the type of electrolyte material used [1]. Electrolyte is the conductive substance located between the positive and negative electrode, acting as the conductor, yet it does not conduct electrons for the ion exchange that produces electrical current [2]. There are five different types of fuel cell that are currently studied, developed and demonstrated, in various stages of commercial availability. These five types of fuel cell are significantly different from each other in many aspects but the key distinguishing feature is the electrolyte material (Table 2.1). All fuel cells have the same basic operating principle.

Table 2.1: The table below shows different types of fuel cells [3-5]

Fuel cell Type	Proton Exchange Membrane Fuel Cells (PEMFC)	Molten Carbonate fuel cells (MCFC)	Alkaline Fuel Cell (AFC)	Solid Oxide fuel cells (SOFC)	Phosphoric Acid Fuel Cells (PAFC)
Electrolyte used	Proton exchange membrane	Typically, molten $\text{Li}_2\text{CO}_3/\text{K}_2\text{CO}_3$ eutectics	Typically aqueous KOH solution	Stabilized ceramic matrix with free oxide ions	H_3PO_4 solutions
Typical construction	Plastic, metal, or carbon	High temperature metals, porous ceramic	Plastic, metal	Ceramic, high temp metals	Carbon, porous ceramics
Operational temperature	(60-120 °C)	(650-700 °C)	(60-260 °C)	(650-1000 °C)	(150-210 °C)
Primary contaminate sensitivities	CO, Sulfur, and NH_3	Sulfur	CO, CO_2 , and Sulfur	Sulfur	CO < 1 %, Sulfur
Applications	Electric utility, portable power, transportation	Electric utility	Military space	Electric utility	Electric utility, transportation
Advantages	Solid electrolyte reduces corrosion & management	High temperature advantages	Cathode reaction faster in alkaline electrolyte — therefore high performance	High temperature advantages. Solid electrolyte	Up to 85 % efficiency in co-generation of electricity and heat.

	problems. Low temperature. Quick start-up			advantages	Impure H ₂ as fuel
Disadvantages	Low temperature requires expensive catalysts. High sensitivity to fuel impurities	High temperature enhances corrosion and breakdown of cell components	Expensive removal of CO ₂ from fuel and air streams required	High temperature enhances breakdown of cell components	Pt catalyst. Low current and power. Large size.



2.1.1 Polymer Electrolyte Membrane Fuel Cells (PEMFCs)

The proton-exchange membrane or PEM fuel cell, is made up of two electrodes separated by an electrolyte. It is the type of electrolyte used which distinguishes the PEM fuel cell from others. Hydrogen-PEMFC and direct methanol fuel cells (DMFC) are categorized as PEMFC because of the solid proton exchange membrane used in them as the electrolyte. The main difference between the DMFC and the H₂-PEMFC is the fuel used for the production of electrical energy, with hydrogen in the case of H₂-PEMFC and methanol in the case of DMFC [10]. The unique physical and operational properties of the polymer membrane electrolyte provide significant advantages over liquid and high temperature solid electrolytes in materials selection, component design and manufacturing, and power plant systems design [6].

Polymer electrolyte membrane (PEM) fuel cells have the potential to alleviate major problems associated with the production and consumption of energy. PEMFCs offer high energy

conversion efficiency, at low operating temperatures, which can rapid start-up. These characteristics and the ability to rapidly change power output are some of the traits that makes the PEMFCs the most promising fuel cell technique for large-scale application in, such as portable electronics, automobiles or stationary power supplies [7-9]. The proton-exchange membrane fuel cell uses one of several ion-exchange polymers as its electrolyte. These polymers are electronic insulators, but excellent conductors of hydrogen ions.

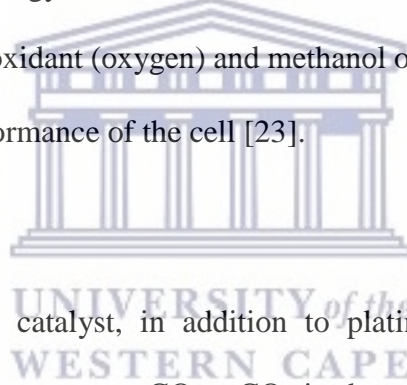
2.1.1.1 H₂-Proton exchange membrane fuel cells (H₂-PEMFCs)

The first H₂-PEMFC device was developed in the 1960's by the General Electric Company, for use as a military power sources in the Gemini space missions. A H₂-PEM fuel cell converts chemical energy stored in the fuel (hydrogen) into electrical energy through electrochemical reactions between H₂ and O₂ [11-13]. H₂-PEM fuel cell uses platinum (Pt) as electrodes, on the anodic side it uses platinum catalyst together with hydrogen fuel and Pt and oxygen for the cathodic side. Because of the sensitivity of Pt to carbon monoxide (CO), the fuel need to be purified which enables the best fuel cell performance [14-16]. But the problem in storage and transportation of hydrogen, has led to a search for an alternate fuel. Methanol has been suggested as a better alternative because it is known to be an excellent carrier for hydrogen [17]

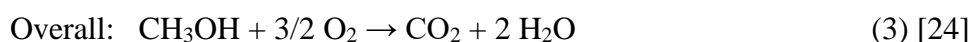
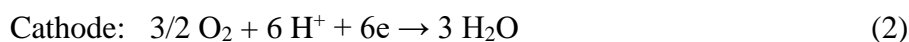
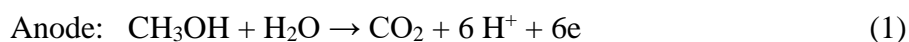
2.1.1.2 Direct Methanol Fuel Cells (DMFCs)

The DMFC technology has gained wide acceptance as a viable fuel cell technology and DMFC has a proven track record in powering cell phones, and laptops [18-20]. DMFC uses methanol

which has a higher energy density than hydrogen and is liquid, making it easy to adapt to existing fuel infrastructure with the benefit of its application in small portable devices. DMFCs will be widely used for years to come. In the DMFC system, liquid methanol enters the fuel cell directly, without the need for an intermediate step to convert the fuel into hydrogen. Methanol is an inexpensive liquid at room temperature, easy to store, high in energy density, and can be produced from various sources such as natural gas, coal, and even biomass. It is also biodegradable. It is not corrosive to the DMFC frame. DMFC provides unlimited possibilities for many applications [21-22]. These advantages allow DMFCs to be commercialized for use in portable electronic devices. One of the disadvantages of methanol used as fuel in fuel cell technology is methanol crossover. Methanol tends to diffuse to the cathode side where there is an oxidant (oxygen) and methanol oxidation occurs on the cathode catalyst, thus reducing the performance of the cell [23].

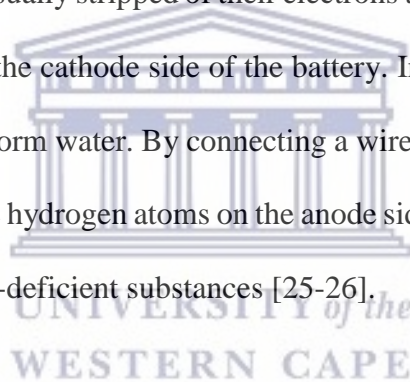


Compared to the H₂-PEMFC catalyst, in addition to platinum, other catalysts such as ruthenium (Ru) must be added to convert CO to CO₂ in the anodic reaction. The electrolyte and operating temperature in DMFC are essentially the same as used in H₂-PEMFC normally operating in the temperature range of 50 to 100 ° C. Higher efficiency is achieved at high temperatures. The main difference is the reaction at the anode where methanol is oxidized instead of hydrogen as in H₂-PEMFC. DMFC uses a catalyst and a solution of methanol (usually 1-2 M) at the anode, a Pt catalyst and O₂ at the cathode. The electrochemical oxidation of methanol is more complex than that of hydrogen [24].



2.1.1.3 Operating principle of the direct methanol fuel cell

The DMFC is a specialized PEMFC that operates on methanol instead of hydrogen on the anode side. It consists of several layers, the three key layers include membrane electrode assemble (MEA) (which is formed by the electrodes (anode and cathode)), proton conducting membrane, catalyst layer and hardware. The mixture of methanol and water is fed into the anode catalyst, where the catalyst particles present in the anode help separate methanol molecules into hydrogen atoms and carbon dioxide (CO₂) (as shown in Figure 2.1). The separated hydrogen atoms are usually stripped of their electrons to form protons and the protons pass through the membrane to the cathode side of the battery. In the cathode catalyst, protons react with oxygen in the air to form water. By connecting a wire from the anode to the cathode side, electrons stripped from the hydrogen atoms on the anode side can propagate to the cathode side and combine with electron-deficient substances [25-26].



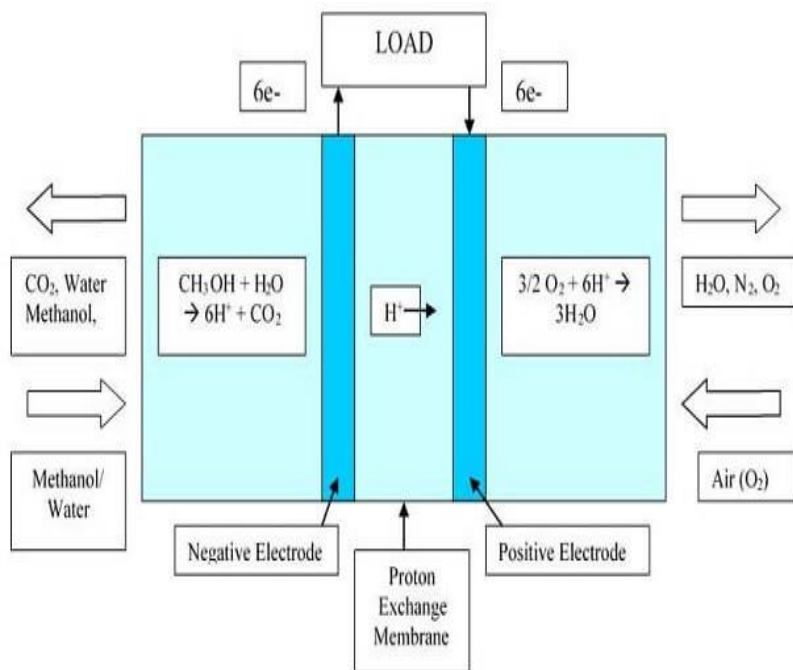


Figure 2.1 Schematic diagram of a Direct Methanol Fuel Cell [27].

2.1.1.4 Challenges in the direct methanol fuel cell

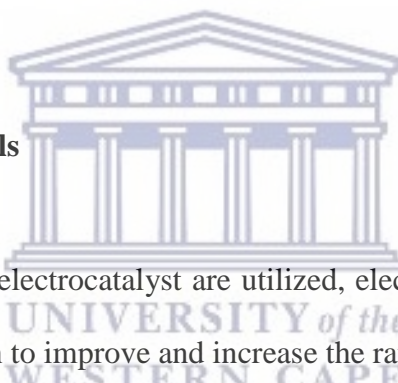
Although DMFC is already in the market, there are still some drawbacks that needs to be addressed in order to improve the efficiency and commercialization of this device. Most DMFCs operates in acidic electrolyte where platinum (Pt) catalyst is utilized as the anode with a solid Nafion proton exchange membrane. Nevertheless DMFCs have some drawbacks which lowers cell voltage and fuel utilization. These drawbacks include poisoning of electro-oxidation by adsorbed intermediate like CO, carbon material corrosion, membrane degradation and alcohol crossover. Construction and operational costs are one of crucial aspects on the successful development and commercialization of these fuel cells. The metal used as the catalyst which is platinum (Pt) is highly expensive. Research has been done to reduce noble metal catalyst loading without affecting fuel cell performance [28-30]. In order to solve this problem extensive research has been conducted using platinum based binary and ternary

metallic electrocatalysts. The platinum ruthenium (Pt-Ru) catalyst have been found to be the one of the good electrocatalysts for the direct methanol anode catalyst [31].

2.2 Catalyst

A catalyst is a substance that has the ability to fasten the chemical reaction by forming a bond with reacting species and reducing the activation energy. A catalyst enables reactants to form a product which later detaches leaving the catalyst in its original form in such a way that it can be used for the next reaction.

2.2.1 Catalysts used in fuel cells

The logo of the University of the Western Cape, featuring a classical building with columns and a pediment, with the text 'UNIVERSITY of the WESTERN CAPE' below it.

In fuel cells catalyst known as electrocatalyst are utilized, electrocatalyst is a catalyst that is used in electrochemical reaction to improve and increase the rate of a chemical reaction. They are a form of catalysts that are specifically designed for a sole purpose of working as either an electrode itself or at the surface of the electrode. Different catalysts are used in fuel cell because of the urge of trying to enhance the fuel cell's performance, which includes the stability, stability, cost reduction and activity of the fuel cell. Fuel cell uses heterogeneous catalyst, which is a metal dispersed on the conductive support material, this done to improve the catalytic activity by increasing the surface area. [31-32]. Heterogeneous catalyst exist in a different phase to the reactant.

In DMFCs catalysts are classified according to their role in the electrochemical reaction, namely cathode catalyst and anode catalyst. For reducing reactants at the cathodic end the cathode catalyst is used. Alcohol oxidation happens at the anodic side, hence the anode catalyst

is used to carry out the alcohol oxidation process. The most commonly used catalysts are platinum (Pt), palladium (Pd), and their alloys they can be used either as pure metals doped on the carbon support material or alloyed with other metals like gold, ruthenium and nickel [33-34]. In this project Pd and Pd-Co are used as the catalysts for methanol oxidation. There has been a lot of work done on the anode catalyst and Table 2.2 reviewed some work as given in below table.

Table 2.2: The application of different catalyst in direct alcohol fuel cells and their performance

Catalysts Composition	Experimental conditions	Specific/mass activity	References
Pd/MnO ₂ /graphene	0.5 M KOH and 1 M CH ₃ OH	20.4 mA/cm ²	[35]
Pd/PPY/graphene	0.5 M NaOH and 1 M CH ₃ OH	359.8 mA/mg	[36]
PtNi/C	1 M NaOH and 1 M CH ₃ OH	48.5 mA/cm ²	[37]
PtPd/graphene	0.1 M HClO ₄ and 1 M CH ₃ OH	198 mA/mg	[38]
Pd/MnO ₂ /CNT	0.5 M NaOH and 1 M CH ₃ OH	432.02 mA/mg	[39]
Pd/graphene	0.5 M NaOH and 1 M CH ₃ OH	61.6 mA/cm ²	[40]
Pd/PANI	1 M NaOH and 1 M CH ₃ OH	0.82 mA/cm ²	[41]
PdCo/RGO	1 M KOH and 1 M CH ₃ OH	303.8 mA/mg	[42]
Pd/PPy PNCs	1 M KOH and 1M C ₂ H ₅ OH	13.08 mA/cm ²	[43]
Pd/PPyC	1 M KOH and 1M C ₂ H ₅ OH	983 mA/cm ² .mg	[44]
PdNi/MWCNT	0.5 M NaOH and 1 M CH ₃ OH	482.2 mA/mg	[39]
Pt/MWCNT	1 M KOH and 1 M CH ₃ OH	730.0 mA/mg	[45]

2.2.2 Platinum based electro-catalyst

In many years of research and development of fuel cells platinum group metal has been the most used and promising as a catalyst, platinum (Pt) is commonly used as the catalyst because of its high electrocatalytic activity. Platinum has the highest catalytic activity for oxygen reduction more than any of the pure metals and when supported on a conductive carbon serves as state of the art electrocatalysts in DMFC air cathodes. However, due to kinetic limitations of the oxygen reduction reaction (ORR), a considerable loss in efficiency occurs in the cathode electrode, as the result of cathode overpotential [46]. Platinum based catalyst has shown to enhance the fuel cell performance if it is used in higher amount. Using high quantities of Pt raises concerns with the cost because Pt metal is expensive meaning the total fuel cell cost will be high and unaffordable, therefore it is impossible to take the fuel cell into the market while the cost is too high. Due to the above mentioned reason many scientists have conducted research with the aim of improving fuel cell performance and reducing the cost using small quantities of Pt in Pt based catalyst [47-48]. With the aim to decrease the Pt loading and improve the ORR kinetics several new classes of the Pt based ORR catalysts such as Pt-based binary and ternary alloys/ nanocomposites have been discovered as active ORR catalysts [49]. Platinum is also commonly used as the anode catalyst supported on carbon based material in low-temperature fuel cells. The activity for the methanol oxidation reaction (MOR) of Pt alone, however, it is too low for an industrial use, thus research efforts have been addressed to improve the MOR activity of platinum. A way to increase the catalytic activity is the addition of a second metal, in particular ruthenium, to Pt. According to the bifunctional mechanism, the second metal supplies oxygen to oxidise the Pt-adsorbed methanol oxidation intermediate species known as CO and form CO₂, while according to the electronic effect, the second metal modifies

the Pt electronic configuration, weakening the adsorption of methanol oxidation intermediate species on Pt [50].

2.2.3 Palladium (Pd) based catalyst for fuel cells

The high cost and less availability of platinum has led to the research looking for other metals that can be used as catalyst for fuel cell with cheaper cost. Not only that platinum has pose the challenge of higher cost but has been found to be poisoned by CO formed as a by-product when used in methanol fuel cells. Palladium has proven to a promising most abundant alternative to be used as catalyst in fuel cells. Unlike Pt-based catalyst which can be easily poisoned by intermediate product, Pd has shown to have tolerance against poisoning by intermediate products and being able to oxidise some alcohols like methanol, glycerol during the alcohol oxidation reaction in alkaline media [51-52]. The difficulties that are faced by platinum based catalyst are not encountered by palladium binary catalysts, because of the oxophilic nature of Pd which allows the oxidative desorption of intermediate products. Hence Pd has higher activity for ethanol oxidation reaction (EOR) as compared to Pt [53]. Pd based catalyst will be used as the anode for methanol oxidation in this study.

2.3 Support material for catalysts

The issue of low stability and stability and poor performance of fuel cells has led the researchers to look for a material that can be used to solve such problem. Catalyst support material has been found to be a promising solution, proving a better and improved fuel cell performance through an increased surface area. A good support material is the one that has high electric

conductivity, high surface area to improve catalytic dispersion, electrochemically stable in the electrolyte, corrosion resistant, and it must be porous enough to allow the easy flow of the reactants [54].

Traditionally, carbon black has been used as the support material of choice in DMFCs as it offers high electronic conductivity, high surface area and is cost effective. Recently, carbon-based nanomaterial with high graphitic structure, such as carbon nanotubes (CNTs), and carbon nanofibers (CNFs) are being extensively studied as new generation of catalyst support [54]. This is due to their distinctive characteristics as they offer more crystalline structure with high electrical conductivity, excellent corrosion resistance and high purities compared to conventional carbon black powders. CNTs are particularly of great interest due to their unique structural, electrical and mechanical properties. Carbon-based support, however, generally suffers from corrosion in different levels depending on the carbon material used, carbon blacks being the most affected by corrosion under fuel cell conditions. The instability of carbon based support material under fuel cell conditions, is a major concern and accordingly a drawback in the performance of electro-catalyst supported on these materials because the corrosion of the carbon support leads to Pt sintering and lowers the electro-chemical active surface area of the catalyst and ultimately results in the undesired degradation of the fuel cell system. Thus, a new class of support material is needed that will be extremely resistant to corrosion under fuel cell conditions [55].

2.3.1 Multi-walled carbon nanotubes (MWCNT)

Layers of graphite rolled into round and hollow frame and are frequently closed on both ends are known as carbon nanotubes. They can be made and/or orchestrated in laboratory and appear amazing mechanical and warm conductivity. Multi-walled carbon nanotubes (MWCNTs), have received a rising attention in recent years for their use as catalyst support materials, because of their appealing properties like high chemical stability and a large surface to volume ratio. Several papers have focused on the application of carbon nanotubes in fuel cell as catalyst supports [56].

It is evident from previous studies that for low temperature fuel cells like PEMFC and DMFC that have Pt catalyst supported on multi-walled carbon nanotubes shows better performance for electro-oxidation of methanol than that on carbon black [57]. Nano-structured carbon materials have been used due to their improved physical chemical properties. In this study MWCNT was chosen due to improved properties. Either than good catalytic activity, a good support material should possess good corrosion resistance; it has been proposed that carbon material with more graphite component can be more stable. Carbon nanotubes have been proposed as promising support material for fuel cell catalyst due to their unique characteristics, which include high electron conductivity, and high mass transport capability. Active metal particles may be dispersed on the external walls or be encapsulated in the interior of the nanotubes due to the size and morphology of the MWCNTs. The metal particles on the external walls and the reactant molecules make contact more easily compared to those encapsulated in the internal channels of the MWCNTs [58].

2.3.2 Polypyrrole as a catalyst support material

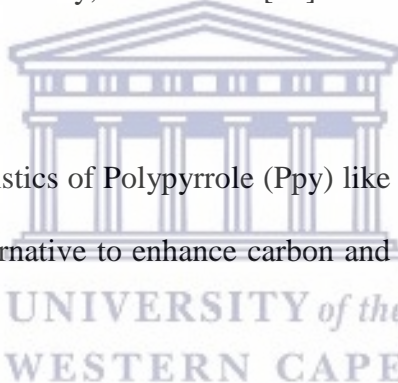
In previous years carbon materials like carbon black has been largely used as the catalyst support for low temperature fuel cells like DAFC's. However there are several drawbacks of

these support material, limiting the catalyst performance, which leads to a total fuel cell performance and stability being lowered. These drawbacks include their micro-pores which limits the surface accessibility lowering the surface area, easy corrosion at high potentials. Therefore an advanced or modified carbon material is required to enhance the fuel cell performance [59-60].

More research have been conducted to mitigate the problems related to carbon support materials. One of the solution was the introduction of metal oxides and conductive polymers to improve the surface of the support material. To overcome the drawbacks of pure carbon supports and achieve a breakthrough in catalytic performance, a wide range of modified carbon materials have been and are being explored as special, more exciting and promising support material for catalysts in PEMFCs. Their unique physicochemical structures have resulted in improved stability and catalytic activity via the chemical and physical modification of carbon supports. Some metal oxides have been tested and found to have a necessary characteristic to make advanced support materials. Metal oxides like tungsten oxide, molybdenum oxide, ruthenium oxide, tin oxide, cerium oxide and manganese oxide, and multi-component perovskite oxides are abundantly available, have high chemical and electrochemical stability, abundant hydroxyl groups on the surface, and strong interaction with metal nanoparticles, and thus are promising to reduce the present problems in PEFCs. For example Magnéli-phase titanium oxides, which shows no oxidation peaks between 0 and 2.0 V in 1 M sulfuric acid meaning that it is resistant to electrochemical corrosion[61-62].

Conductive Polymers such as Polypyrrole (PPy), polyaniline (PANI), poly 3,4-ethylenedioxythiophene), poly (methylene blue), poly (methoxyaniline) and poly (O-amino phenol) have been used as electrocatalysts for methanol oxidation, due to their excellent

electrical and electrochemical properties [63]. For example Eris et al. fabricated the rGO/PANI/Pt composite and applied it as catalyst for methanol oxidation. It was reported that PANI bridges the rGO and Pt through Pt-N bond and improves the stability of rGO/PANI/Pt [64]. In some cases metal oxides have been used together with polymers to modify the support material. For instance Wei, L et al reported the use of manganese oxide (MnO_x) and poly (3,4-ethylenedioxythiophene) (PEDOT) nanocomposite on multi-walled carbon nanotubes (MnO_x -PEDOT-MWCNTs) as a support for Pt. The catalyst showed a significant improved electro-oxidation activity and stability [65]. Lastly Polypyrrole have been also used in cobalt-polymer-MWCNT composite which displayed improved power densities for hydrogen, methanol and ethanol fuel cells as reported by Reddy, A.L.M et al [66].



Due to the distinctive characteristics of Polypyrrole (Ppy) like its high conductivity, has been suggested as the promising alternative to enhance carbon and nanostructured carbon support material.

Polypyrrole is the conjugated polymer formed by the polymerization of pyrrole, when oxidized it turn to be a conductive polymer as shown in figure 2.2 below. This polymer can be synthesized in two different ways namely chemically and electrochemically methods. Chemical method can be achieved by mixing the solution of pyrrole with an appropriate oxidant such as iron (III) chloride ($FeCl_3$) [59&67]. The use of a molecular solvent/electrolyte like lithium perchlorate/acetonitrile to carry out the synthesis of conductive polymers like Polypyrrole is known as the customary electrochemical synthesis, but recently new ways has been reported. Pringle, J.M et al, reported the use of ionic liquids like 1-ethyl-3-methylimidazolium bis(trifluoromethanesulfonyl) amide as electrolyte and growth medium [68].

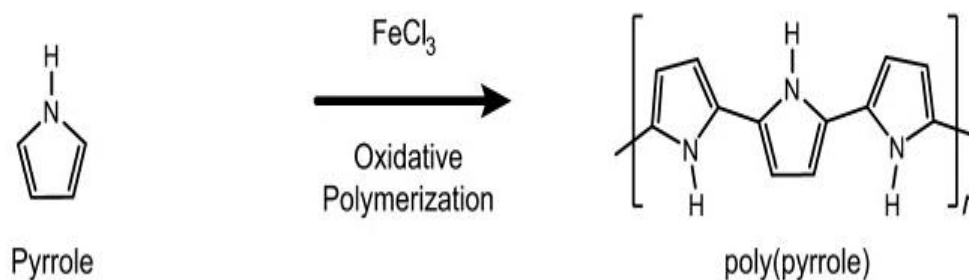


Figure 2.2 Schematic diagram of Pyrrole polymerization to form Polypyrrole [69]

Amongst the known conductive polymers PPy stands out because of its unique conductivity and the ability to resist corrosion under high positive potentials. Hence it will be used on this project as an ionomer on the catalysts support material.



2.4 Fuel cells catalyst preparation methods

The catalyst activity is mainly affected by the preparation method employed to form the catalyst. There are various methods used to prepare catalysts such as polyol method, impregnation method and sulphite complex route to name a few.

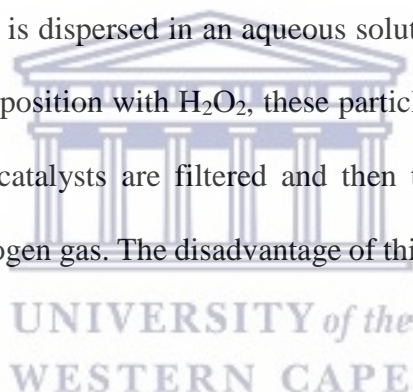
2.4.1 Impregnation method

Impregnation method is said to be the most common and easiest methods to prepare the fuel cell catalysts. This method it simple involve the infusion of a metal salt solution onto a support material at specific time intervals. The most common used salts are chloride salts RuCl_3 and H_2PtCl_6 , because of their simple availability. During this method the metallic catalyst precursor

is impregnated first into a support before reducing it into metallic nanoparticles. The reduction process involves two steps namely chemical and electrochemical reduction of which both of the steps can be conducted either in gas or liquid phase. The slurry is put through heat to eliminate the solvent and thereafter the residue is successively reduced at increased temperature to decompose the salt and obtain the required catalyst [70].

2.4.2 Sulphite complex route

In this method the Pt sulphite complexes are synthesized in an aqueous solution. The starting precursor salt which is H_2PtCl_6 is dispersed in an aqueous solution containing NaHSO_3 . This will undergo oxidative composition with H_2O_2 , these particles are then adsorbed onto the carbon support material. The catalysts are filtered and then treated with heat and further reduced under the flow of hydrogen gas. The disadvantage of this method presence of chlorine contaminants [71-72].



2.4.3 Polyol method

The polyol method falls under the catalysts synthesis methods known as colloidal methods. It uses the bottom-up approach. This technique is typically used to synthesis bimetallic metallic nanoparticles in a solution by means of reducing their ionic salts. During polyol method an inorganic metallic compound powder is dispersed in a liquid polyol (ethylene glycol). The suspension is mixed by stirring followed by heating at a given temperature. It takes few hours to complete the reduction of the compound and thereafter fine powder metal is recovered. The method is advantageous because it is less energy demanding, it can be conducted at a room

temperature because it does not require any external heat. At room temperature this reaction employs sodium borohydride as a reducing agent [73-74].



References

1. Badwal, S.P.S. and K. Foger, *Solid oxide electrolyte fuel cell review*. Ceramics International, 1996. **22**(3): p. 257-265.
2. Carrette, L., K.A. Friedrich, and U. Stimming, *Fuel Cells: Principles, Types, Fuels, and Applications*. ChemPhysChem, 2000. **1**(4): p. 162-193.
3. Steele, B.C.H. and A. Heinzl, Materials for fuel-cell technologies. Nature, 2001. 414(6861): p. 345-52.
4. Larminie, J. and A. Dicks, *Fuel Cell Systems Explained*. Second Edition ed. 2003: John Wiley and Sons. 15.
5. Gregor, H., *Fuel cell technology handbook*. 2003, CRC Press, New York.
6. Prater, K.B., 1994. Polymer electrolyte fuel cells: a review of recent developments. *Journal of Power Sources*, 51(1-2), pp.129-144.
7. Borup, R., Meyers, J., Pivovar, B., Kim, Y.S., Mukundan, R., Garland, N., Myers, D., Wilson, M., Garzon, F., Wood, D. and Zelenay, P., 2007. Scientific aspects of polymer electrolyte fuel cell stability and degradation. *Chemical reviews*, 107(10), pp.3904-3951.
8. Carrette, L., Friedrich, K.A. and Stimming, U., 2001. Fuel cells-fundamentals and applications. *Fuel cells*, 1.
9. Cacciola, G., V. Antonucci, and S. Freni, Technology up date and new strategies on fuel cells. *Journal of Power Sources*, 2001. 100(1-2): p. 67-79.
10. Meier-Haack, J., et al., Membranes from sulfonated block copolymers for use in fuel cells. *Separation and Purification Technology*, 2005. 41(3): p. 207-220.
11. Zhang, J., Zhang, H., Wu, J. and Zhang, J., 2013. Chapter 1-PEM fuel cell fundamentals. *PEM Fuel Cell Testing and Diagnosis*, pp.1-42.

12. Perry, M.L. and Fuller, T.F., 2002. A historical perspective of fuel cell technology in the 20th century. *Journal of the electrochemical society*, 149(7), p.S59.
13. Kalhammer, F.R., 2000. Polymer electrolytes and the electric vehicle. *Solid State Ionics*, 135(1-4), pp.315-323.
14. Haile, S.M., 2003. Fuel cell materials and components. *Acta materialia*, 51(19), pp.5981-6000.
15. Papageorgopoulos, D.C., Keijzer, M. and De Bruijn, F.A., 2002. The inclusion of Mo, Nb and Ta in Pt and PtRu carbon supported electrocatalysts in the quest for improved CO tolerant PEMFC anodes. *Electrochimica Acta*, 48(2), pp.197-204.
16. Trimm, D.L. and Önsan, Z.I., 2001. Onboard fuel conversion for hydrogen-fuel-cell-driven vehicles. *Catalysis Reviews*, 43(1-2), pp.31-84.
17. Friedlmeier, G., Friedrich, J. and Panik, F., 2002. Test experiences with the DaimlerChrysler: Fuel cell electric vehicle NECAR 4. *Hemijaska industrija*, 56(6), pp.287-290.
18. Carrette, L., Friedrich, K.A. and Stimming, U., 2000. Fuel cells: principles, types, fuels, and applications. *ChemPhysChem*, 1(4), pp.162-193.
19. McNicol, B.D., Rand, D.A.J. and Williams, K.R., 2001. Fuel cells for road transportation purposes—yes or no?. *Journal of Power Sources*, 100(1-2), pp.47-59.
20. Maynard, H.L. and Meyers, J.P., 2002. Miniature fuel cells for portable power: Design considerations and challenges. *Journal of Vacuum Science & Technology B: Microelectronics and Nanometer Structures Processing, Measurement, and Phenomena*, 20(4), pp.1287-1297.
21. Park, G.G., Yang, T.H., Yoon, Y.G., Lee, W.Y. and Kim, C.S., 2003. Pore size effect of the DMFC catalyst supported on porous materials. *International Journal of Hydrogen Energy*, 28(6), pp.645-650.

22. Osaka, T. and Datta, M.EDS., 2000. *Energy storage systems in electronics*. CRC Press.
23. Salgado, J.R.C., Antolini, E. and Gonzalez, E.R., 2005. Carbon supported Pt–Co alloys as methanol-resistant oxygen-reduction electrocatalysts for direct methanol fuel cells. *Applied Catalysis B: Environmental*, 57(4), pp.283-290.
24. Antolini, E., 2011. The problem of Ru dissolution from Pt–Ru catalysts during fuel cell operation: analysis and solutions. *Journal of Solid State Electrochemistry*, 15(3), pp.455-472.
25. Lee, J.H., Lalk, T.R. and Appleby, A.J., 1998. Modeling electrochemical performance in large scale proton exchange membrane fuel cell stacks. *Journal of power sources*, 70(2), pp.258-268.
26. Wang, L., Husar, A., Zhou, T. and Liu, H., 2003. A parametric study of PEM fuel cell performances. *International journal of hydrogen energy*, 28(11), pp.1263-1272.
27. Spiegel, C., 2016. *Direct Methanol Fuel Cell Improvements*. [online] Fuelcellstore.com. Available at: <<https://www.fuelcellstore.com/blog-section/direct-methanol-fuel-cell-improvements>> [Accessed 5 June 2021].
28. Rao, C.R. and Trivedi, D.C., 2005. Chemical and electrochemical depositions of platinum group metals and their applications. *Coordination Chemistry Reviews*, 249(5-6), pp.613-631.
29. Chang, H., Kim, H., Choi, Y.S. and Lee, W., 2009. Critical Issues in the Commercialization of DMFC and Role of Membranes. In *Polymer Membranes for Fuel Cells* (pp. 307-339). Springer, Boston, MA.
30. Thompsett, D., 2003. Catalysts for the proton exchange membrane fuel cell. *Fuel cell technology handbook*.
31. Antolini, E., 2009. Carbon supports for low-temperature fuel cell catalysts. *Applied Catalysis B: Environmental*, 88(1-2), pp.1-24.

32. Janardhanan, V.M. and Deutschmann, O., 2006. CFD analysis of a solid oxide fuel cell with internal reforming: Coupled interactions of transport, heterogeneous catalysis and electrochemical processes. *Journal of Power Sources*, 162(2), pp.1192-1202.
33. Liu, H., Song, C., Zhang, L., Zhang, J., Wang, H. and Wilkinson, D.P., 2006. A review of anode catalysis in the direct methanol fuel cell. *Journal of Power Sources*, 155(2), pp.95-110.
34. Lamy, C., Léger, J.M. and Srinivasan, S., 2002. Direct methanol fuel cells: From a twentieth century electrochemists dream to a twenty-first century emerging technology. *In Modern aspects of electrochemistry* (pp. 53-118). Springer US.
35. Liu, R., Zhou, H., Liu, J., Yao, Y., Huang, Z., Fu, C. and Kuang, Y., 2013. Preparation of Pd/MnO₂-reduced graphene oxide nanocomposite for methanol electro-oxidation in alkaline media. *Electrochemistry communications*, 26, pp.63-66.
36. Zhao, Y., Zhan, L., Tian, J., Nie, S. and Ning, Z., 2011. Enhanced electrocatalytic oxidation of methanol on Pd/polypyrrole-graphene in alkaline medium. *Electrochimica Acta*, 56(5), pp.1967-1972.
37. Jiang, Q., Jiang, L., Hou, H., Qi, J., Wang, S. and Sun, G., 2010. Promoting effect of Ni in PtNi bimetallic electrocatalysts for the methanol oxidation reaction in alkaline media: experimental and density functional theory studies. *The Journal of Physical Chemistry C*, 114(46), pp.19714-19722.
38. Lu, Y., Jiang, Y., Wu, H. and Chen, W., 2013. Nano-PtPd cubes on graphene exhibit enhanced activity and durability in methanol electrooxidation after CO stripping-cleaning. *The Journal of Physical Chemistry C*, 117(6), pp.2926-2938.
39. Zhao, Y., Zhan, L., Tian, J., Nie, S. and Ning, Z., 2010. MnO₂ modified multi-walled carbon nanotubes supported Pd nanoparticles for methanol electro-oxidation in alkaline media. *International Journal of Hydrogen Energy*, 35(19), pp.10522-10526.

40. Huang, H. and Wang, X., 2012. Pd nanoparticles supported on low-defect graphene sheets: for use as high-performance electrocatalysts for formic acid and methanol oxidation. *Journal of Materials Chemistry*, 22(42), pp.22533-22541.
41. Prodromidis, M.I., Zahran, E.M., Tzakos, A.G. and Bachas, L.G., 2015. Preorganized composite material of polyaniline–palladium nanoparticles with high electrocatalytic activity to methanol and ethanol oxidation. *international journal of hydrogen energy*, 40(21), pp.6745-6753.
42. Rodríguez-Pérez, L., Herranz, M.Á. and Martín, N., 2013. The chemistry of pristine graphene. *Chemical Communications*, 49(36), pp.3721-3735.
43. Ghosh, S., Bhandary, N., Basu, S. and Basu, R.N., 2017. Synergistic effects of polypyrrole nanofibers and Pd nanoparticles for improved electrocatalytic performance of Pd/PPy nanocomposites for ethanol oxidation. *Electrocatalysis*, 8(4), pp.329-339.
44. Han, H., Noh, Y., Kim, Y., Yadav, V.S.K., Park, S., Yoon, W., Lee, S. and Kim, W.B., 2017. Electrocatalytic Oxidations of Formic Acid and Ethanol over Pd Catalysts Supported on a Doped Polypyrrole-Carbon Composite. *ChemistrySelect*, 2(22), pp.6260-6268.
45. Wang, Y., Clancey, J., Lu, G., Liu, J., Liu, L., Chaudhuri, J., George, S., Xie, M., Wei, S. and Guo, Z., 2015. Enhanced methanol oxidation with annealed atomic layer deposited platinum nanoparticles on carbon nanotubes. *Journal of The Electrochemical Society*, 163(2), p.F1.
46. Antolini, E., Lopes, T.R.V.P. and Gonzalez, E.R., 2008. An overview of platinum-based catalysts as methanol-resistant oxygen reduction materials for direct methanol fuel cells. *Journal of Alloys and Compounds*, 461(1-2), pp.253-262.

47. Samad, S., Loh, K.S., Wong, W.Y., Lee, T.K., Sunarso, J., Chong, S.T. and Daud, W.R.W., 2018. Carbon and non-carbon support materials for platinum-based catalysts in fuel cells. *international journal of hydrogen energy*, 43(16), pp.7823-7854.
48. Pollet, B.G., Staffell, I. and Shang, J.L., 2012. Current status of hybrid, battery and fuel cell electric vehicles: From electrochemistry to market prospects. *Electrochimica Acta*, 84, pp.235-249.
49. Singh, R.N., Awasthi, R. and Sharma, C.S., 2014. An overview of recent development of platinum-based cathode materials for direct methanol fuel cells. *Int J Electrochem Sci*, 9(5607), p.e39.
50. Antolini, E., 2018. Photo-assisted methanol oxidation on Pt-TiO₂ catalysts for direct methanol fuel cells: A short review. *Applied Catalysis B: Environmental*, 237, pp.491-503.
51. Bambagioni, V., Bianchini, C., Marchionni, A., Filippi, J., Vizza, F., Teddy, J., Serp, P. and Zhiani, M., 2009. Pd and Pt-Ru anode electrocatalysts supported on multi-walled carbon nanotubes and their use in passive and active direct alcohol fuel cells with an anion-exchange membrane (alcohol= methanol, ethanol, glycerol). *Journal of Power Sources*, 190(2), pp.241-251.
52. Zhiani, M., Majidi, S. and Rostami, H., 2014. 'Comparative study of aliphatic alcohols electrooxidation on zero-valent palladium complex for direct alcohol fuel cells', *International Journal of Hydrogen Energy*, 40(1), pp. 568–576.
53. Cheng, X., Shi, Z., Glass, N., Zhang, L., Zhang, J., Song, D., Liu, Z.S., Wang, H. and Shen, J., 2007. A review of PEM hydrogen fuel cell contamination: Impacts, mechanisms, and mitigation. *Journal of Power Sources*, 165(2), pp.739-756.

54. Bianchini, C. and Shen, P.K., 2009. Palladium-based electrocatalysts for alcohol oxidation in half cells and in direct alcohol fuel cells. *Chemical Reviews*, 109(9), pp.4183-4206.
55. Vishnyakov, V.M., 2006. Proton exchange membrane fuel cells. *Vacuum*, 80(10), pp.1053-1065.
56. Liu, Z., Lin, X., Lee, J.Y., Zhang, W., Han, M. and Gan, L.M., 2002. Preparation and characterization of platinum-based electrocatalysts on multiwalled carbon nanotubes for proton exchange membrane fuel cells. *Langmuir*, 18(10), pp.4054-4060.
57. Shao, Y., Liu, J., Wang, Y. and Lin, Y., 2009. Novel catalyst support materials for PEM fuel cells: current status and future prospects. *Journal of Materials Chemistry*, 19(1), pp.46-59.
58. Rajalakshmi, N., Ryu, H., Shaijumon, M.M. and Ramaprabhu, S., 2005. Performance of polymer electrolyte membrane fuel cells with carbon nanotubes as oxygen reduction catalyst support material. *Journal of Power Sources*, 140(2), pp.250-257.
59. Yuan, X., Ding, X.L., Wang, C.Y. and Ma, Z.F., 2013. Use of polypyrrole in catalysts for low temperature fuel cells. *Energy & Environmental Science*, 6(4), pp.1105-1124.
60. Huang, S.Y., Ganesan, P. and Popov, B.N., 2009. Development of conducting polypyrrole as corrosion-resistant catalyst support for polymer electrolyte membrane fuel cell (PEMFC) application. *Applied Catalysis B: Environmental*, 93(1-2), pp.75-81.
61. Wang, Y.J., Fang, B., Li, H., Bi, X.T. and Wang, H., 2016. Progress in modified carbon support materials for Pt and Pt-alloy cathode catalysts in polymer electrolyte membrane fuel cells. *Progress in Materials Science*, 82, pp.445-498.
62. Zhang, Z., Liu, J., Gu, J., Su, L. and Cheng, L., 2014. An overview of metal oxide materials as electrocatalysts and supports for polymer electrolyte fuel cells. *Energy & Environmental Science*, 7(8), pp.2535-2558.

63. Arukula, R., Vinothkannan, M., Kim, A.R. and Yoo, D.J., 2019. Cumulative effect of bimetallic alloy, conductive polymer and graphene toward electrooxidation of methanol: An efficient anode catalyst for direct methanol fuel cells. *Journal of Alloys and Compounds*, 771, pp.477-488.
64. Eris, S., Daşdelen, Z., Yıldız, Y. and Sen, F., 2018. Nanostructured Polyaniline-rGO decorated platinum catalyst with enhanced activity and stability for Methanol oxidation. *International Journal of Hydrogen Energy*, 43(3), pp.1337-1343.
65. Wei, L., Fan, Y.J., Ma, J.H., Tao, L.H., Wang, R.X., Zhong, J.P. and Wang, H., 2013. Highly dispersed Pt nanoparticles supported on manganese oxide–poly (3, 4-ethylenedioxythiophene)–carbon nanotubes composite for enhanced methanol electrooxidation. *Journal of power sources*, 238, pp.157-164.
66. Reddy, A.L.M., Rajalakshmi, N. and Ramaprabhu, S., 2008. Cobalt-polypyrrole-multiwalled carbon nanotube catalysts for hydrogen and alcohol fuel cells. *Carbon*, 46(1), pp.2-11.
67. Duchet, J., Legras, R. and Demoustier-Champagne, S., 1998. Chemical synthesis of polypyrrole: structure–properties relationship. *Synthetic metals*, 98(2), pp.113-122.
68. Pringle, J.M., Efthimiadis, J., Howlett, P.C., Efthimiadis, J., MacFarlane, D.R., Chaplin, A.B., Hall, S.B., Officer, D.L., Wallace, G.G. and Forsyth, M., 2004. Electrochemical synthesis of polypyrrole in ionic liquids. *Polymer*, 45(5), pp.1447-1453.
69. Watson, S.M., Hedley, J.H., Galindo, M.A., Al-Said, S.A., Wright, N.G., Connolly, B.A., Horrocks, B.R. and Houlton, A., 2012. Synthesis, Characterisation and Electrical Properties of Supramolecular DNA-Templated Polymer Nanowires of 2, 5-(Bis-2-thienyl)-pyrrole. *Chemistry–A European Journal*, 18(38), pp.12008-12019.
70. S.K. Young's, *Material Matters*. 1, (2006): p. 29-47.

71. Watanabe, M., Uchida, M. and Motoo, S., 1987. Preparation of highly dispersed Pt+Ru alloy clusters and the activity for the electrooxidation of methanol. *Journal of electroanalytical chemistry and interfacial electrochemistry*, 229(1-2), pp.395-406.
72. Siracusano, S., Stassi, A., Modica, E., Baglio, V. and Aricò, A.S., 2013. Preparation and characterisation of Ti oxide based catalyst supports for low temperature fuel cells. *International journal of hydrogen energy*, 38(26), pp.11600-11608.
73. Fievet, F., Lagier, J.P. and Figlarz, M., 1989. Preparing monodisperse metal powders in micrometer and submicrometer sizes by the polyol process. *Mrs Bulletin*, 14(12), pp.29-34.
74. Song, K.C., Lee, S.M., Park, T.S. and Lee, B.S., 2009. Preparation of colloidal silver nanoparticles by chemical reduction method. *Korean Journal of Chemical Engineering*, 26(1), pp.153-155.



Chapter 3

Experimental

3. Introduction

The chapter presents the details of the experimental and characterization methods employed in the synthesis and analysis of Pd/MWCNT, Pd/rGO, Pd/PPy-rGO, Pd/PPy-MWCNT, Pd-Co/MWCNT, Pd-Co/rGO, PdCo/PPy, PdCo/PPy-rGO and PdCo/PPy-MWCNT.

3.1 Chemicals

All chemicals used are listed in Table 3.1. Ultrapure water from Millipore was used for all preparations.

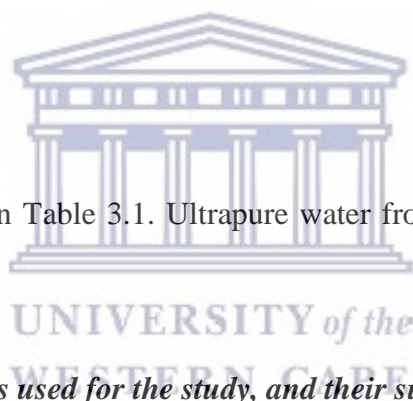


Table 3.1: The list of chemicals used for the study, and their suppliers.

Chemicals	Company
PdCl ₃	SA Precious Metals (PTY) (LTD)
Co ₃ O ₄	Alfa easar
EG	Kimix
KOH	Kimix
HNO ₃	Kimix
NAOH	Sigma alrich
H ₂ SO ₄	Kimix
Hydrazine	Sigma aldrich
Ultra-pure water	Milli-Q system

MWCNT's	Carbon Nano-material Technology, South Korea
Graphite	Sigma aldrich
Nafion	Alfa Aesar
Isopropanol	Alfa Aesar
Pyrrole	Sigma Aldrich
FeCl ₃	Sigma Aldrich
Methanol	Alfa Aesar

All the reagents were of analytical grade and were used as received from the suppliers without further purification.



3.2 Methodology

This section goes over the specifics of how the catalysts were prepared. First, before using the MWCNT, they were treated with acid to remove impurities and to introduce functional groups on the surface of the MWCNTs, which are known to be essential in improving catalyst loading and dispersing on the surface of the support [24].

3.2.1 Pre-treatment of carbon nanotubes

The treatment was performed by using 5 g of Multi-walled carbon nanotubes treated in an aqueous solution composed of 90 mL concentrated sulphuric acid and 30 mL of concentrated nitric acid, the mixture was refluxed for 6 hours at 160 °C.

The carbon nanotube sediments were separated from the reaction mixture, washed with ultrapure water. The synthesis solution pH was adjusted to ~7 by using 2M NaOH solution.

The purified, acid-functionalized MWCNT slurry was then oven-dried at 80°C overnight to obtain the solid black product.

3.2.2 Preparation of Graphene oxide

Graphene oxide was synthesized by means of modified Hummers method. 1 g of natural flake graphite powder, 0.5 g of sodium nitrate and 50 mL of sulphuric acid were mixed at a 0 °C ice-water bath. 3 g of potassium permanganate was slowly added into the solution every half an hour, three times in total. After that 46 mL of hot de-ionized water was added into the suspension drop-wise. The temperature was kept at 90 °C and maintained for 1 hour. Subsequently to that 20 mL of H₂O₂ was added into the suspension drop-wise. The solution was taken to an ultrasonicator for 30 minutes with the power of 200 W. The suspension was centrifuged and a mud-like material was obtained. The material was washed with de-ionized water and ethanol for several times, respectively. Lastly, the material was dried in oven at 40 °C and maintained for several days to get the completely dry GO material.

3.2.3 Preparation of Reduced-Graphene Oxide (rGO)

1 g of graphene oxide (GO) was dispersed in 1L water by means of 30 minutes' ultrasonic treatment. As a result a homogeneous brown GO aqueous suspension was obtained.

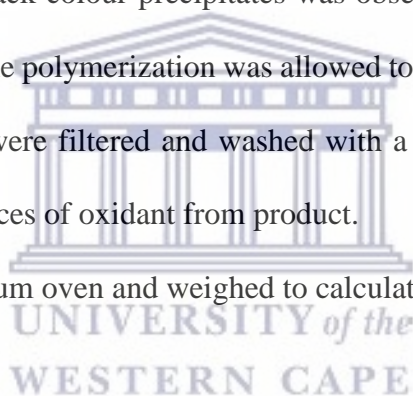
The pH of the suspension was adjusted to ~10 by dropping NH₃H₂O. An amount of 1.4 mL hydrazine hydrate was added into suspension and heated under reflux at 80°C for a period of 24 hours.

A kind of black flocculent substance was gradually precipitated out of the solution. The product was obtained by filtered with the qualitative filter paper. Finally, the resulting black product was washed with methanol and water and dried at 80°C for 24 hours.

3.2.4 Preparation of Polypyrrole (Ppy)

25mL of de-ionized water was added into round bottom flask. Pyrrole monomer (8.5mL) from sigma Aldrich was added into it and mixing was carried out for ten minutes using magnetic stirrer. Further FeCl₃ solution (2.5M) was added very slowly as an oxidant to the monomer solution. The appearance of black colour precipitates was observed in the flask immediately after the addition of oxidant. The polymerization was allowed to continue for 24 hours at room temperature. The precipitates were filtered and washed with a mixture of water and ethanol several times to remove any traces of oxidant from product.

The filtrate was dried in a vacuum oven and weighed to calculate the yield of final product.



3.2.5 Preparation of the Catalysts

All catalysts prepared in the study were prepared using the modified polyol method.

3.2.5.1 Preparation of mono catalysts Pd/MWCNT, Pd/rGO, Pd/PPy

The catalysts were prepared using modified polyol method as follows:

0.4g of MWCNT, rGO and PPy were each dispersed in 15 mL of ethylene glycol (EG) under stirring followed by sonication in an ultrasonic bath for 15 minutes. To the dispersion, a

solution of a catalyst made of 0.1 g PdCl₃ and 15 mL EG was added followed by stirring for 15 minutes. The pH of the solution was adjusted with 2M of NaOH/EG solution to ~12 and the mixture was sonicated for 15 minutes, a homogeneous adsorption of the metal precursor onto the surface of the support occurred. For the reduction of the metal ions, the solution was transferred to a round bottom flask which was put in an oil bath and heated for 6 hours at 160°C under stirring and reflux. After completing the reduction, the reaction mixture was left under stirring overnight. Finally the product Pd/MWCNT, Pd/rGO and Pd/PPy was filtered and washed with ultra-pure water. The catalyst was dried in an oven at 80°C overnight.

The binary catalysts were prepared as follows:

The PdCo/MWCNT, PdCo/rGO and PdCo/PPy were prepared using the similar procedure to the Pd/MWCNT, but the metals Pd and Co were added in 1:1 mol ratio.

Preparation of mono-catalysts with hybrid supports (Pd/PPy-MWCNT and Pd/PPy-rGO)

For supports hybrids (Pd/MWCNT-Ppy and Pd/rGO-Ppy) the supports were mixed in a 1:1 mass ratio under magnetic stirring for 24 hours before the catalyst was added the mixture was put under sonication in an ultrasonic bath for 15 minutes

To the dispersion, a solution of a catalyst made of 0.1 g PdCl₃ and 0.13 g Co₃O₄, 15 mL EG was added followed by stirring for 15 minutes. The pH of the solution was adjusted with 2M of NaOH/EG solution to ~12 and the mixture was sonicated for 15 minutes, a homogeneous adsorption of the metal precursor onto the surface of the support occurred.

For the reduction of the metal ions, the solution was transferred to a round bottom flask which was put in an oil bath and heated for 6 hours at 160°C under stirring and reflux. After completing the reduction, the reaction mixture was left under stirring overnight.

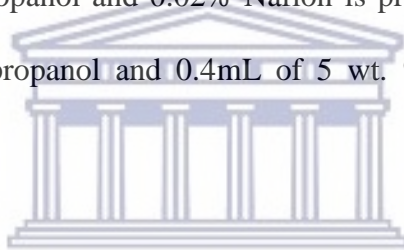
Finally the product Pd/PPy-MWCNT and Pd/PPy-rGO was filtered and washed with ultra-pure water. The catalyst was dried in an oven at 80°C overnight.

Preparation of binary catalysts with hybrid supports (PdCo/PPy-MWCNT and PdCo/PPy-rGO)

The PdCo/PPy-MWCNT and PdCo/PPy-rGO were prepared using the similar procedure to the mono catalyst hybrid support above, but the metals Pd and Co were added in 1:1 mol ratio.

3.2.6 Ink preparation

A stock solution of 20% isopropanol and 0.02% Nafion is prepared by mixing 79.6 mL of ultrapure water, 20mL of isopropanol and 0.4mL of 5 wt. % Nafion solution in 100mL volumetric flask.



10mg of the catalyst is measured into a 10mL vial and 5mL of stock solution is added; mixed through and sonicated for 1 hour. A 10 μ l volume or 0.01 mg of the catalyst ink was then transferred via a syringe onto a freshly polished (mirror finish) Glassy Carbon (GC) electrode with a diameter of 3 mm (Single), Size: 25 x 25 mm.

3.2.7 Cleaning of the glassy carbon rotating disk electrode (GCRDE) tip

The GCRDE was cleaned before and after every use, by polishing the electrode for 5 minutes on Microcloth TM (Buehler) using 0.3 and 0.05 micron alumina slurries in sequence. The polished electrodes were rinsed well with UHP water. The electrodes were then dried at room temperature before use.

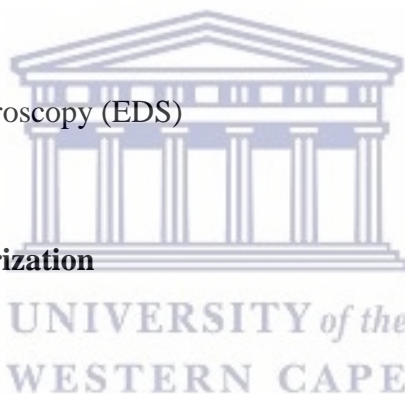
3.3 CHARACTERIZATION TECHNIQUES

For structural identification of the catalyst the following instruments were used

- High-resolution transmission electron microscopy (HRTEM)
- X-ray diffraction microscopy (XRD)
- Fourier Transmission Infrared (FTIR) spectroscopy

For elemental analysis

- Energy dispersive spectroscopy (EDS)



For electrochemical characterization

- Cyclic voltammetry (CV)
- Linear sweep voltammetry (LSV)
- Electrochemical Impedance Spectroscopy (EIS)
- Chronoamperometry (CA)

3.3.1 PHYSICAL CHARACTERIZATION

3.3.1.1 HIGH RESOLUTION TRANSMISSION ELECTRON MICROSCOPY (HRTEM)

High Resolution Transmission electron microscopy is a microscopy technique where a beam of electrons produces a micrograph when transmitted through a specimen. HRTEM has become a powerful and is considered to be an indispensable tool for studying the properties of nanostructured materials such as nanoparticles, and sp^2 bonded carbon such as carbon nanotubes and graphite. Due to the electrons having both wave and particle nature and the de Broglie wavelength of electrons are significantly smaller than that of light and so they higher resolution capability. This enables the finer detail examination, to even as small as a single column of atoms [1-2].

Working principle of HRTEM

The HRTEM works by utilizing a high voltage electron beam to create an image. The electron beam is produced by an electron gun, normally fitted with a tungsten filament cathode as an electron source. The electron beam is accelerated by an anode typically at plus 100 KeV (40-400 KeV) with respect to the cathode, and the electron beam is focused by electro-static and electro-magnetic lenses. The focused beam is then transmitted through the specimen that is in part transparent to the electrons and in part scatters them out of the beam. When the electron beam emerges from the specimen it contains information about the structure of the specimen that is magnified by the objective lenses of the microscope. The image is viewed by projecting the magnified electron image onto a fluorescent viewing screen coated with a phosphor or scintillator material such as zinc sulphide. Differently, the image can be photographically recorded by exposing a photographic film or plate directly to the electron beam, or use a high resolution sensor that may be coupled by means of a lens optical or fibre optic guide to the

sensor of a charge-coupled-device (CCD) camera. The image detected by the CCD is then displayed on either a monitor or computer [1-3].

HRTEM was utilized in this study to examine the metal nanoparticle size, nanoparticle size distribution, homogeneity of dispersion, and agglomeration of the nanoparticles in supported nanophase electrocatalysts [4].

Sample preparation

HRSEM samples were prepared by placing double-sided conductive carbon tape on an aluminium specimen stub. A very small amount of the sample was deposited on the specimen stub and flattened with a spatula, then gently tapped to remove the excess and loose sample. The nanoparticles supported on rGO, MWCNTs, PPy and hybrid support catalysts did not require any coating, as they were conductive enough to be imaged without charging. The samples were then introduced into the vacuum chamber of the microscope for analysis. In this study HRSEM Auriga was used with the experimental parameters listed below as:

Working distance: 10 nm

Accelerating Voltage: 5 KeV

Tilt Angle: 0°

3.3.1.2 X-RAY DIFFRACTION (XRD)

The discovery of X-rays enabled scientists to probe crystalline structure at the atomic level. X-ray diffraction has been heavily used in science, for the fingerprint characterization of crystalline materials and determination of their structure. Each crystalline solid has its unique characteristic X-ray powder pattern which may be used as an information for its identification

[5]. XRD in this study was used for the direct examination of crystalline structure, phase identification, average particle size, and lattice parameter.

Working principle of XRD

In a typical XRD analysis, X-rays are generated in a cathode ray tube by heating the filament to produce electrons. The produced electrons are then accelerated toward the target material by applying voltage and bombarding the target material with electrons [6-7]. When the electrons have enough energy to dislodge the inner shell electrons of the target material, characteristic X-ray spectra are produced.

The structural properties of the electro-catalysts were investigated using XRD. From the obtained results the average crystallite size, (d , Å) was calculated from line broadening analysis using the Scherrer formula. The Scherrer equation was used as shown in Equation to estimate the crystallite size from the XRD data[8].

$$d = \frac{0.9\lambda}{\beta \cos \theta} \quad (3.1)$$

Where d = crystallite size, 0.9 = shape factor, λ = x-ray wavelength, β = peak width at half peak height and θ = angle of reflection.

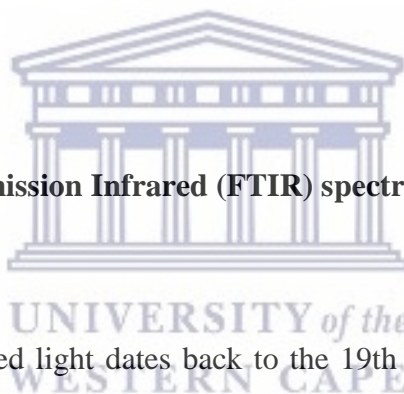
Sample preparation

In the XRD analysis, dry nanophase electrocatalyst samples were mounted in plastic sample holders and the surface was flattened to allow maximum X-ray exposure. Experimental parameters for XRD analysis are given as follows: X-ray Diffractometer: Bruker AXS D8 Advance from Ithemba labs.

Table 3.1 XRD sample preparation

Parameter	settings
Tube	Copper
Detector	Sodium Iodide
Monochromator	Graphite
Electron intensity	40 kV
X-ray Source	CuK α ($\lambda= 1.5418\text{\AA}$)
Current	40mA
Scan range	$10^\circ < 2\theta < 100^\circ$

3.3.1.3 Fourier Transmission Infrared (FTIR) spectroscopy



The discovery of infrared light dates back to the 19th century. Since then, scientists have established multiple methods for using infrared light. Infrared absorption spectroscopy is a method used by scientists to determine the structure of the molecule, in which the functional groups of the molecule absorb infrared radiation. Infrared spectrum is a molecular vibration spectrum. When exposed to infrared radiation, sample molecules selectively absorb radiation of unique wavelengths, causing changes in the dipole moment of the sample molecules. Therefore, the vibrational energy levels of sample molecules changed from the ground state to the excited state. The frequency of the absorption peak is determined by the vibration energy gap. The diversity of absorption peaks is related to the diversity of degrees of freedom of molecular vibration. The intensity of the absorption peak is related to the change of the dipole moment and

the possibility of the transition of the energy levels. Therefore, by studying infrared spectroscopy, you can easily obtain a great deal of information about the molecular structure of a substance. Most molecules are infrared active except for several mononuclear diatomic molecules (such as O₂, N₂ and Cl₂) because of the zero dipole change within the vibration and rotation of these molecules. What makes the Infrared Absorption Spectrometer even more useful is that it can successfully study all gas, liquid and solid samples [9-10]. The commonplace used region for infrared absorption spectroscopy is 4000 ~ 400 cm⁻¹ because the absorption radiation of maximum natural compounds and inorganic ions is within this region [11].

Working principle of FTIR

The IR beams from the light source passes through an interferometer, which consists of a beam splitter, a fixed mirror and a moving mirror. The interferometer is a well-designed optical device that splits the spectral components of the beam in time. As the moving mirror makes reciprocating movements, the optical path difference to the fixed mirror changes, in such a way that the phase difference changes with time. The light beams are recombined in the interferometer to produce interference light. The intensity of the interference light is recorded in an interferogram, with the optical path difference recorded along the horizontal axis. The corresponding absorbance spectrum is received from a Fourier transform of the interferogram [12]. Figure 3.1 shows the collection of devices used for FTIR analysis.

Sample preparation

The KBr pressed disc technique was used. Discs were thoroughly washed and dried before use. An amount of KBr in a tip of spatula was added into the grinding mortar

and a small amount of the sample in a tip of the spatula was added followed by grinding until the powder was completely mixed and fine. The prepared powder was then slowly dropped into the discs and hardly pressed to form a thin film. The film plane was placed normal to the IR beam sample holder for analysis.



Figure 3.1 Working station of FTIR [13]

3.3.2 ELEMENTAL ANALYSIS

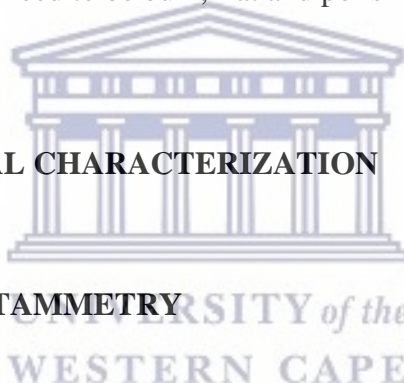
3.3.2.1 ENERGY DISPERSIVE SPECTROSCOPY (EDS)

Energy dispersive spectroscopy (EDS) detector which is connected to the HRSEM was used in this study to investigate the elemental composition of the electrocatalysts synthesized. After taking HRSEM images, the samples would then be scanned on six different areas to obtain the average wt. % of the metals.

Working principle of EDS

EDS analysis works by letting an electron beam hit the inner shell of an atom, knocking off electrons from the shell and leaving positively charged electron hole. As an electron moves, it attracts another electron from the outer shell and fills the void space. As electrons move from the outer high-energy shell to the inner low-energy shell, this energy difference is emitted in the form of an X-ray beam. The energy of this X-ray beam is unique to a particular element and transition [14]. EDS requires no special sample preparation, other than that which is required to image the sample in the SEM or TEM, for qualitative analysis, but for quantitative analysis in the SEM the sample need to be bulk, flat and polished.

3.3.3 ELECTROCHEMICAL CHARACTERIZATION



3.3.3.1 CYCLIC VOLTAMMETRY

Cyclic voltammetry is probably the most versatile electro analytical technique for the study of electro active species. Its ease of measurement and versatility has resulted in it being in extensive use in many scientific fields like, electrochemistry, organic chemistry, inorganic chemistry and biochemistry. Cyclic voltammetry is an great approach to study the reactivity of new materials or compounds and can offer information about (i) the potential at which oxidation or reduction processes transpire, (ii) the oxidation state of the redox species, (iii) the number of electrons involved, (iv) the rate of electron transfer, (v) viable chemical processes corresponding with the electron transfer, and (vi) adsorption effects etc [15-16]. Cyclic voltammetry is usually done using a three electrode system consisting of a working electrode, reference electrode and counter electrode in the presence of a supporting electrolyte. The

reference electrode can be a standard hydrogen electrode, saturated calomel electrode or silver electrode chloride. Counter electrodes can be gold, platinum or carbon while the working electrode is normally a glassy carbon electrode deposited with the catalyst being studied. The supporting electrolyte is present to repress migration of charged reactants and products [17]

In cyclic voltammetry the potential of the working electrode is swept linearly with time and between two potential ends. By adjusting the potential of the working electrode, electrons are transferred between the electrode and the molecules in the electrolyte, which records the current response of the working electrode when the potential is swept back and forth between two selected potentials [18-19]. Cyclic voltammetry was used in this study to examine the electro-active surface area (ECSA) and stability of nanophase supported electrocatalysts. In figure 3.2 is the CV graph used for illustration to show how the ECSA is calculated.

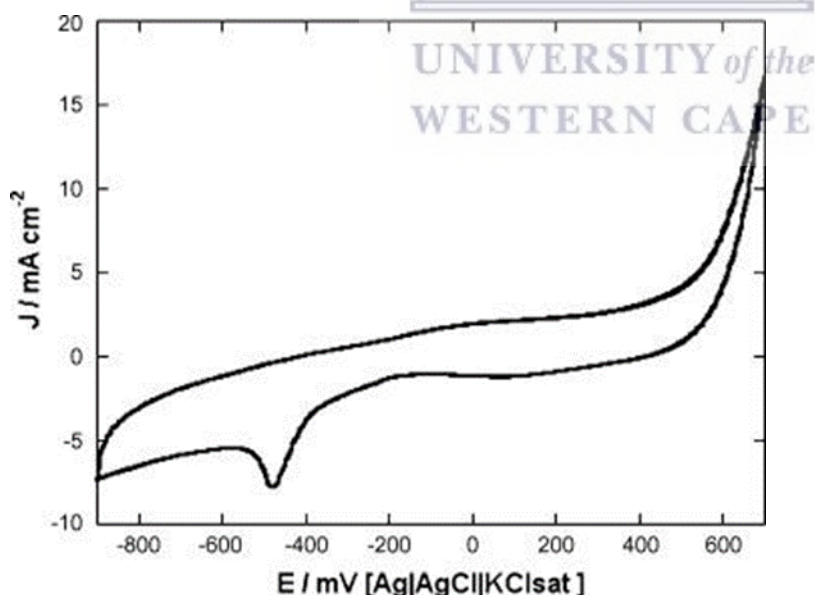
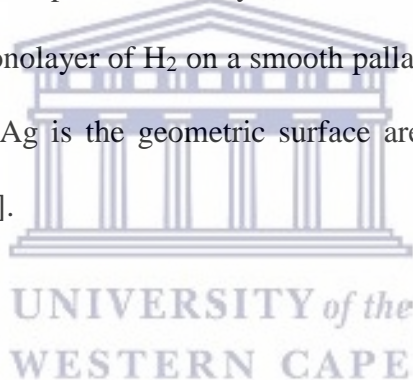


Figure 3.2 cyclic voltammogram of Pd/MWCNT (at the fifth cycle) in 2 M KOH solution. Pd loading $17 \mu\text{g cm}^{-2}$. Scan rate: 50 mV s^{-1} [20].

The Pd reduction peak is used to calculate the electro-active surface area (ECSA). ECSA is a property which is used to validate the electro-catalytic activity of the prepared catalyst. The ECSA is an indication of the electro-active surface of the catalyst, calculated by using the equation:

$$\text{ECSA}(\text{m}^2 \text{ g}^{-1} \text{ Pd}) = [\text{Q}_H / 420 \cdot \text{L} \cdot \text{A}_g] 10^5 \quad (3.2)$$

Q_H = is the area of the Pd reduction peak divided by the scan rate (V/s), $420 \mu\text{C cm}^{-2}$ is required to charge the formation of a monolayer of H_2 on a smooth palladium surface. L is the loading of catalyst in mgPd cm^{-2} and A_g is the geometric surface area of the electrode (5 mm in diameter, $\text{A}_g = 0.196 \text{ cm}^2$) [21].



3.3.3.2 Linear sweep voltammetry (LSV)

Linear sweep voltammetry is a type of voltammetry in which a current is measured in the working electrode, while the potential between the working electrode and the reference electrode is linearly scanned over time. The oxidation or reduction of a substance is recorded as the peak or through the current signal at the potential at which the substance starts to oxidize or reduce [22]. Linear sweep voltammetry is used to determine the current density and onset potential of the catalyst used for alcohol oxidation.

Table 3.3: Sample preparation and operating parameters for LSV

Parameter	Specification
Electrolyte	Potassium hydroxide
Alcohol oxidation	Methanol
Working electrode	Glassy carbon electrode
Counter electrode	Platinum electrode
Reference electrode	Silver chloride electrode
Scan rate	20 mV/s
Scan range	-1.0– 0.4V

3.3.3.3 Electrochemical Impedance Spectroscopy (EIS)

AC impedance measurements may be helpful in identifying the kinetic, ohmic, electrolytic, and diffusion layer resistances, as well as the delivery limitations inside the machine. This technique makes use of a small sinusoidal perturbation potential at one or several frequencies, and the reaction is an alternating current (AC) sign of the identical frequency with a probable phase shift and amplitude trade. In a few dimension systems, the AC current is imposed on top of the DC current generated by way of the fuel cell, and the voltage is recorded in place of the current. The recorded response is used to calculate the impedance using a mathematical method. Via repeating this at numerous frequencies, an electrochemical impedance spectrum is received. EIS is a non-invasive method that varies the current or voltage of the fuel cell by some percentage. The magnitude of the fluctuations is depending on the peak-peak current of the AC signal imposed and the impedance of the fuel cell at every frequency [23]. The AC-Impedance measurement is obtained with an electronic load, a function generator, and a computer. This is additionally the equal setup also can be used for obtaining a fuel cell

polarization or IC curves. EIS is useful in characterizing rapid and gradual delivery phenomena as it tests each single and a big variety of frequencies. This check helps to signify mass transfer resistance, resistance to electron transfer at some stage in electrochemical reactions, and ionic resistance through the membrane. This data can then be used to evaluate the numerous impedances inside the gas cell [24]. A charge transfer resistance (R_{ct}) for the kinetically controlled reactions may be represented by the diameter of the semicircle in the medium frequency and is related to the charge transfer reaction kinetics according to the following equation.

$$R_{ct} = \frac{RT}{nFi_o} \quad (3.3)$$

$$i = nFAK_o C_o^{(1-\alpha)} C_R^\alpha \quad (3.4)$$

Where R: molar gas constant ($J.mol^{-1} k^{-1}$); T: temperature (K); n: number of electrons transferred; F: Faraday constant (C); i_o : exchange current (A); A: reaction area (cm^2); k_o : standard heterogeneous rate constant ($cm.sec^{-1}$); C_o , C_R : bulk concentration of oxidant and reductant species ($mol.L^{-1}$); α : transfer coefficient [25].

The symbol for impedance is usually Z and it may be represented by writing its magnitude and phase in the form $|Z|\angle\theta$. The electrochemical impedance spectroscopy was used to study the electrode kinetics of the catalysts.

3.3.3.4 Chronoamperometry (CA)

Chronoamperometry is one of the simplest voltammetric methods, but one of the most used voltammetric methods. In its simplest form, chronoamperometry consists of applying a single

voltage step at time t_0 and then measuring the current resulting from the applied potential.

The simplicity of chronoamperometry makes it an ideal analytical technique as an example of basic voltammetry operations. In chronoamperometry the potential of the working electrode is stepped and the resulting current faradaic processes are monitored. Chronoamperometry is an electrochemical technique that generates high charging currents, which decay exponentially with time as any RC circuit. The faradaic current which is due to electron transfer is almost always the factor of interest [26]. Chronoamperometry has been applied in many studies independently or alongside other electrochemical techniques such as CV. In most case it used to examine the electrochemical activity and stability of the electrocatalysts [27-28]. In this work the Chronoamperometry was used to determine the stability of the catalysts.



References

1. Kumar, S.S., Hidyatai, N., Herrero, J.S., Irusta, S. and Scott, K., 2011. Efficient tuning of the Pt nano-particle mono-dispersion on Vulcan XC-72R by selective pre-treatment and electrochemical evaluation of hydrogen oxidation and oxygen reduction reactions. *International journal of hydrogen energy*, 36(9), pp.5453-5465.
2. Tang, X., Zhang, B., Li, Y., Xu, Y., Xin, Q. and Shen, W., 2004. Structural features and catalytic properties of Pt/CeO₂ catalysts prepared by modified reduction-deposition techniques. *Catalysis letters*, 97(3), pp.163-169.
3. Dutrow, B.L. and Clark, C.M., 2016. X-ray powder diffraction (XRD), geochemical instrumentation and analysis. *Carleton College*.
4. Chiang, Y.C., Lin, W.H. and Chang, Y.C., 2011. The influence of treatment duration on multi-walled carbon nanotubes functionalized by H₂SO₄/HNO₃ oxidation. *Applied Surface Science*, 257(6), pp.2401-2410.
5. Bunaciu, A. A., Udriștioiu, E. gabriela and Aboul-Enein, H. Y. (2015) 'X-Ray Diffraction: Instrumentation and Applications', *Critical Reviews in Analytical Chemistry*, 45(4), pp. 289–299.
6. Maass, S., Finsterwalder, F., Frank, G., Hartmann, R. and Merten, C., 2008. Carbon support oxidation in PEM fuel cell cathodes. *Journal of Power Sources*, 176(2), pp.444-451.
7. F. Rodríguez-Reinoso, *Carbon* 1998. 36: p.159-175
8. Goldstein, J. ed., 2012. *Practical scanning electron microscopy: electron and ion microprobe analysis*. Springer Science & Business Media.
9. Sun, D.W. ed., 2009. *Infrared spectroscopy for food quality analysis and control*. Academic press.

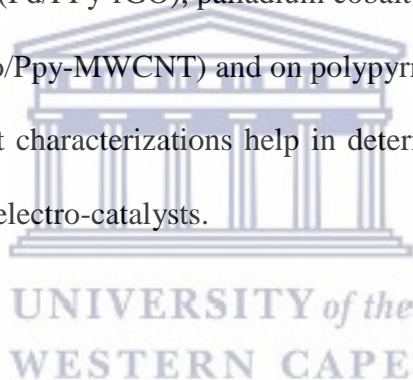
10. Saptari, V., 2003. *Fourier transform spectroscopy instrumentation engineering*. Bellingham Washington, DC: SPIE Optical Engineering Press.
11. Nicolet, T. and All, C. (2001) 'Thermogravimetric Analysis', 199(1), pp. 1–8
12. Janssens, M., 2006. Fundamental measurement techniques. In *Flammability Testing of Materials Used in Construction, Transport and Mining* (pp. 22-62). Woodhead Publishing.
13. <https://www.labcompare.com/Spectroscopy/165-Infrared-Spectroscopy-IR-FTIR/>
14. Singh, M.N.K., *An Investigation on Oxidation behaviour of Heavy Alloy Tungsten Scrap Fines using High-Temperature Fluidization* (Doctoral dissertation, National Institute of Technology, Rourkela).
15. Marken, F., Neudeck, A. and Bond, A. M. (2005) 'Cyclic Voltammetry', in *Electroanalytical Methods*. Berlin, Heidelberg: *Springer Berlin Heidelberg*, pp. 51–97.
16. Elgrishi N, Rountree K, McCarthy B, et. al. (2017) 'A Practical Beginner's Guide to Cyclic Voltammetry'. *J. Chem. Educ.* 2018, 95, 197–206
17. Evans, D.H., O'Connell, K.M., Petersen, R.A. and Kelly, M.J., 1983. *Cyclic voltammetry*.
18. Spence, John C.H. (1988) [1980]. *Experimental high resolution electron microscopy*. New York: Oxford U. Press. ISBN 0-19-505405-9
19. Electron microscope- Ask.com Encyclopedia last modified on 20 July 2013 available at www.dstuns.iitm.ac.in/microscopy-instruments.php
20. Bambagioni, V., Bianchini, C., Marchionni, A., Filippi, J., Vizza, F., Teddy, J., Serp, P. and Zhiani, M., 2009. Pd and Pt–Ru anode electrocatalysts supported on multi-walled carbon nanotubes and their use in passive and active direct alcohol fuel cells

- with an anion-exchange membrane (alcohol= methanol, ethanol, glycerol). *Journal of Power Sources*, 190(2), pp.241-251.
21. Grdeń, M., Łukaszewski, M., Jerkiewicz, G. and Czerwiński, A., 2008. Electrochemical behaviour of palladium electrode: *oxidation, electrodisolution and ionic adsorption*. *Electrochimica Acta*, 53(26), pp.7583-7598.
22. Aoki, K., Akimoto, K., Tokuda, K., Matsuda, H. and Osteryoung, J., 1984. Linear sweep voltammetry at very small stationary disk electrodes. *Journal of electroanalytical chemistry and interfacial electrochemistry*, 171(1-2), pp.219-230.
23. Spiegel, C. (2017) Techniques for Measuring Fuel Cell Resistance.
24. Latorrata, S. et al. (2018) 'Use of Electrochemical Impedance Spectroscopy for the Evaluation of Performance of PEM Fuel Cells Based on Carbon Cloth Gas Diffusion Electrodes', *Journal of Spectroscopy. Hindawi*, 2018, pp. 1–13.
25. Hsing, I.M., Wang, X. and Leng, Y.J., 2002. Electrochemical impedance studies of methanol electro-oxidation on Pt/C thin film electrode. *Journal of the Electrochemical Society*, 149(5), p.A615.
26. Bard A. J.(1994) 'Electroanalytical Chemistry', Marcel Dekker, New York pp.13
27. Guy, O.J. and Walker, K.A.D., 2016. Graphene functionalization for biosensor applications. *Silicon Carbide Biotechnology*, pp.85-141.
28. Tusi, M.M., Brandalise, M., Verjúlio-Silva, R.W., Correa, O.V., Villalba, J.C., Anaissi, F.J., Neto, A.O., Linardi, M. and Spinacé, E.V., 2010. Preparation of PtRu/C electrocatalysts by hydrothermal carbonization using different carbon sources. In *Studies in surface science and catalysis* (Vol. 175, pp. 551-554). Elsevier.

Chapter 4

Results and Discussion

This chapter focuses on analysing the results obtained from various characterization techniques performed on the synthesized catalysts of palladium and palladium cobalt supported on multi-walled carbon nanotubes (Pd/MWCNT & PdCo/MWCNT), reduced graphene oxide (Pd/rGO & PdCo/rGO) and on polypyrrole (Pd/PPy & PdCo/PPy) and palladium on polypyrrole - multi-walled carbon nanotubes hybrid (Pd/PPy-MWCNT), palladium on polypyrrole – reduced graphene oxide hybrid catalyst (Pd/PPy-rGO), palladium cobalt oxide on polypyrrole – multi-walled carbon nanotubes (PdCo/PPy-MWCNT) and on polypyrrole – reduced graphene oxide (PdCo/PPy-rGO). The different characterizations help in determining the various properties exhibited by these synthesized electro-catalysts.



4.1 Functionalization of The Support material

4.1.1 Multi-walled carbon nanotubes (MWCNT)

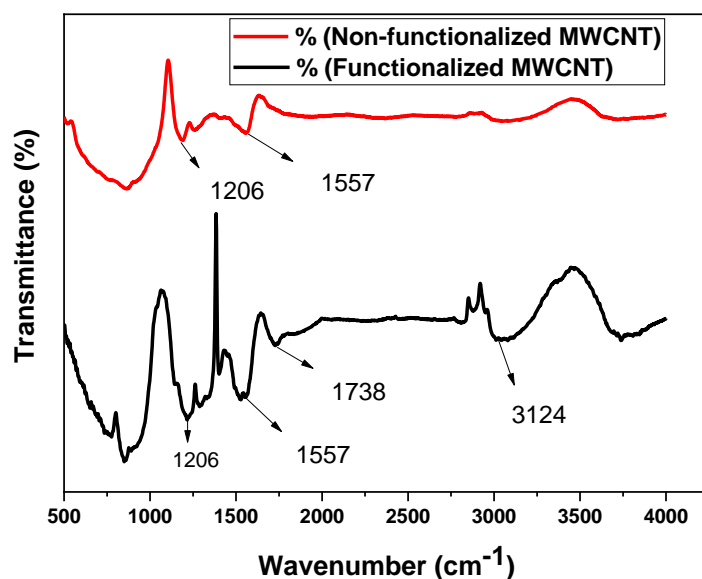


Figure 4.1.1 FTIR spectra of Functionalized MWCNTs with COOH

The functionalized and non-functionalized MWCNTs were analysed through Fourier transform infra-red spectroscopy (FTIR). The vibration bands obtained from the spectra of the MWCNTs shows a formation of new peaks in functionalized MWCNT compared to the non-functionalized MWCNT. The spectra of functionalized MWCNTs depicts related vibrational bands characteristic of carboxylic groups on MWCNTs. FTIR spectra from the MWCNTs show a broad peak at $\sim 3124 \text{ cm}^{-1}$ in Figure 4.1.1 above which is assigned to the O–H stretch from carboxylic groups (C–OH and O=C–OH), these peaks were not present on the non-functionalized MWCNTs [1]. The peak at 1738 cm^{-1} , associated with the stretch mode of carboxylic groups C=O as observed in the IR spectrum of the functionalized MWCNTs which indicates that carboxylic groups are formed due to the oxidation of some carbon atoms on the surface of the MWCNTs by nitric acid. . The peak at 1557 cm^{-1} is allocated to the –C–C– stretch in a ring (aromatic) and the peak at 1206 cm^{-1} is associated with C–O stretch of carboxylic group. The overall peaks found in the spectrum are ν (O–H) ($3750\text{--}3250 \text{ cm}^{-1}$), ν (C–H) ($3000\text{--}2750 \text{ cm}^{-1}$), ν (C=O) ($1760\text{--}1650 \text{ cm}^{-1}$), ν (C–C) ($1600\text{--}1550 \text{ cm}^{-1}$) and ν (C–O) (1350--

900 cm^{-1}). These vibrations are in good agreement with the spectrum of the functionalized MWCNTs as reported by Moosa, et al [2].

4.1.2 Graphene oxide and reduced graphene oxide (rGO)

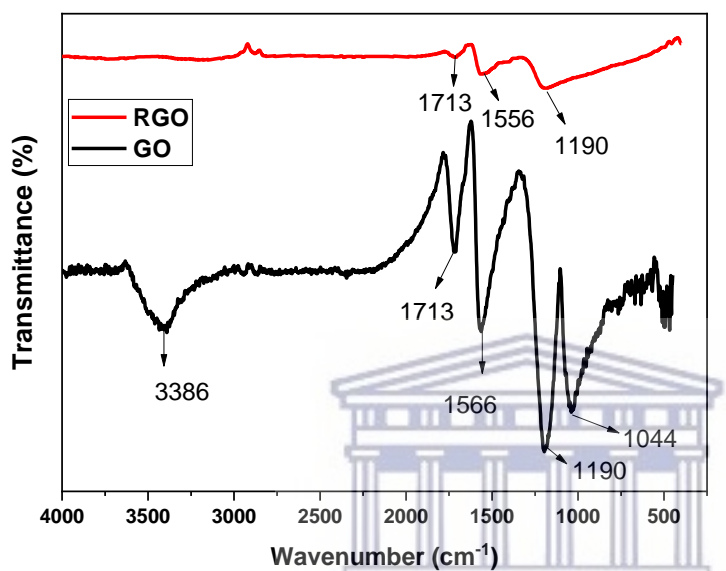


Figure 4.1.2 FTIR spectra of GO and rGO

UNIVERSITY of the
WESTERN CAPE

The synthesized GO and rGO were analysed through FTIR. The vibration bands obtained from the spectra of the GO and reduced GO shows related vibrational bands characteristic of carboxylic groups on GO and rGO as expected. The broad peak at 3386 cm^{-1} is attributed to the O-H stretching, which is associated with the OH stretch of carboxylic acid, is due to the presence of absorbed water molecules and alcohol groups. The peak at 1566 cm^{-1} is ascribed to C=C stretches from un-oxidized graphitic domain. The peak at around 1713 cm^{-1} is ascribed to C=O stretch of carboxyl group. The peak at 1190 cm^{-1} corresponds to C-OH stretch of alcohol group and the peak at 1044 cm^{-1} is ascribed to C-O stretching vibrations of C-O-C. These vibrations corresponds to the spectrum of GO reported by Emiru, et al [3].

The reduction of GO was also characterized by FTIR. As seen in Figure 4.1.2. The rGO peaks displays the reduction of oxygen-containing functional groups on GO by KMnO_4 . These peaks were confirmed by the removal and the reduction of the peaks as displayed in figure 4.1.2. The peaks in 1044 , 1190 , 1713 and 3386 cm^{-1} enormously decreased and disappeared, which indicates that the oxygen-containing groups in GO were removed. The observations on rGO spectra confirmed that most oxygen-containing functional groups in the GO were removed even though some residual oxygen functionalities on GO still remains on the rGO surface with weaker intensity after reduction [4].

4.1.4 Polypyrrole (PPy)

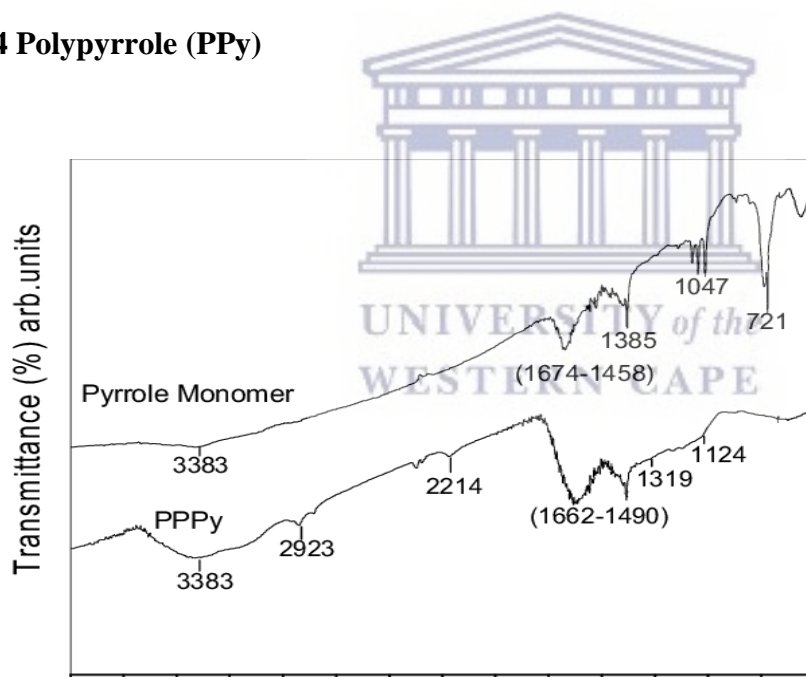


Figure 4.1.3: The FTIR spectrum of pyrrole monomer [5]

The pyrrole (Py) was analysed through FTIR by Bruno, et al. Figure 4.1.3 above shows the FTIR spectrum of pyrrole. The broad peak at 3383 cm^{-1} is attributed to the presence of N–H stretching vibrations. The absorption around 1650 cm^{-1} is attributed to the amines in the pyrrole structure these peaks were confirmed on the literature by Kamal, M.M et al [5].

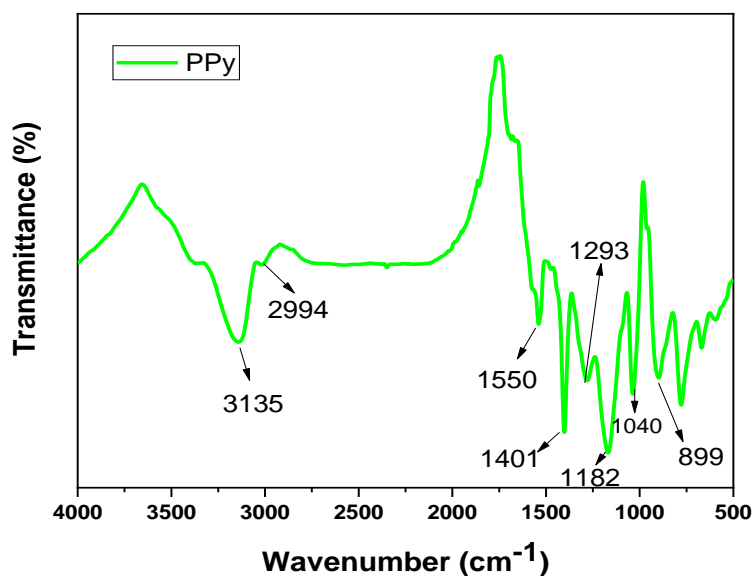


Figure 4.1.4 FTIR spectra of PPy

The polymerized pyrrole or polypyrrole was analysed through FTIR. The observed peaks are in agreement with the spectrum shown in the figure above from the work done by Kamal, et al [5]. Figure 4.1.4 above shows the FTIR spectra of PPy powder. The broad peak at 3135 cm^{-1} is attributed to the presence of N–H stretching vibrations. The peaks at 1550 cm^{-1} and 1182 cm^{-1} represents C=N and C–N bonds respectively. Whereas the peaks at 1401 cm^{-1} and 1293 cm^{-1} correspond to the C=C stretching. The peaks at 1040 cm^{-1} , 899 cm^{-1} are attributed to C–H wagging. At about 2994 cm^{-1} , there is a small sharp peak in PPy spectrum but not in monomer spectrum. The peak is due to asymmetric and symmetric C–H stretching vibration of saturated hydrocarbon in PPy. The peaks observed in figure 4.1.4 relates well with the ones available in the literature [6-7] confirming the formation of PPy.3fv

4.2 XRD Analysis

4.2.1 XRD of the prepared support material

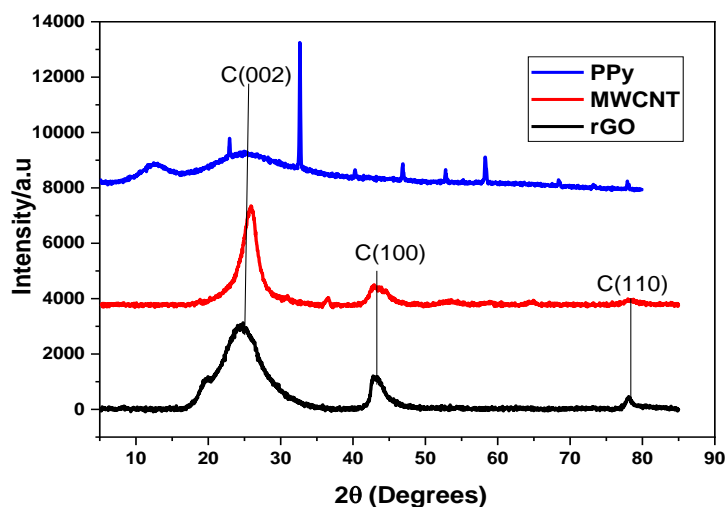


Figure 4.2.1 XRD patterns of the in house supports material (PPy, MWCNT and rGO)

The XRD patterns of the PPy, rGO and MWCNTs samples are presented in Figure 4.2.1 above. The strongest and sharpest diffraction peak for all samples at around $2\theta = 25.6^\circ$ could be indexed as (002) reflection of the graphite [8]. The other characteristic diffraction peaks of MWCNT and rGO at 2θ of $\sim 43.6^\circ$, 78.8° corresponded to (100), and (110), respectively. All diffraction peaks were observed at the same 2θ values for both samples. Distinctly, the intensity of the diffraction peak at (002) in functionalized MWCNTs and rGO was more intense in comparison with the PPy. This shows that the loosely of the MWCNTs floss after the acid treatment formed more ordered MWCNTs floss in the functionalized MWCNTs, whereas in rGO it indicates the more graphitic character of rGO nano-sheets[9-10]. XRD pattern showed that two broad peaks related to the scattering from PPy chains at the inter-planar spacing are centred at $2\theta \sim 11.7^\circ$; 25.7° , these broad peaks were observed indicating some structural ordering of nanometric dimensions, distinctive of nanostructured polymers with low degree of crystallinity. It is clear that there are several strong diffraction peaks at ~ 23 , 33 , 47 and 59 degrees for PPy which indicates the presence of some Fe impurities in the PPy sample [11].

4.2.2 XRD of the prepared palladium catalysts

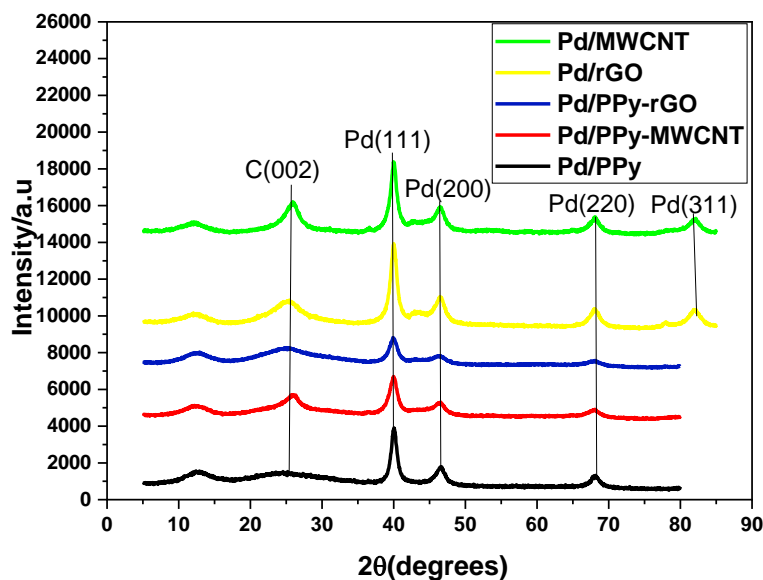


Figure 4.2.2 The XRD patterns of the in-house catalysts namely Pd/rGO, Pd/MWCNT, Pd/PPy, Pd/PPy-rGO, Pd/PPy-MWCNT.

The crystalline structure of the synthesized nanoparticles were investigated by XRD. The XRD patterns for the in-house catalysts are presented in figure 4.2.2 above. New peaks were formed after the addition of Pd compared to the peaks observed in Figure 4.2.1 above. The peaks at 39.99° , 46.7° and 68.1° can be assigned to (111), (200), and (220) for reflection of Pd on Pd/rGO, Pd/MWCNT, Pd/PPy, Pd/PPy-rGO and Pd/PPy-MWCNT. Meanwhile the peaks at 82.5° can be assigned to (311) index of Pd/rGO and Pd/MWCNT [8]. The peaks of Pd/rGO, Pd/MWCNT, Pd/PPy, Pd/PPy-rGO and Pd/PPy-MWCNT at 25.1° may be assigned to (002) index which is attributed to the carbon [11]. A very broad humped peak appeared at about 12.5 degrees which indicates that the synthesized material is amorphous with short range ordering [32]. In addition, PPy compared with Pd / PPy, the diffraction peaks (at ~ 23 , 33 , 47 and 59 degrees) of PPy disappeared.

4.2.3 XRD of Palladium Cobalt catalysts

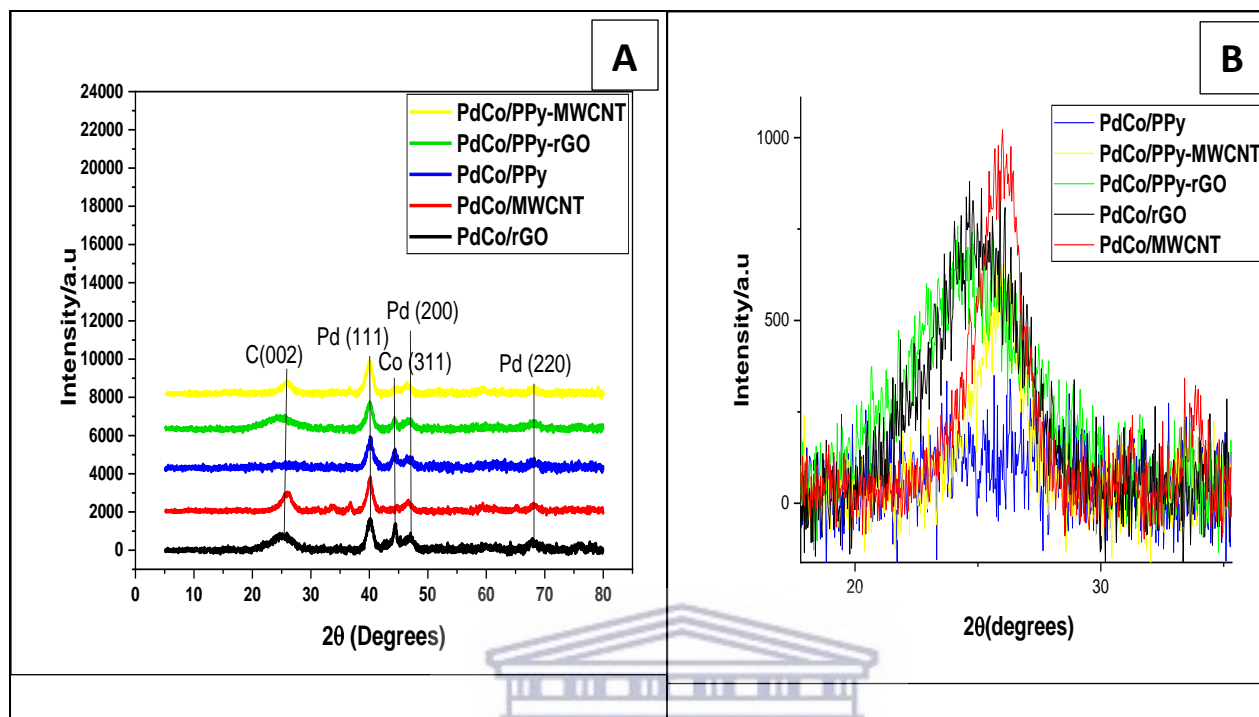


Figure 4.2.3A The XRD patterns of the palladium cobalt catalysts namely PdCo/rGO, PdCo/MWCNT, PdCo/PPy, PdCo/PPy-rGO, PdCo/PPy-MWCNT with a zoomed patterns in the diagram labelled B.

UNIVERSITY of the
WESTERN CAPE

The crystalline structure of the synthesized nanoparticles were investigated by XRD. The XRD patterns for the in-house catalysts are presented in figure 4.2.3A above. The prepared binary PdCo electro-catalyst display characteristic patterns similar to that of the standard Pd electro-catalyst, an indication that all catalysts have prevailed the Pd face-centred-cubic (fcc) crystal structure. These diffraction peaks in all samples corresponded to (111), (200), and (311) of the Pd- rich fcc crystalline structure. However, the 2θ values of the binary catalyst shifted slightly to higher values, showing that cobalt was alloyed well with this preparation method. The diffraction peak for carbon attributed by the supports material at about $2\theta = 25^\circ$ which corresponds to (002) is one of the five major peaks, this peak can be clearly observed in a zoomed diffractograms in Figure 4.2.3B. The peaks at 39.99° shifted to 40.2° , 46.7° to 47.2° and

68.1° to 68.4° [8]. The combined XRD patterns for PdCo/rGO, PdCo/MWCNT, PdCo/PPy, PdCo/PPy-rGO and PdCo/PPy-MWCNT show the peaks corresponding to Pd peaks and also show the diffraction peaks corresponding to the Co peaks and these shows that they coexist in the sample [12]. The average size of the metal particles is calculated according to Scherrer's equation.

The Scherrer equation was used to calculate the crystal size and the equation is given as:

$$D = \frac{k\lambda}{B\cos\theta} \quad (4.1)$$

Where k is Scherrer constant which can take values from 0.9 to 1, for this calculation we chose to use 0.9, λ is the wavelength of the x-ray which has a value of 1.540598 in Angstroms, B is full width at half maximum, and θ is the angle. Plus, the FWHM value is converted to radians. The plane calculated was the (111) which had the most intense peak. Table 4.1 below gives the various data points acquired to make the calculations.

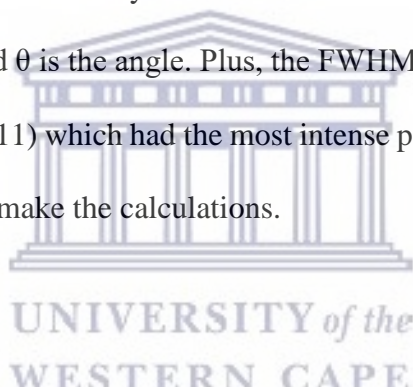
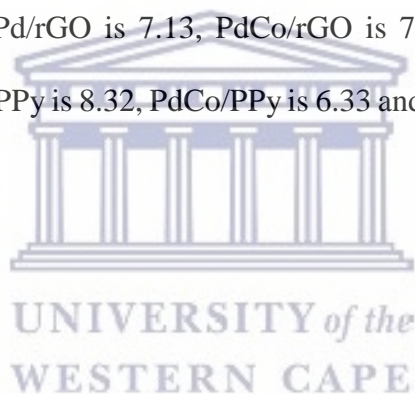


Table 4. 1: XRD data of Gaussian Fit for (111) plane and HRTEM for crystal size calculation

Catalyst	2 θ	θ	FWHM	FWHM (radians)	Crystallite size (nm)	HRTEM Particle size (nm)
Pd/rGO	40.001	20.001	1.186	0.021	7.13	13.5
Pd/MWCNT	39,995	19.998	1.253	0.022	6.75	10.4
Pd/PPy	40.088	20.044	1.016	0.018	8.32	7.9
Pd/PPy-rGO	39.999	19.999	1.361	0.024	6.21	7.7
Pd/PPy- MWCNT	39.995	19.998	1.338	0.023	7.13	10.4

PdCo/rGO	40.081	20.040	1.175	0.021	7.19	8.2
PdCo/MWCN T	40.097	20.049	1.154	0.020	7.33	7.9
PdCo/PPy	40.131	20.065	1.337	0.023	6.33	8.9
PdCo/PPy- rGO	40.039	20.019	1.216	0.021	6.95	10.9
PdCo/PPy- MWCNT	39.985	19.992	1,392	0.024	6.07	11.1

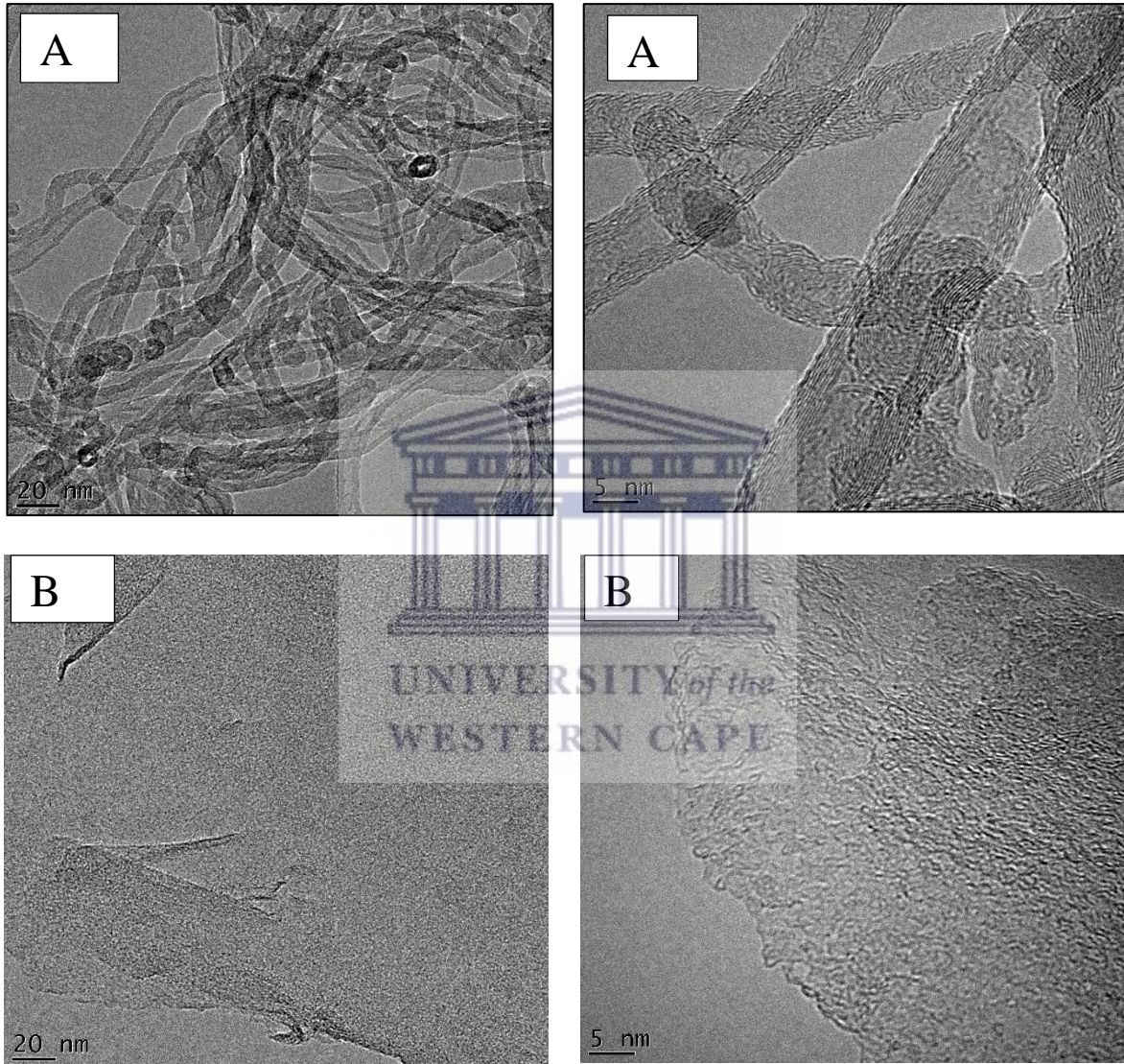
The average particle size for Pd/rGO is 7.13, PdCo/rGO is 7.19, Pd/PPy-rGO is 6.21 and PdCo/PPy-rGO is 6.95. For Pd/PPy is 8.32, PdCo/PPy is 6.33 and for Pd/PPy-MWCNT is 7.13, PdCo/PPy-MWCNT is 6.07.



4.3. Internal structure

The internal structure of the synthesized nanoparticles was evaluated by High resolution transmission electron microscope (HR-TEM). From the HR-TEM images particle sizes of the catalysts were calculated using J-image software and reported below in the histogram plots in Figure 4.3.3.

4.3.1 HRTEM of the support material used in electrocatalysts



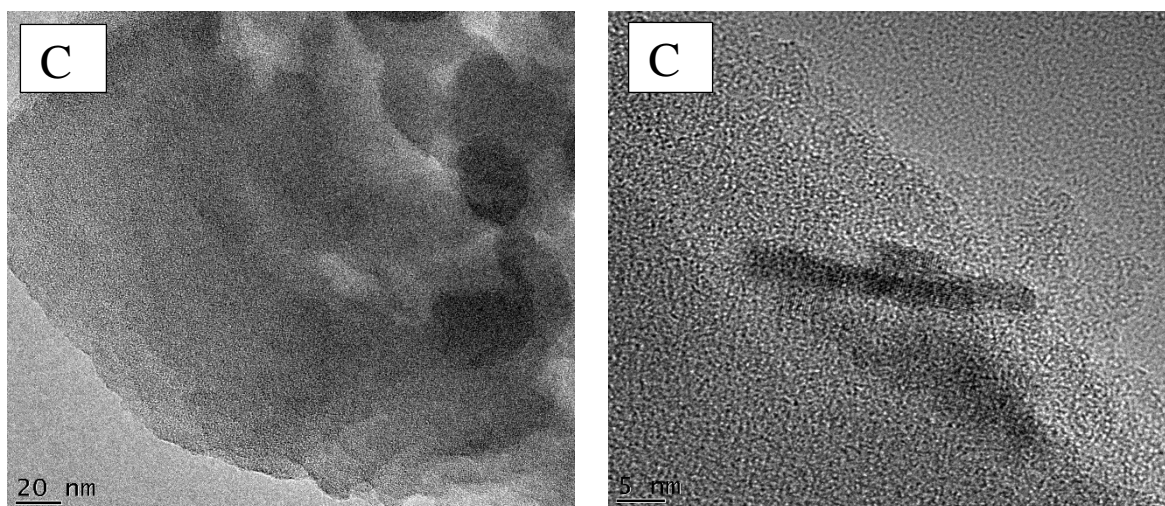


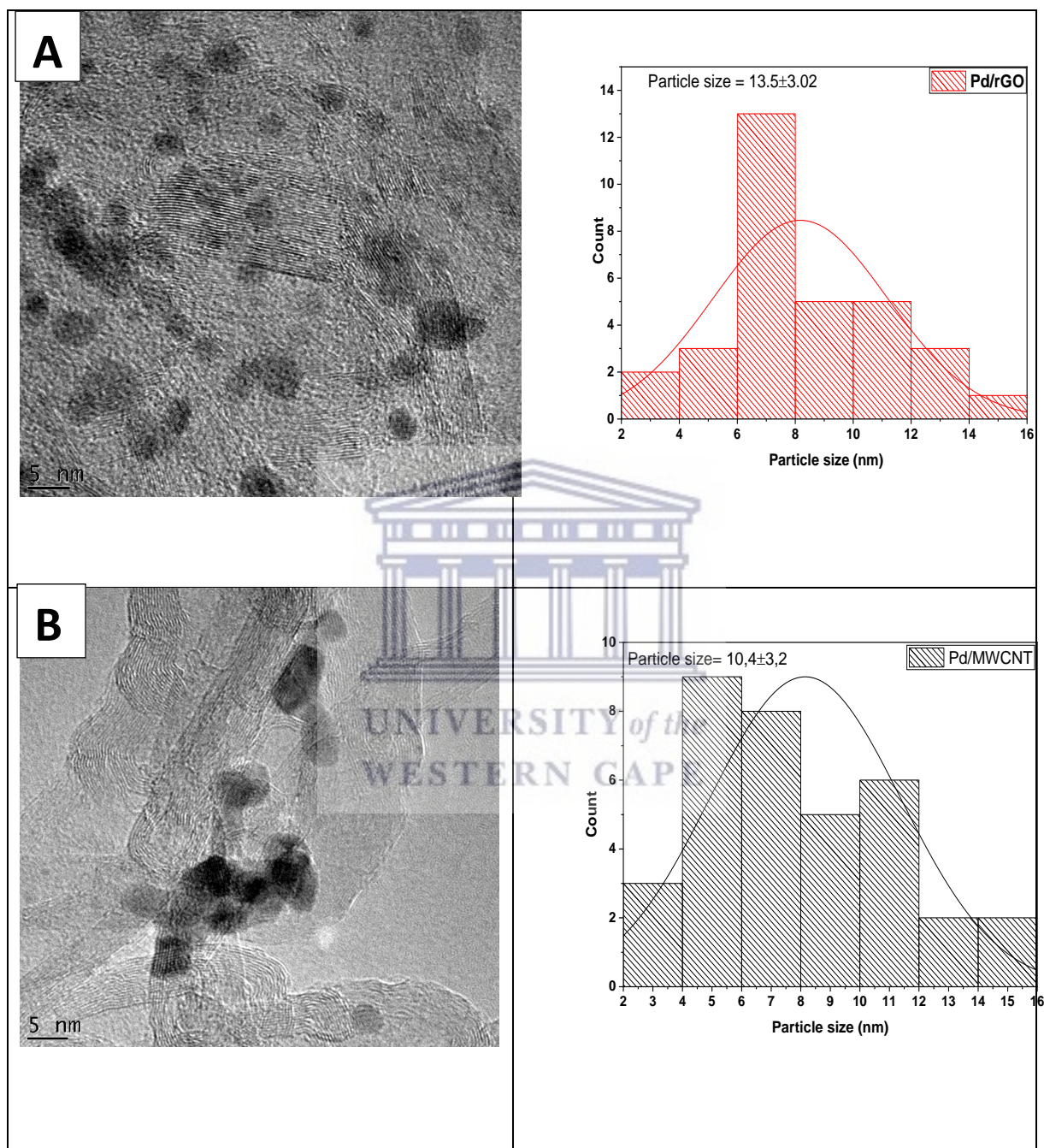
Figure 4.3.1 HRTEM images of the prepared supports material of (A) MWCNT, (B) rGO and (C) PPy at low and high magnification.

The internal structure of the prepared support materials was investigated through HRTEM as displayed in Figure 4.3.1 above to view the morphology of each support at high and low resolution of 20 nm and 5 nm. MWCNT (A) are clearly visible with thick thread like appearance which indicates that MWCNTs were finely prepared without any perceptible deformation. The rGO (B) is visible as the nano-layers in the 20 nm magnification and showing some porosity within the nano-sheets at 5 nm magnification. PPy (C) shows smooth layer on the surface and clear micro-pores.

4.3.2 HRTEM analysis (Particle size and size distribution)

The particle size and particle morphology has a great influence in the electro-chemical activity of the catalyst owing to the relationship between catalytic activity and surface structure. Therefore, HRTEM analysis of the supported electro-catalyst was therefore carried out before

the comparison of their catalytic activity. Their particle size were calculated and presented in Table 4.1 above.



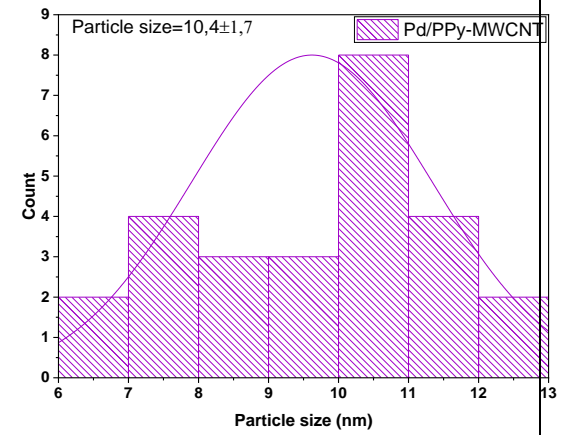
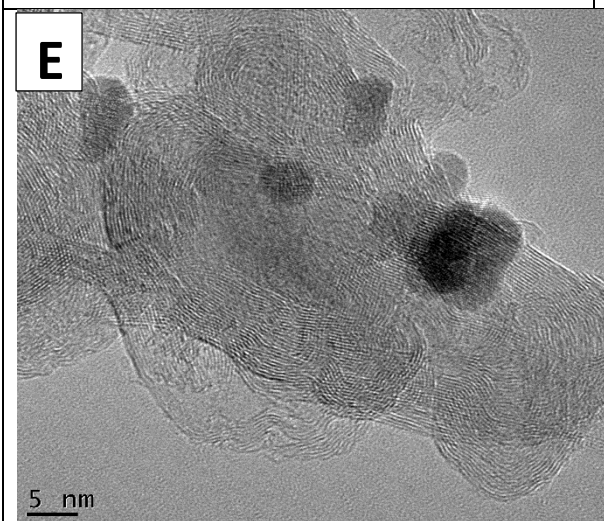
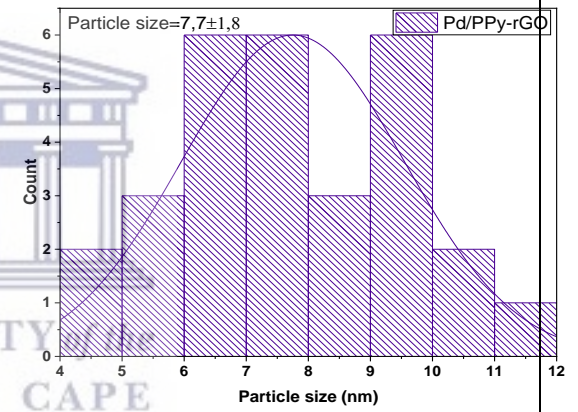
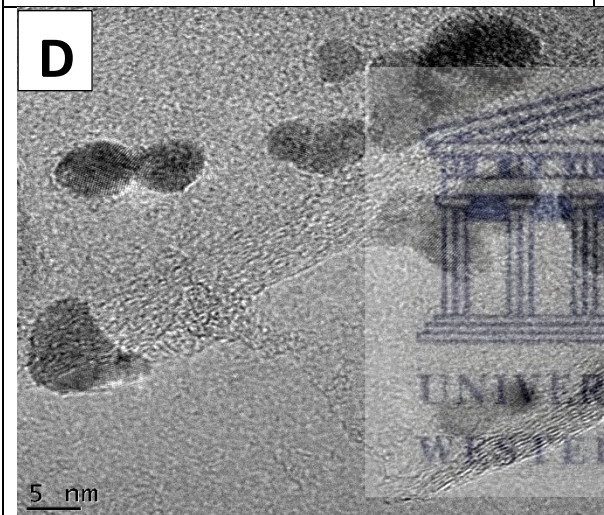
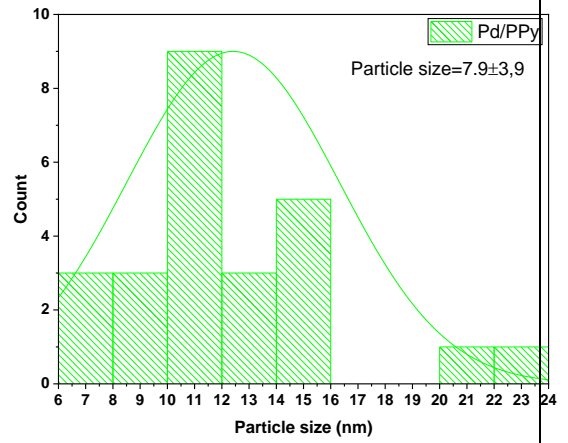
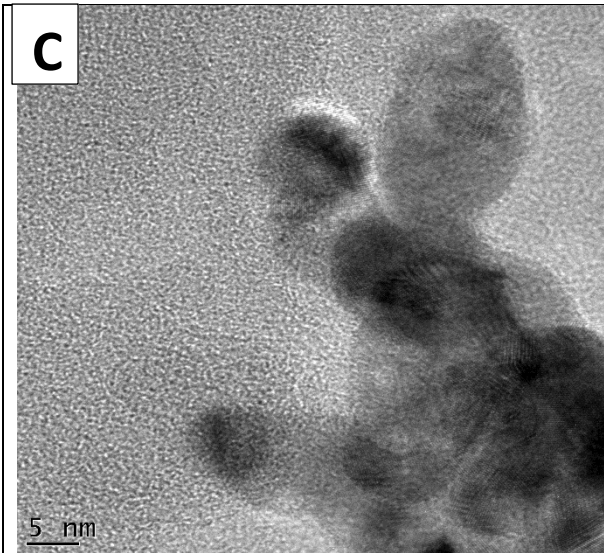
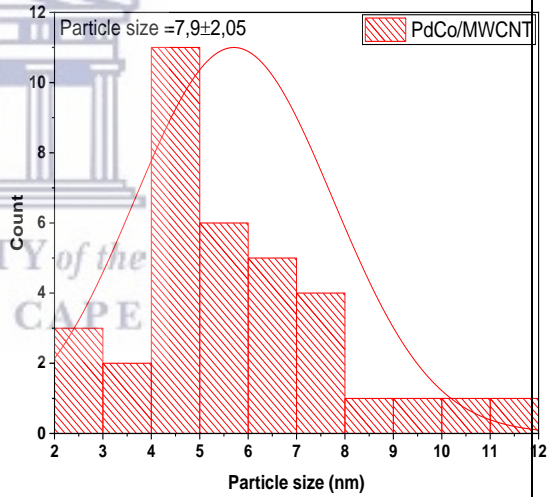
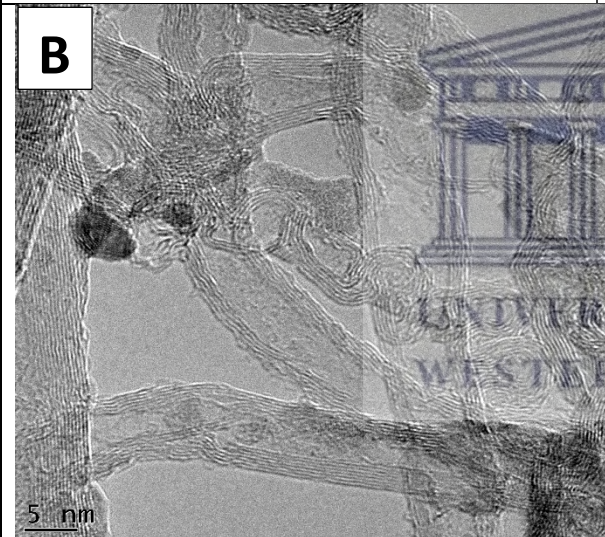
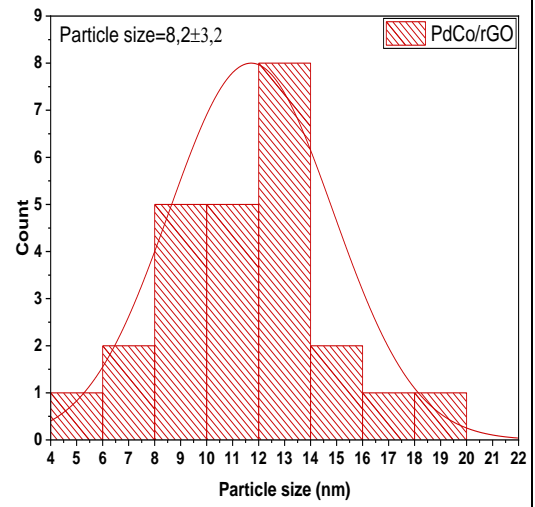
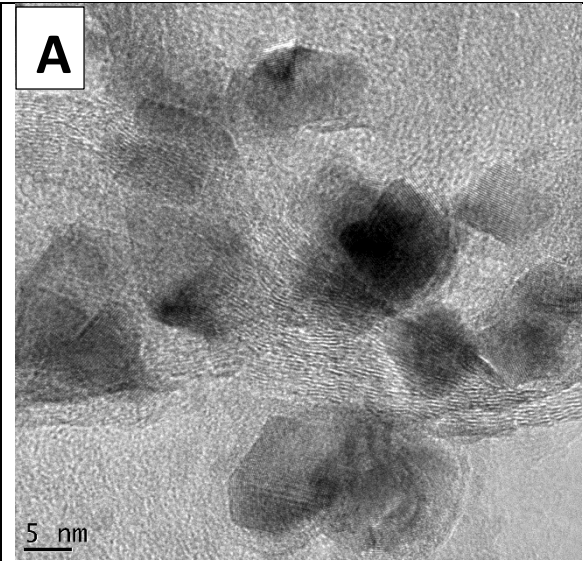
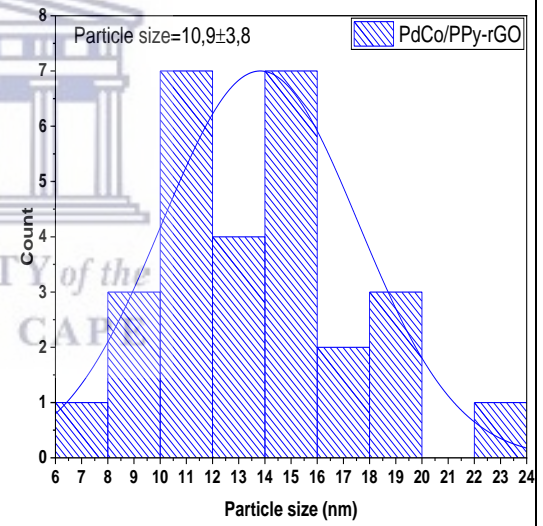
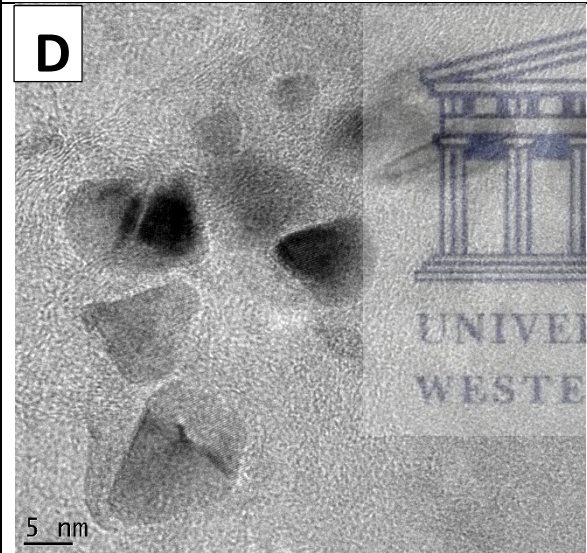
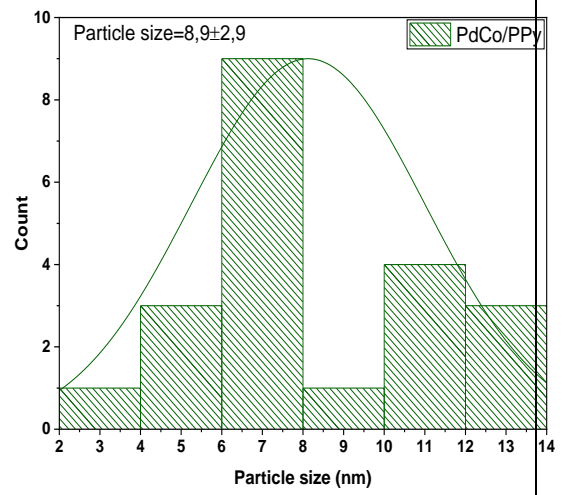
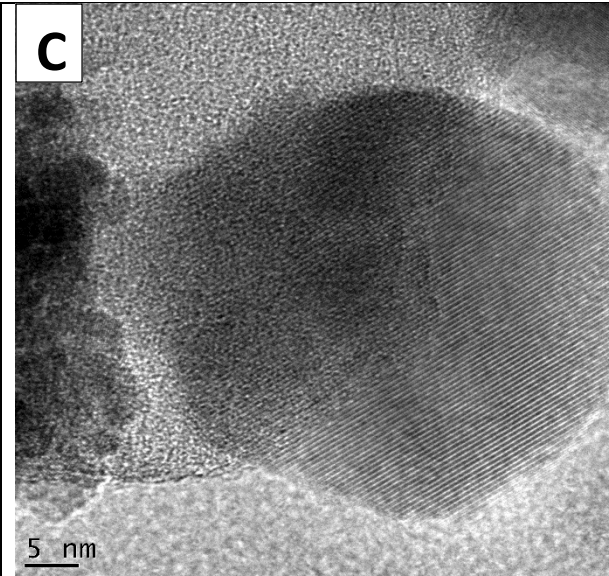


Figure 4.3.2 HRTEM images of the synthesized catalysts together with the Mean particle size plots from HRTEM namely (A) Pd/rGO, (B) Pd/MWCNT, (C) Pd/PPy, (D) Pd/PPy-rGO, (E) Pd/PPy-MWCNT.

Images A-E of Figure 4.3.2 above shows the particle distribution of the mono-catalysts Pd/rGO, Pd/MWCNT, Pd/PPy, Pd/PPy-rGO and Pd/PPy-MWCNT. At low magnification the catalysts showed agglomeration on the rGO, PPy and MWCNT surface and at high magnification the d-spacing values of the catalysts were calculated from the XRD and reported in Table 4.1 above. The inner shape of the synthesized catalysts is unclear additionally the images show that catalysts they may be agglomerated except for Pd/rGO with a better inner structure and they have small particle size. The particle sizes obtained for the catalysts were summarized in histogram plots. The typical histograms of the HRTEM images of the synthesized catalysts were estimated from 100 particles selected from random regions using the J-image software. The average particle size was collected and presented in Table 4.1 above. It was observed that the alloyed metals nanoparticles are uniformly dispersed on the supports material with few agglomerates on some parts of the sample for the PPy, MWCNT and the hybrid supports. The uniform distribution of the catalyst particle is known to be a crucial factor for electro-catalytic activity [13-14].





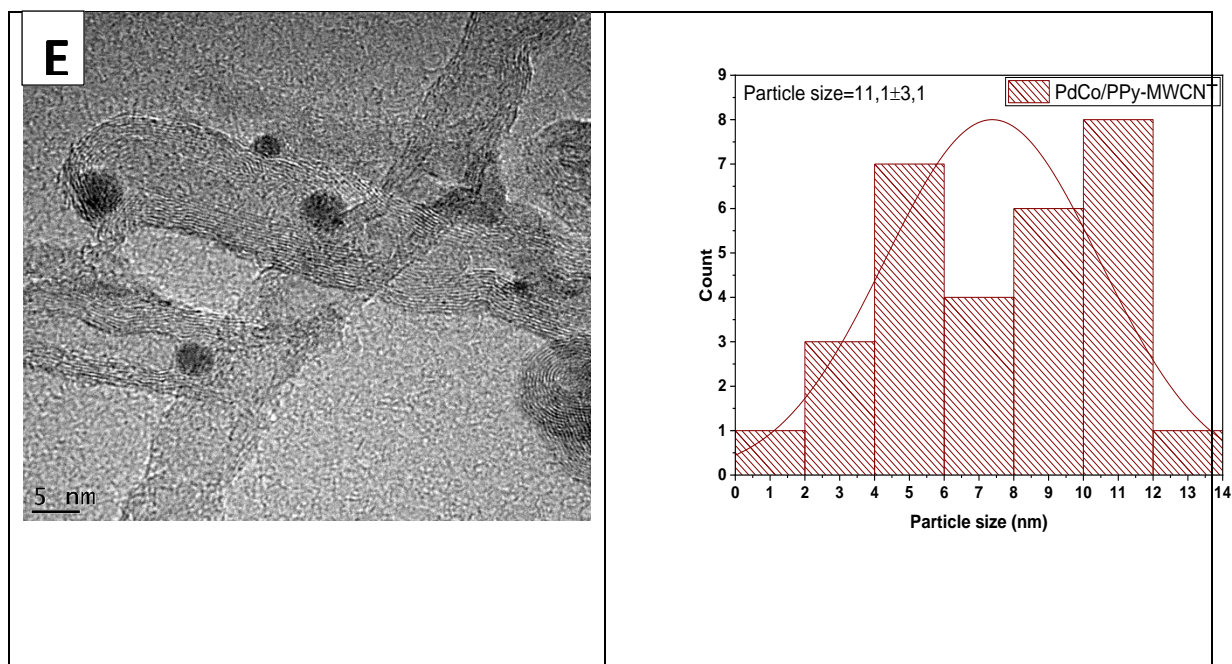
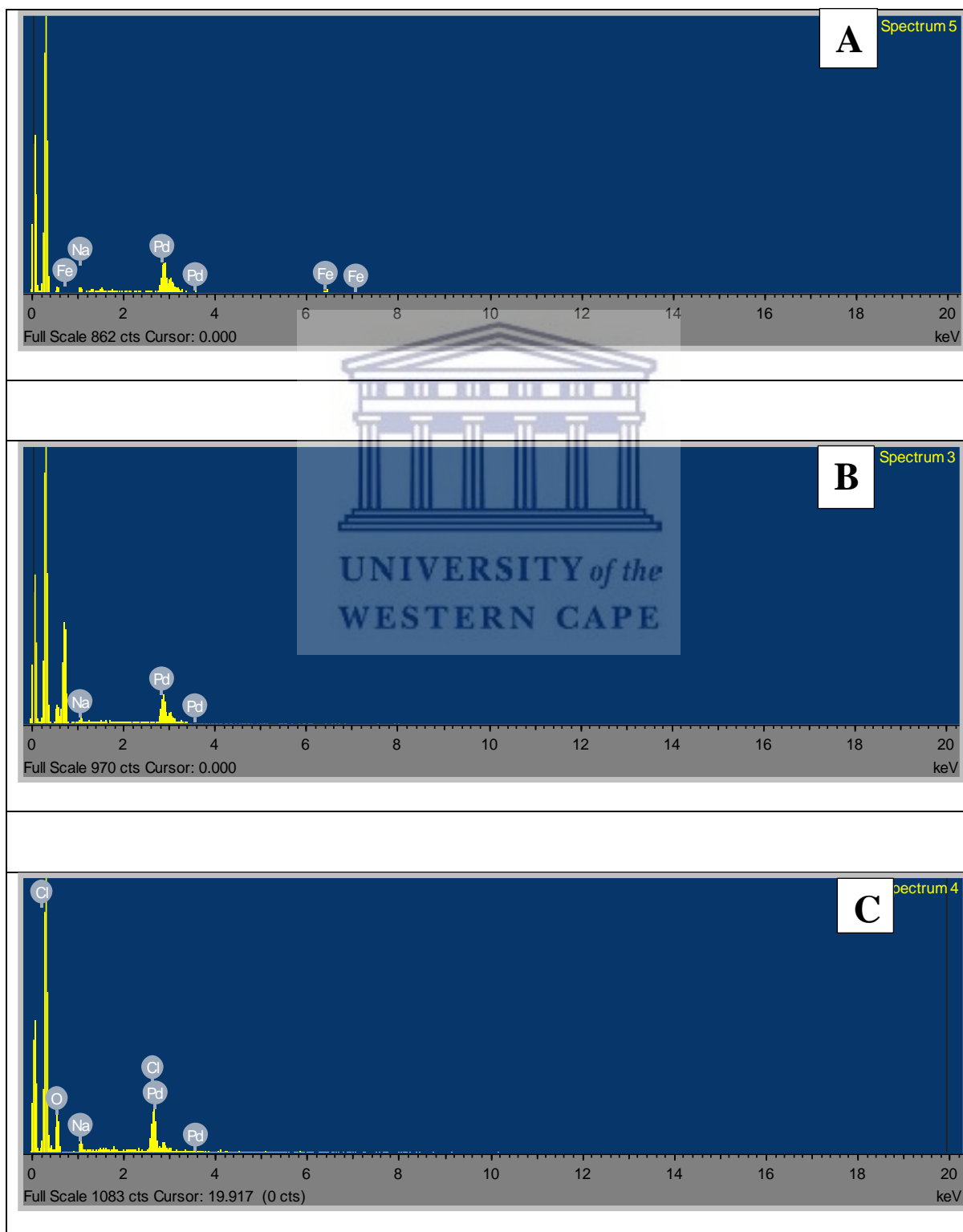


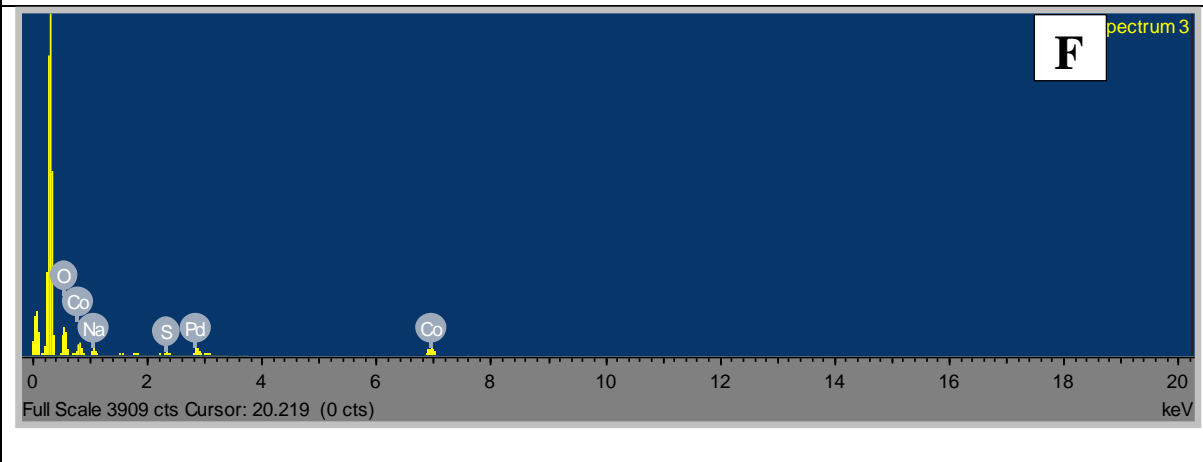
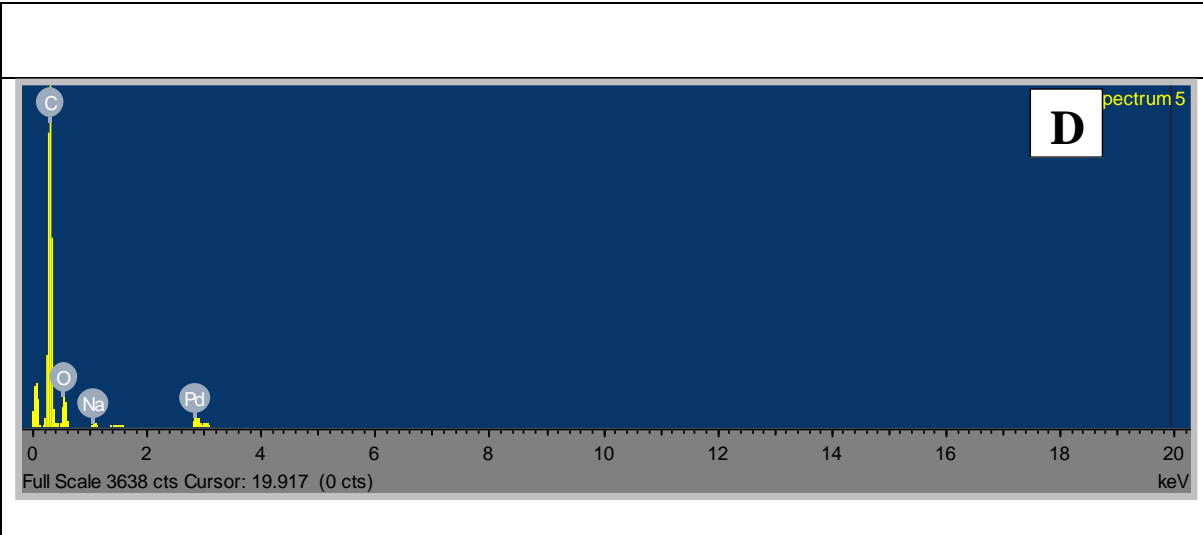
Figure 4.3.3 HRTEM images together with Mean particle size plots from HRTEM images of the synthesized catalysts namely (A) PdCo/rGO, (B) PdCo/MWCNT, (C) PdCo/PPy, (D) PdCo/PPy-rGO and (E) PdCo/PPy-MWCNT.

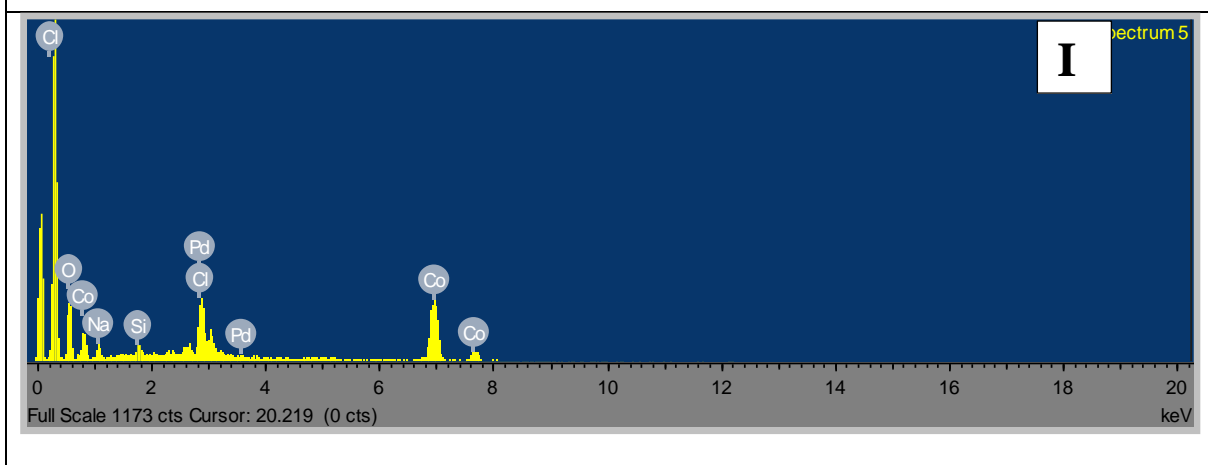
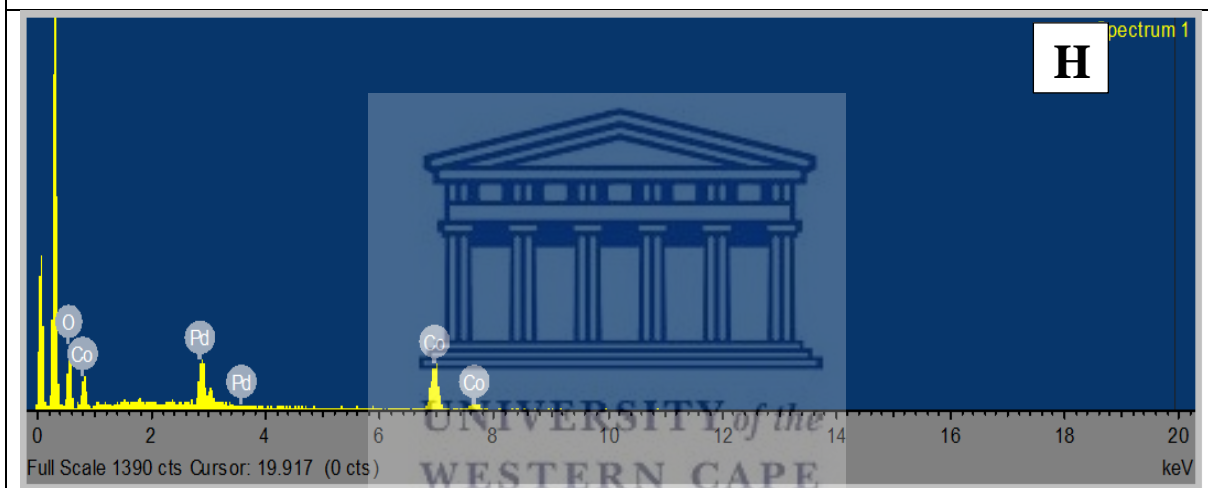
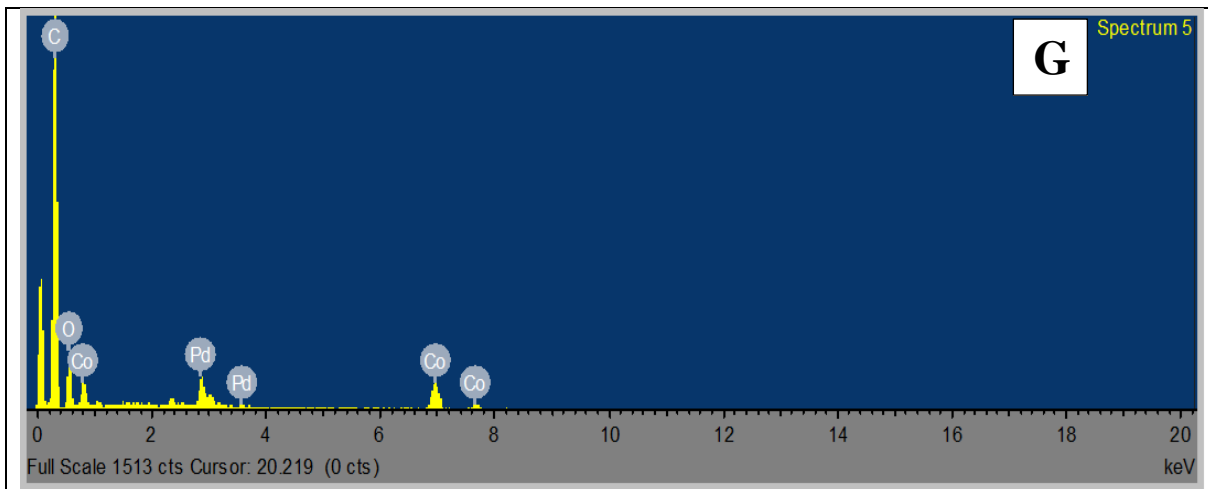
Images A-E of Figure 4.3.3 above shows the particle distribution of the catalysts PdCo/rGO, PdCo/MWCNT, PdCo/PPy, PdCo/PPy-rGO, and PdCo/PPy-MWCNT at low and high magnification. The particle sizes obtained for the catalysts were summarized in histogram plots. The typical histograms of the HRTEM images of the synthesized catalysts were estimated from 100 particles selected from random regions. The average particle size was collected and presented in Table 4.1 above. The uniform distribution of the catalyst particle is known to be a crucial factor for electro-catalytic activity [13]. It was observed that the alloyed metals nanoparticles are uniformly dispersed on the supports material with few agglomerates on some parts of the sample for the hybrid supports [15-16].

4.4 Elemental analysis of the synthesized electrocatalysts

EDS was used to confirm the elements in the synthesized catalysts as shown in Figure 4.4 below.







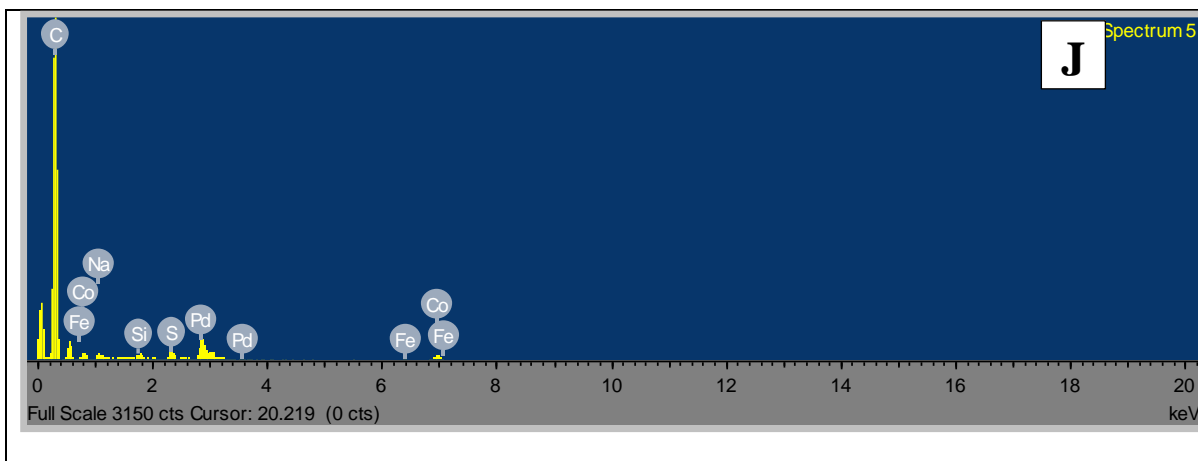


Figure 4.4 EDS plots of the synthesized catalysts of (A) Pd/rGO, (B) Pd/MWCNT, (C) Pd/PPy, (D) Pd/PPy-rGO, (E) Pd/PPy-MWCNT, (F) PdCo/rGO, (G) PdCo/MWCNT, (H) PdCo/PPy, (I) PdCo/PPy-rGO and (J) PdCo/PPy-MWCNT.

Figure 4.4 shows the EDS spectra of the synthesized catalysts confirming the presence of the elements in the prepared catalysts. Pd/rGO, Pd/MWCNT, Pd/PPy and the hybrid support catalysts Pd/PPy-rGO and Pd/PPy-MWCNT spectra shows the presence of palladium and carbon. PdCo/rGO, PdCo/MWCNT, PdCo/PPy and their hybrid catalysts spectra shows the presence of palladium, Cobalt and carbon. It was observed that are some unwanted metals which may be impurities that remain after preparation of PPy [17].

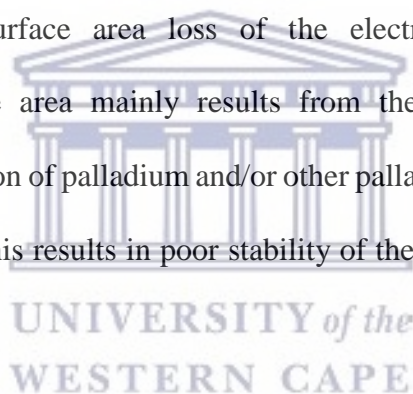
4.5 Electrochemistry Analysis

The electrochemical techniques (that is CV, LSV, EIS and Chrono) were used to investigate the electrochemical properties of the synthesized electrocatalysts. The cyclic voltammetry was used to study the electro-activity of the synthesized catalysts with 1 M KOH as electrolyte and 1 M methanol as an alcohol. The potential window used for the investigation ranges from -1 V to +0.4 V. The synthesized catalysts that were investigated were Pd/rGO, Pd/MWCNT, PdCo/rGO, PdCo/MWCNT, Pd/PPy, Pd/PPy-rGO and PdCo/PPy-rGO. A three-electrode system made-up of working electrode, counter electrode and reference electrode was used. The

working electrode used was glassy-carbon electrode while the counter electrode was platinum electrode and the reference electrode used was Ag/AgCl saturated in KCl.

4.5.1 Cyclic Voltammetry and ECSA Investigation

It is generally believed that the electro-chemical surface area of palladium is one of the most important parameters for characterizing a fuel cell electrode [18]. A large electro-chemical surface area is a sign for a better electrode, as more catalyst sites are available for electro-chemical reactions. It is reported that the performance degradation of DMFC is largely due to the electrochemical active surface area loss of the electrodes. The decrease in the electrochemical active surface area mainly results from the growth of palladium alloy nanoparticles size, the dissolution of palladium and/or other palladium alloy nanoparticles from the carbon support material. This results in poor stability of the fuel cell catalyst and the fuel cell system [19].



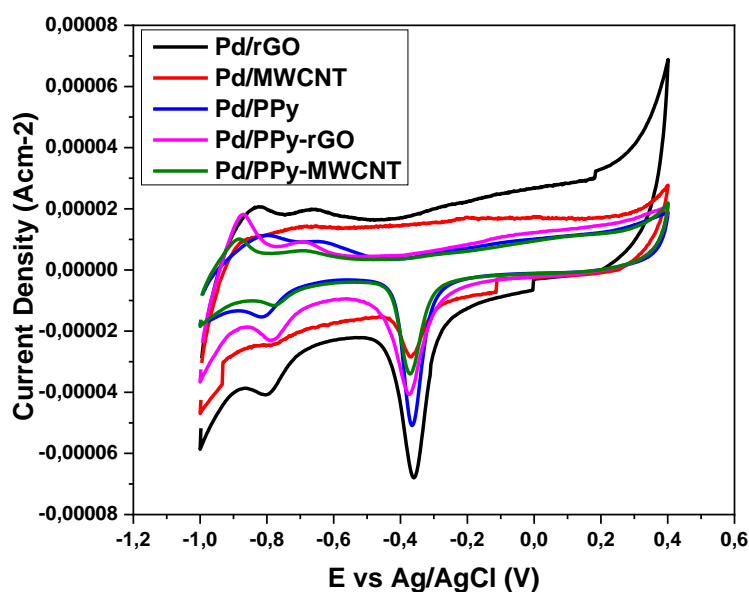


Figure 4.5.1 Cyclic voltammetry of Pd in house electro-catalyst supported on rGO, MWCNT, PPy and on a hybrid support of PPy-rGO and PPy-MWCNT in N_2 saturated 1.0 M of KOH at a scan rate of 20 mV.s^{-1}

Figure 4.5.1 compares the electrochemical responses of Pd/rGO, Pd/MWCNT, Pd/PPy and Pd/PPy-rGO in 1.0 MKOH measured in the potential range of -1.0V and 0.4V vs Ag/AgCl. The H_2 adsorption-desorption voltammetric peak in alkaline media was observed between the potentials of -0.23V and -0.86V. The Pd reduction peak was observed at the potential of -0.36V and the electrochemical active surface area (ECSA) of Pd/rGO, Pd/MWCNT, Pd/PPy, Pd/PPy-rGO and Pd/PPy-MWCNT catalysts was then calculated using the reduction peak. The Electrochemical Active Surface Area (ECSA) was calculated from the density of charge associated with the reduction of a full monolayer of Pd oxides [20]. This area was then converted into the effective active surface area by using the factor $420 \mu\text{C.cm}^{-2}$ for the monolayer of Pd Oxides. The results were collected and presented in Table 4.5.1 below. All ECSA calculations for this study were done following equation 4.5 given below:

$$\text{ECSA} = \frac{QH-\text{adsorption}(c)}{420 \mu\text{C.cm}^{-2} \cdot (LPd) \cdot (Ag)} \quad (4.5)$$

Q_H = is the charge area from Pd(reduction) peak; $420\mu\text{C}\cdot\text{cm}^{-2}$ is the charge of full coverage for clean polycrystalline Pd and is used as the conversion factor; L_{Pd} is the working electrode Pd loading ($\mu\text{g}\cdot\text{cm}^{-2}$); and A_g is the geometric surface area of the glassy carbon electrode (i.e. 0.196 cm^2). The values for ECSA are reported in $\text{m}^2\cdot\text{g}^{-1}$.

Table 4.5.1: Summary data of ECSA

Catalyst	ECSA ($\text{m}^2\cdot\text{g}^{-1}$)
Pd/rGO	50.7
Pd/MWCNT	14.0
Pd/PPy	68.0
Pd/PPy-rGO	40.3
Pd/PPy-MWCNT	27.6
PdCo/rGO	33.9
PdCo/MWCNT	49.3
PdCo/PPy	1.4
PdCo/PPy-rGO	17.3
PdCo/PPy-MWCNT	4.8

The table above displays the obtained data of ECSA for the synthesized catalysts, with Pd/PPy having the larger ECSA followed by Pd/rGO, PdCo/MWCNT, Pd/PPy-rGO, PdCo/rGO and Pd/MWCNT. This is most likely ascribed to the smaller size and much better dispersion of the Pd nanoparticles on PPy as compared to reduced-graphene oxide and multi-walled carbon nanotubes which is agglomerated due to growth in palladium alloyed nanoparticle size. This is in agreement with the results as it can be observed that most of the catalysts with larger particle

size leads to a smaller ECSA and those with the smaller particle size shows a larger ECSA. The mono-catalysts showed to have higher ECSA than most of the binary catalyst. This can be observed when comparing their HR-TEM particle size with ECSA. The ECSA values for mono catalysts are 50.7 m²/g for Pd/rGO, 14.0 m²/g for Pd/MWCNT, 68.0 m²/g for Pd/PPy, 40.3 m²/g for Pd/PPy-rGO and 27.6 m²/g for Pd/PPy-MWCNT. Adding the second metal to form binary catalysts did not increase the ECSA due to agglomeration [30]. The ECSA values for binary catalysts are 33.9 m²/g for PdCo/rGO, 49.3 m²/g for PdCo/MWCNT, 1.4 m²/g for PdCo/PPy, 17.3 m²/g for PdCo/PPy-rGO and 4.8 m²/g for PdCo/PPy-MWCNT. The HR-TEM particle size values for mono catalysts are 13.5 nm for Pd/rGO, 10.4 nm for Pd/MWCNT, 7.9 nm for Pd/PPy, 7.7 nm for Pd/PPy-rGO and 10.4 for Pd/PPy-MWCNT of which are mostly lower than that of binary catalysts. The HR-TEM values for binary catalysts are 8.2 nm for PdCo/rGO, 7.9 nm for PdCo/MWCNT, 8.9 nm for PdCo/PPy, 10.9 nm PdCo/PPy-rGO and 11.1 nm for PdCo/PPy-MWCNT. The high ECSA value for Pd-based mono-catalysts can be attributed to their lower particle sizes and electrochemical reaction kinetics [21]. The higher ECSA is associated with good catalytic activity [22].

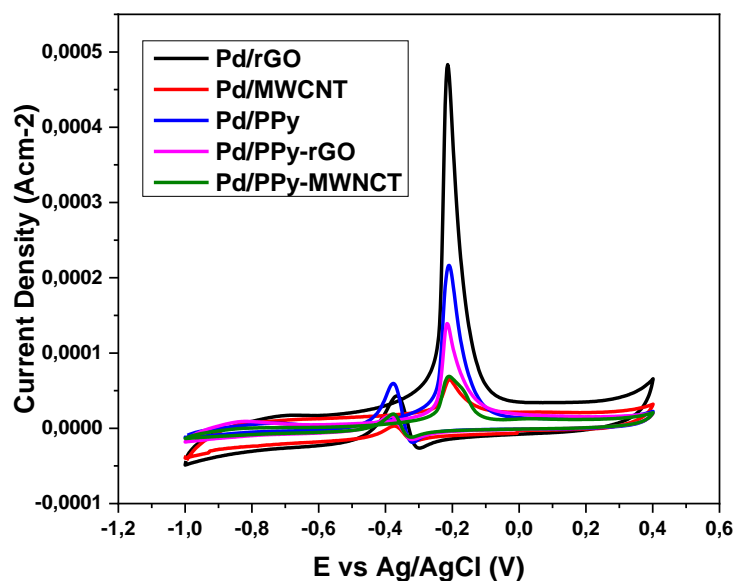


Figure 4.5.2 Cyclic voltammetry of Pd in house electro-catalyst supported on rGO, MWCNT, PPy and on a hybrid support of PPy-rGO and PPy-MWCNT in N_2 saturated 1.0 M of KOH and 1.0 M of Methanol at a scan rate of $20 \text{ mV}\cdot\text{s}^{-1}$

Figure 4.5.2 displays the CVs for methanol oxidation by different catalysts. Two peaks of methanol oxidation under anodic condition are clearly observed: the oxidation peak in the forward scan is corresponding to the oxidation of freshly chemisorbed species coming from methanol adsorption; the reverse oxidation peak is primarily associated with removal of carbonaceous species not completely oxidized in the forward scan, rather than caused by freshly chemisorbed species [23]. The magnitude of the peak current on the forward scan indicated the electrocatalytic activity of the electrocatalysts for methanol oxidation. It can be clearly observed from figure 4.5.2 above that the Pd supported on rGO has the highest oxidation peak followed by PPy and PPy-rGO composite, with Pd/MWCNT showing the smallest peak. The current density of the other three catalysts is very low, which may be associated with agglomeration on the surface of these catalysts as it can be seen from the HRTEM images from

figure 4.3.2 above. The onset overpotential is around -0.2 V for all the catalysts which is better in terms of overpotential [24].

Table 4.5.2: All the data collected from figure 4.5.2 of methanol oxidation.

Catalyst	$E_{\text{Onset(reduction)}}$ (mV vs Ag/AgCl)	$I_{\text{f(oxidation)}}$ (mA/cm ²)	$E_{\text{Onset(oxidation)}}$ (mV vs Ag/AgCl)	$I_{\text{r(reduction)}}$ (mA/cm ²)	$\frac{I_{\text{O}}}{I_{\text{r}}}$
Pd/rGO	-231.01	0.479	-329.2	-0.042	11.40
Pd/MWCNT	-250.5	0.065	-284.7	-0.009	7.22
Pd/PPy	-252.9	0.229	-294.5	-0.064	3.58
Pd/PPy-rGO	-213.9	0.136	-282.3	-0.016	8.50
Pd/PPy-MWCNT	-284.7	0.069	-277.4	-0.033	2.09

All the data in Table 4.5.2 were collected from Figure 4.5.2. The current density of Pd/rGO is 0.479 mA/cm² which is higher than all of the other prepared catalysts followed by Pd/PPy, Pd/PPy-rGO with 0.229 mA/cm² and 0.136 mA/cm² respectively and Pd/MWCNT with the lowest current density of 0.065 mA/cm². In addition, the ratio of the forward anodic peak current density (I_{f}) to the reverse anodic peak current density (I_{r}), $I_{\text{f}}/I_{\text{r}}$, can be used to describe the catalyst ability to tolerate carbonaceous species accumulation. A higher ratio indicates more effective removal of the poisoning species on the catalyst surface during the anodic scan and little accumulation of carbonaceous residues on the electrode surface, a low $I_{\text{f}}/I_{\text{r}}$ ratio shows the reverse case [25]. The $I_{\text{f}}/I_{\text{r}}$ ratio for PPy-rGO was 8.5 which is lower than that of rGO 11.4 but higher than all of other catalysts, indicating more intermediate carbonaceous species were

oxidized to carbon dioxide in the forward scan on Pd/PPy-rGO surface than on the surface of the other catalysts.

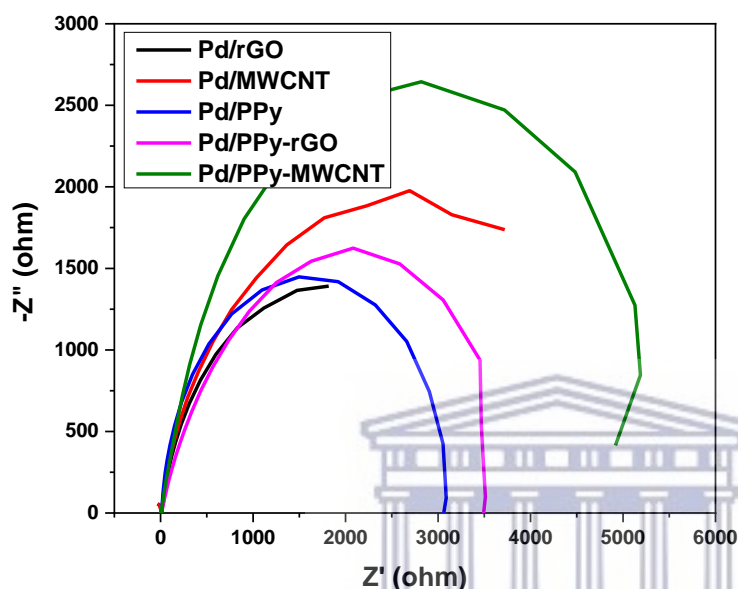


Figure 4.5.3 EIS of the synthesized electrocatalysts of Pd/rGO, Pd/MWCNT, Pd/PPy, Pd/PPy-rGO and Pd/PPy-MWCNT in 1.0M KOH with 1.0M methanol.

Figure 4.5.3 shows the nyquist plot which is characterized by a resistive behaviour for Pd/MWCNT, Pd/rGO, Pd/PPy, Pd/PPy-rGO and Pd/PPy-MWCNT. The plot resembles a semicircle, which can be attributed to a kinetically controlled reaction. The small arc in the high frequency region is associated with the dehydrogenation and chemisorption of the methanol molecule at the initial stage of the oxidation process [26]. A charge transfer resistance (R_{ct}) for the kinetically controlled reactions may be represented by the diameter of the semicircle in the medium frequency and is related to the charge transfer reaction kinetics according to the following equation:

$$R_{ct} = \frac{RT}{nFi_o} \quad (4.2)$$

$$i = nFAK_o C_o^{(1-\alpha)} C_R^\alpha \quad (4.3)$$

Where R: molar gas constant ($\text{J}\cdot\text{mol}^{-1}\text{ k}^{-1}$); T: temperature (K); n: number of electrons transferred; F: Faraday constant (C); i_0 : exchange current (A); A: reaction area (cm^2); k_0 : standard heterogeneous rate constant ($\text{cm}\cdot\text{sec}^{-1}$); C_o , C_R : bulk concentration of oxidant and reductant species ($\text{mol}\cdot\text{L}^{-1}$); α : transfer coefficient [20].

Table 4.5.3 the table below shows charge transfer resistance (R_{ct}) of the synthesized mono-catalysts

Catalysts	R_{ct} (charge transfer resistance) in ohms (Ω)	Current density in (mA/cm^2)
Pd/rGO	29.38	0.479
Pd/MWCNT	229.27	0.065
Pd/PPy	77.81	0.229
Pd/PPy-rGO	106.99	0.136
Pd/PPy-MWCNT	256.64	0.069

In Table 4.5.3 above it can be observed that the catalyst with higher oxidation current density has lower charge transfer resistance. Pd/rGO has the lowest charge transfer resistance and the highest current density followed by Pd/PPy, Pd/PPy-rGO, Pd/MWCNT and Pd/PPy-MWCNT respectively which can be attributed to the methanol oxidation reaction. Meaning that there is less difficulty encountered when electrons are transferred during MOR in Pd/rGO, Pd/MWCNT and Pd/PPy. This behaviour indicates that the reaction kinetics were affected by the adsorption of methanol on the electrode surface. However, the hybrid supported catalysts namely Pd/PPy-rGO and Pd/PPy-MWCNT were not favoured by the reaction kinetics. The high values of charge transfer resistance for all hybrid supported catalysts suggests low reaction kinetics. These results are in agreement with those obtained from voltammetric studies [26].

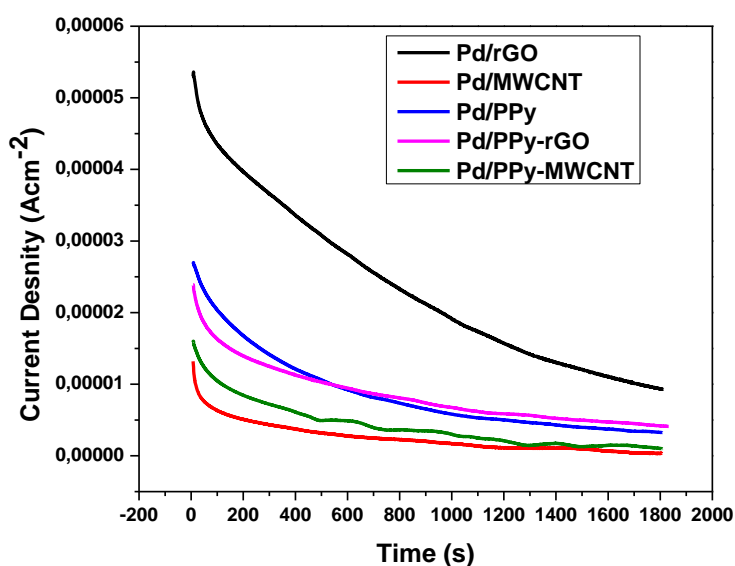


Figure 4.5.4 Chronoamperometry of Pd in-house electro-catalysts on rGO, MWCNT, PPy, PPy-rGO and PPy-MWCNT support in N_2 saturated 1.0M KOH and 1.0 M methanol comparing their stability at a -0.3V.

Shown in Figure 4.5.4 is the chronoamperometry for the synthesized catalysts, a decay of current value in the time interval measured for the studied electrocatalysts was observed. However, after the initial drops the performance become stable for all the catalyst tested. Pd/rGO shows a better stability compared to Pd/MWCNT, Pd/PPy, Pd/PPy-rGO and Pd/PPy-MWCNT respectively. This was to test the impact of the PPy support material on Pd stability when compared with other support materials like rGO and MWCNT. The stability test showed a better stability when Pd is supported on PPy compared to MWCNT but less stable than the Pd supported on rGO. Secondly the introduction of PPy on MWCNT to form a hybrid support for Pd catalyst showed a better stability compared to the Pd/MWCNT mono catalyst support as it can be observed on Figure 4.5.3 above. The ability for PPy to function as a support material with a good stability observed in this study was in agreement with the results obtained from other studies that compared this support material with other carbon based support materials [24&27].

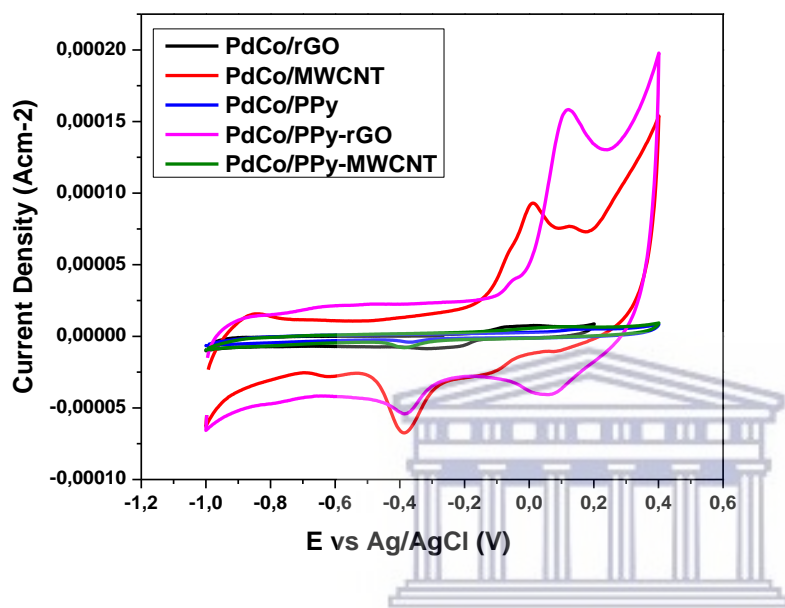


Figure 4.5.5 Cyclic voltammetry of PdCo in house electro-catalyst supported on rGO, MWCNT, PPy and on a hybrid support of PPy-rGO and PPy-MWCNT in N_2 saturated 1.0 M of KOH at a scan rate of $20 \text{ mV}\cdot\text{s}^{-1}$

Figure 4.5.5 compares the electrochemical responses of PdCo/rGO, PdCo/MWCNT, PdCo/PPy, PdCo/PPy-rGO and PdCo/PPy-MWCNT in 1.0 MKOH measured in the potential range of -1.0 and 0.4 vs Ag/AgCl. The second metal which is cobalt was introduced to confirm the effect of the supports material in presence of the bimetallic electro-catalyst. The adsorption-desorption voltammetric peaks of PdCo was observed between the potential of -0.26 V and -0.53 V [28]. The electrochemical active surface area (ECSA) of the synthesized catalysts was then calculated using the reduction peak at the potential of -0.39 V. The Electrochemical Active Surface Area (ECSA) was calculated from the density of charge associated with the reduction of a full monolayer of Pd oxides [20]. This area was then converted into the effective active

surface area by using the factor $420\mu\text{C}\cdot\text{cm}^{-2}$ for the monolayer of Pd Oxides. The results were collected and presented in Table 4.5.1 above.

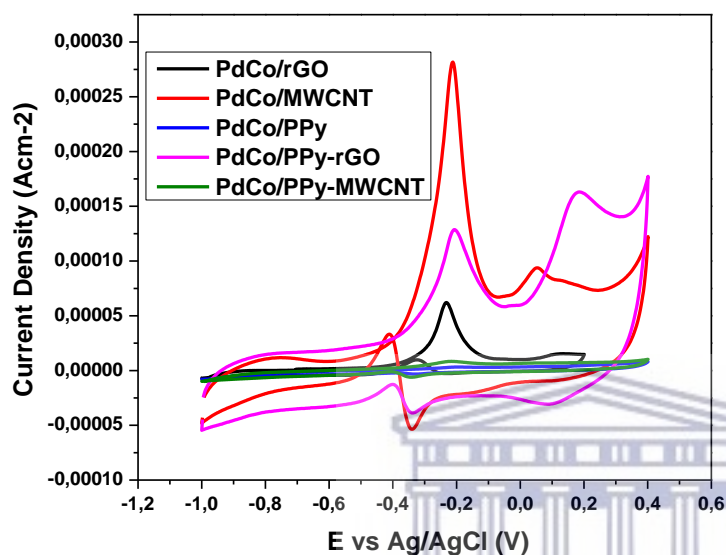


Figure 4.5.6 Cyclic voltammetry of PdCo in house electro-catalyst supported on rGO, MWCNT, PPy and on a hybrid support of PPy-rGO and PPy-MWCNT in N_2 saturated 1.0 M of KOH and 1.0 M of Methanol at a scan rate of $20\text{ mV}\cdot\text{s}^{-1}$

Figure 4.5.6 displays the CVs for methanol oxidation by synthesized PdCo catalysts supported on rGO, MWCNT, PPy, PPy-rGO and PPy-MWCNT. Two peaks of methanol oxidation are clearly observed: the oxidation peak in the forward scan is corresponding to the oxidation of freshly chemisorbed species coming from methanol adsorption; the reverse oxidation peak is primarily associated with removal of carbonaceous species not completely oxidized in the forward scan, rather than caused by freshly chemisorbed species. PdCo/MWCNT showed a higher current density followed by PdCo/PPy-rGO, PdCo/rGO, PdCo/PPy-MWCNT and PdCo/PPy respectively. Introducing the second metal on the Pd catalyst seems to be improving the catalytic activity for the PdCo supported on MWCNT compared to the ones supported on rGO and PPy where current density was lowered. According to the studies addition of Co on

Pd improves the catalytic activity as it can be observed with PdCo/MWCNT [29-30]. The onset potential (E_{onset}) for methanol oxidation is an important factor. The most negative onset potential is preferred, the lower it is the better in terms of overpotential and less over-potential. Increasing the E_{onset} may be due to the CO adsorbed on the electrode surface that leads to overpotential [29]. PdCo/MWCNT shows a high current density with a more negative onset potential which indicates higher catalytic performance compare to the other 4 catalysts namely PdCo/rGO, PdCo/PPy, PdCo/PPy-rGO and PdCo/PPy-MWCNT. The onset potential and current density of the prepared catalysts is shown in the table below.

Table 4.5.4: Current density values and onset potentials of PdCo/rGO, PdCo/MWCNT, PdCo/PPy, PdCo/PPy-rGO and PdCo/PPy-MWCNT in 1.0MKOH with 1.0M methanol at a scan rate of $20\text{mV}\cdot\text{s}^{-1}$

Catalyst	Current density (mAcm^{-2})	Onset potential (V)
PdCo/rGO	0.12	-0.40
PdCo/MWCNT	0.37	-0.57
PdCo/PPy	0.007	-0.25
PdCo/PPy-rGO	0.17	-0.54
PdCo/PPy-MWCNT	0.02	-0.31

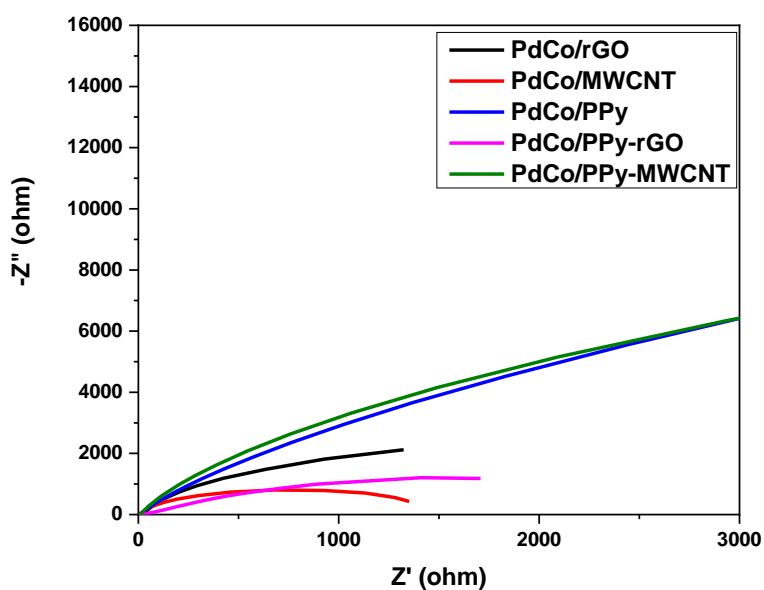


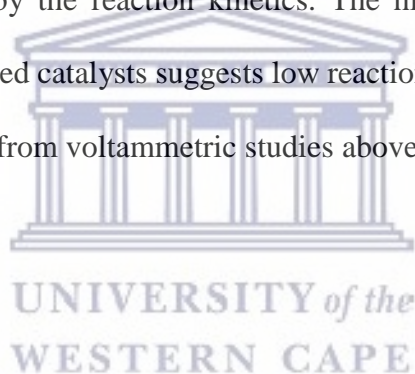
Figure 4.5.7 EIS of PdCo synthesized electro-catalyst supported on rGO, MWCNT, PPy and on a hybrid support of PPy-rGO and PPy-MWCNT in N_2 saturated 1.0 M of KOH and 1.0 M of Methanol.

The Nyquist plot shown in Figure 4.5.7 is characterized by a resistive feature for PdCo/rGO, PdCo/PPy-MWCNT, PdCo/PPy as expected for hydrogen adsorption/desorption and double layer charging/ discharging phenomena as observed in Figure 4.5.7 above the Nyquist plot resembles a semicircle, which can be assigned to kinetically controlled reaction.

Table 4.5.5 the table below shows charge transfer resistance (R_{ct}) of the synthesized binary catalysts

Catalysts	R_{ct} (charge transfer resistance) in ohms (Ω)	Current density in (mA/cm^2)
PdCo/rGO	116.71	0.12
PdCo/MWCNT	142.37	0.37
PdCo/PPy	4392.45	0.007
PdCo/PPy-rGO	109.92	0.17
PdCo/PPy-MWCNT	1069.92	0.02

In Table 4.5.5 above it can be observed that the catalyst with higher oxidation current density has lower charge transfer resistance. PdCo/MWCNT has the lowest charge transfer resistance and the highest current density followed by PdCo/PPy-rGO, PdCo/rGO, PdCo/PPy-MWCNT and PdCo/PPy respectively which can be attributed to the methanol oxidation reaction. Meaning that there is less difficulty encountered when electrons are transferred during MOR in PdCo/MWCNT, PdCo/rGO and PdCo/PPy-rGO compared to PdCo/PPy and PdCo/PPy-MWCNT catalysts. This behaviour indicates that the reaction kinetics were affected by the adsorption of methanol on the electrode surface. However, the catalysts supported on PPy, PPy-MWCNT were not favoured by the reaction kinetics. The high values of charge transfer resistance for the latter mentioned catalysts suggests low reaction kinetics. These results are in agreement with those obtained from voltammetric studies above [26].



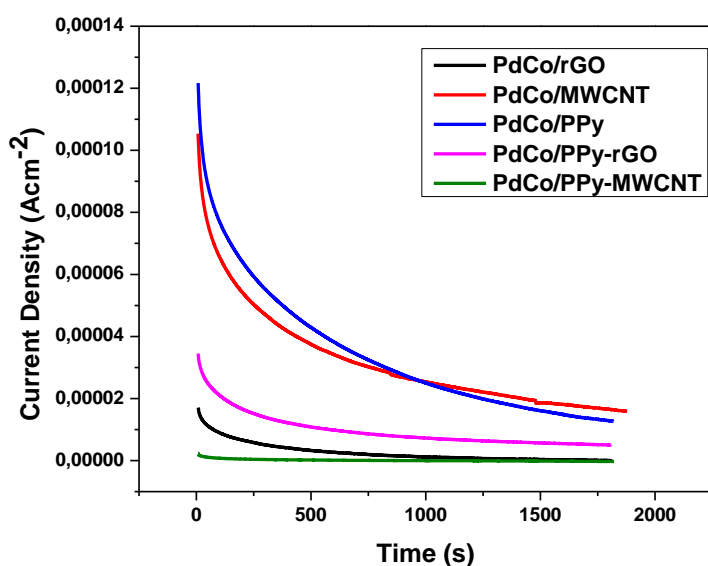


Figure 4.5.8 Chronoamperometry of PdCo in-house electro-catalysts on rGO, MWCNT, PPy, PPy-rGO and PPy-MWCNT support in N_2 saturated 1.0M KOH and 1.0 M methanol comparing their stability at -0.3V.

Figure 4.5.8 shows the chronoamperometry of the synthesized electrocatalysts, a decaying current density value in the time interval measured for the studied electrocatalysts was observed. However, after the initial drops the performance become stable for all the catalyst tested. PdCo/MWCNT and PdCo/PPy shows a better stability compared to PdCo/PPy-rGO, PdCo/rGO and PdCo/PPy-MWCNT respectively, which indicates that the present of PPy has the potential to improve the stability of the catalyst by giving a balanced adsorption between OH species from methanol adsorption on Pd. The results obtained on this study agrees with the study conducted by Zhao, Y, et al [24&31].

4.6 Summary

The Pd mono electro-catalysts and PdCo binary catalysts were synthesized following the modified polyol method outlined in chapter 3 and supported on reduced graphene oxide, multi-walled carbon nanotubes, PPy and hybrid support PPy-rGO and PPy-MWCNT. The home prepared electro-catalysts were then evaluated for their electro-catalytic properties. Physical characterization was evaluated using powerful techniques such as XRD, HRTEM, FTIR and EDS. For electro-chemical characterization CV, EIS and chrono were employed. It was observed that the performance of the electro-catalyst mostly depends on the structural properties of the support material and the morphology of the electro-catalysts. Mono-catalysts performed better than binary catalysts that were supported on the similar material in terms of catalytic activity during methanol oxidation Pd/rGO was better than PdCo/rGO, Pd/MWCNT>PdCo/MWCNT, Pd/PPy>PdCo/PPy, Pd/PPy-rGO>PdCo/PPy-rGO and Pd/PPy-MWCNT>PdCo/PPy-MWCNT. Secondly most of the binary catalyst showed a better stability compared to mono catalysts. Lastly it was observed that adding PPy as an ionomer to MWCNT and rGO can bring a remarkable catalytic stability during methanol oxidation reaction. In terms of catalytic activity PPy did not give us the expected outstanding results, hence further studies need to be conducted to investigate the effect of PPy on the electrocatalysts.

References

1. Atieh, M.A., Bakather, O.Y., Al-Tawbini, B., Bukhari, A.A., Abuilaiwi, F.A. and Fettouhi, M.B., 2010. Effect of carboxylic functional group functionalized on carbon nanotubes surface on the removal of lead from water. *Bioinorganic chemistry and applications*, 2010.
2. Moosa, A.A., Ridha, A.M. and Abdullha, I.N., 2015. Chromium ions removal from wastewater using carbon nanotubes. *International Journal for Innovative Research in Science & Technology*, 4(2), pp.275-282.
3. Emiru, T.F. and Ayele, D.W., 2017. Controlled synthesis, characterization and reduction of graphene oxide: A convenient method for large scale production. *Egyptian Journal of Basic and Applied Sciences*, 4(1), pp.74-79.
4. Andrijanto, E., Shoelarta, S., Subiyanto, G. and Rifki, S., 2016, April. Facile synthesis of graphene from graphite using ascorbic acid as reducing agent. In *AIP Conference Proceedings* (Vol. 1725, No. 1, p. 020003). AIP Publishing LLC.
5. Kamal, M.M. and Bhuiyan, A.H., 2013. Thickness dependent direct current electrical conduction in plasma polymerized pyrrole monolayer thin films. In *Advanced Materials Research* (Vol. 741, pp. 59-64). Trans Tech Publications Ltd.
6. MA, C., SG, P., PR, G. and Shashwati, S., 2011. Synthesis and characterization of polypyrrole (PPy) thin films. *Soft nanoscience letters*, 2011.
7. Huang, Y., Zhang, X., Huang, X., Li, H. and Huang, C., 2015. Preparation of conductive polypyrrole composite particles based on spherical polyelectrolyte brushes. *Materials Express*, 5(1), pp.56-62.
8. Smith, D.K. and Jenkins, R., 1996. The powder diffraction file: past, present, and future. *Journal of research of the National Institute of Standards and Technology*, 101(3), p.259.

9. Kamarudin, S.K. and Hashim, N., 2012. Materials, morphologies and structures of MEAs in DMFCs. *Renewable and Sustainable Energy Reviews*, 16(5), pp.2494-2515.
10. Zainuddin, M.F., Raikhan, N.N., Othman, N.H. and Abdullah, W.F.H., 2018, May. Synthesis of reduced Graphene Oxide (rGO) using different treatments of Graphene Oxide (GO). In *IOP Conference Series: Materials Science and Engineering* (Vol. 358, No. 1, p. 012046). IOP Publishing.
11. Ye, K.H., Zhou, S.A., Zhu, X.C., Xu, C.W. and Shen, P.K., 2013. Stability analysis of oxide (CeO₂, NiO, Co₃O₄ and Mn₃O₄) effect on Pd/C for methanol oxidation in alkaline medium. *Electrochimica Acta*, 90, pp.108-111.
12. Zhu, C., Yang, Y.Y. and Zhao, Z.G., 2018. Surface voltammetric dealloying investigation on PdCu/C electrocatalysts toward ethanol oxidation in alkaline media. *Journal of Nanoparticle Research*, 20(11), pp.1-12.
13. Mukerjee, S., 1990. Particle size and structural effects in platinum electrocatalysis. *Journal of Applied Electrochemistry*, 20(4), pp.537-548.
14. Shen, Y., Lu, S., Xu, W., Lv, A., Wang, Z., Wang, H., Liu, G. and Zhang, Y., 2020. Fabrication of composite material with pd nanoparticles and graphene on nickel foam for its excellent electrocatalytic performance. *Electrocatalysis*, 11(5), pp.522-535.
15. Zhu, M., Sun, G. and Xin, Q., 2009. Effect of alloying degree in PtSn catalyst on the catalytic behavior for ethanol electro-oxidation. *Electrochimica Acta*, 54(5), pp.1511-1518.
16. Morataya, J., 2018. Synthesis and Electrochemical Analysis of PdCo/MWCNT and PdCo/GO Towards Formic Acid Fuel Cells.
17. Nicho, M.E. and Hu, H., 2000. Fourier transform infrared spectroscopy studies of polypyrrole composite coatings. *Solar energy materials and solar cells*, 63(4), pp.423-435.

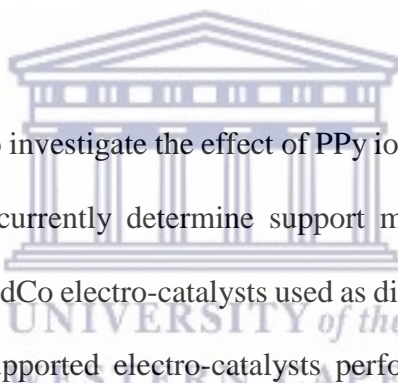
18. Calderón Gómez, J.C., Moliner, R. and Lázaro, M.J., 2016. Palladium-based catalysts as electrodes for direct methanol fuel cells: a last ten years review. *Catalysts*, 6(9), p.130.
19. Talebian-Kiakalaieh, A., Amin, N.A.S., Rajaei, K. and Tarighi, S., 2018. Oxidation of bio-renewable glycerol to value-added chemicals through catalytic and electrochemical processes. *Applied Energy*, 230, pp.1347-1379.
20. Hsing, I.M., Wang, X. and Leng, Y.J., 2002. Electrochemical impedance studies of methanol electro-oxidation on Pt/C thin film electrode. *Journal of the Electrochemical Society*, 149(5), p.A615.
21. Santasalo-Aarnio, A., Kwon, Y., Ahlberg, E., Kontturi, K., Kallio, T. and Koper, M.T., 2011. Comparison of methanol, ethanol and iso-propanol oxidation on Pt and Pd electrodes in alkaline media studied by HPLC. *Electrochemistry Communications*, 13(5), pp.466-469.
22. Corradini, P.G., Pires, F.I., Paganin, V.A., Perez, J. and Antolini, E., 2012. Effect of the relationship between particle size, inter-particle distance, and metal loading of carbon supported fuel cell catalysts on their catalytic activity. *Journal of Nanoparticle Research*, 14(9), pp.1-9.
23. Hosseini, M.G., Abdolmaleki, M. and Ashrafpoor, S., 2013. Methanol electro-oxidation on a porous nanostructured Ni/Pd-Ni electrode in alkaline media. *Chinese Journal of Catalysis*, 34(9), pp.1712-1719.
24. Zhao, Y., Zhan, L., Tian, J., Nie, S. and Ning, Z., 2011. Enhanced electrocatalytic oxidation of methanol on Pd/polypyrrole-graphene in alkaline medium. *Electrochimica Acta*, 56(5), pp.1967-1972.
25. Qin, Y.H., Yang, H.H., Zhang, X.S., Li, P. and Ma, C.A., 2010. Effect of carbon nanofibers microstructure on electrocatalytic activities of Pd electrocatalysts for

- ethanol oxidation in alkaline medium. *International Journal of Hydrogen Energy*, 35(15), pp.7667-7674.
26. Mahapatra, S.S. and Datta, J., 2011. Characterization of Pt-Pd/C electrocatalyst for methanol oxidation in alkaline medium. *International Journal of Electrochemistry*, 2011.
27. Yuan, X., Ding, X.L., Wang, C.Y. and Ma, Z.F., 2013. Use of polypyrrole in catalysts for low temperature fuel cells. *Energy & Environmental Science*, 6(4), pp.1105-1124.
28. Jović, V. and Jović, B., 2002. Surface reconstruction during the adsorption/desorption of OH species onto Cu (111) and Cu (100) in 0.1 M NaOH solution. *Journal of the Serbian Chemical Society*, 67(7), pp.531-546.
29. Kiyani, R., Rowshanzamir, S. and Parnian, M.J., 2016. Nitrogen doped graphene supported palladium-cobalt as a promising catalyst for methanol oxidation reaction: synthesis, characterization and electrocatalytic performance. *Energy*, 113, pp.1162-1173.
30. Ravat, V., Nongwe, I. and Coville, N.J., 2016. N-doped ordered mesoporous carbon supported PdCo nanoparticles for the catalytic oxidation of benzyl alcohol. *Microporous and Mesoporous Materials*, 225, pp.224-231.
31. Ghosh, S., Bhandary, N., Basu, S. and Basu, R.N., 2017. Synergistic effects of polypyrrole nanofibers and Pd nanoparticles for improved electrocatalytic performance of Pd/PPy nanocomposites for ethanol oxidation. *Electrocatalysis*, 8(4), pp.329-339.
32. Biswas, R.K., Khan, P., Mukherjee, S., Mukhopadhyay, A.K., Ghosh, J. and Muraleedharan, K., 2018. Study of short range structure of amorphous Silica from PDF using Ag radiation in laboratory XRD system, RAMAN and NEXAFS. *Journal of Non-Crystalline Solids*, 488, pp.1-9.

Chapter 5

Conclusion and recommendation

5.1. Conclusion



The purpose of this study was to investigate the effect of PPy ionomer on the support materials for electro-catalysts while concurrently determine support materials that can improve the activity and stability of Pd and PdCo electro-catalysts used as direct alcohol fuel cells catalysts. The literature confirms that supported electro-catalysts perform better than non-supported catalysts, hence the focus on support materials. The support material must have certain properties that make it a suitable material for use as a support material for the metal catalyst. So far, carbon, and carbon nanotubes has been regarded as an ideal materials for supporting nanoscale metal particles to the electrodes of low temperature fuel cells such as PEMFC and DMFC. Therefore, PPy was selected for this study because of the special properties such as excellent electronic, physical and mechanical properties it poses. This made it to be proposed as a replacement for traditional carbon black as an alternative support for fuel cell catalysts. In addition, the literature shows that electro-catalysts supported in these materials gives improved activity and stability. Nonetheless, it is known that all support material are corroded under the operating conditions of the fuel cell leading to performance deteriorating over time due to the

accelerated loss of the active surface of the catalyst. To address the instability of support materials, this study selected to investigate the potential of using Pd based catalysts supported on rGO and MWCNT with PPy added as an ionomer for fuel cell electro-catalysts. The main purpose is to enhance the stability of the electro-catalyst by improving the support material, as Pd is known to be resistant to corrosion. Pd and PdCo were chosen as electro-catalysts to examine if they could be methanol tolerant electro-catalysts for DMFC.

This work involved the preparation and characterization of Pd-based catalysts on Polypyrrole, reduced graphene oxide, multi-carbon nanotubes and on PPy-rGO and PPy-MWCNT hybrid supports. Two in-house catalysts, namely Pd and PdCo were synthesized using the modified polyol method. The support materials were synthesized using different methods stated in chapter 3. Electrochemical, chemical and physical properties were investigated by CV, LSV, EIS, chronoamperometry, HRTEM, EDS and XRD. The CV results showed that Pd/PPy had the largest area for the reduction peak which resulted in it having the highest ECSA of 68.01 $\text{m}^2.\text{g}^{-1}$ followed by Pd/rGO with an ECSA of 50.72 $\text{m}^2.\text{g}^{-1}$ and Pd/rGO showed the highest current density and highly negative onset potential in methanol more than any other mono catalysts, with current density at 0.64 mAcm^{-2} and onset potential at -0.48mV. The Pd catalysts containing Co did not perform well in methanol and from XRD it is seen that the catalysts did not alloy well and this affected the catalyst activity. The Pd catalysts supported on rGO showed good stability followed by PPy compared to the Pd supported on MWCNT, also their activity in LSV in the presence of PPy as a hybrid support material can be observed but with decreased oxidation peak showing clearly that the catalysts may not be favoured in methanol as an alcohol of choice. The catalyst kinetics was faster in the Pd mono catalysts supported on PPy compared to those supported on rGO and MWCNT. The particle size observed in TEM showed the smallest particles were for Pd/PPy-rGO, while the average particle size from XRD also showed that Pd/PPy-rGO had the smallest average particle size. Based on all the results obtained in the

study, using PPy as an ionomer to the support material does improve the stability and activity of the catalyst. This study further shows that Pd catalysts favour the use of mono support more than a hybridized support material.

5.2 Recommendations

The effect of using PPy as an ionomer for support material for Pd catalysts shows a promising improvement in the activity and stability. This study therefore recommends that the Polypyrrole should be used as an ionomer for support material for alcohol oxidation tolerant catalyst as they show both activity and stability over the catalysts supported on rGO and MWCNT. Therefore, in terms of reducing the metal loading the role of supporting materials is recommended as these materials have great influence on the cost, activity and stability of the fuel cell catalyst as whole.





UNIVERSITY *of the*
WESTERN CAPE